

OROGRAPHIC EFFECTS ON PRECIPITATING CLOUDS

Robert A. Houze Jr.¹

Received 25 May 2011; revised 7 September 2011; accepted 8 September 2011; published 6 January 2012.

[1] Precipitation over and near mountains is not caused by topography but, rather, occurs when storms of a type that can occur anywhere (deep convection, fronts, tropical cyclones) form near or move over complex terrain. Deep convective systems occurring near mountains are affected by channeling of airflow near mountains, capping of moist boundary layers by flow subsiding from higher terrain, and triggering to break the cap when low-level flow encounters hills near the bases of major mountain ranges. Mesoscale convective systems are triggered by nocturnal downslope flows and by diurnally triggered disturbances propagating away from mountain ranges. The stratiform regions of mesoscale convective systems are enhanced by upslope flow when they move over mountains. In frontal cloud systems, the poleward flow of warm-sector air ahead of the system

may rise easily over terrain, and a maximum of precipitating cloud occurs over the first rise of terrain, and rainfall is maximum on ridges and minimum in valleys. If the low-level air ahead of the system is stable, blocking or damming occurs. Shear between a blocked layer and unblocked moist air above favors turbulent overturning, which can accelerate precipitation fallout. In tropical cyclones, the tangential winds encountering a mountain range produce a gravity wave response and greatly enhanced upslope flow. Depending on the height of the mountain, the maximum rain may occur on either the windward or leeward side. When the capped boundary layer of the eye of a tropical cyclone passes over a mountain, the cap may be broken with intense convection resulting.

Citation: Houze, R. A., Jr. (2012), Oographic effects on precipitating clouds, *Rev. Geophys.*, 50, RG1001, doi:10.1029/2011RG000365.

1. INTRODUCTION

[2] Atmospheric precipitation forming as a result of moist air flowing over and around hills and mountains is a major control on the global precipitation pattern. In a warming world, moist currents approaching and traversing mountains may be expected to adjust in location, strength, and intrinsic instability, resulting in significant changes in the distribution over the Earth of precipitation and associated latent heating of the atmosphere. Because mountainous terrain is highly variable and detailed in its forms and locations relative to moisture sources, its effect on atmospheric precipitation processes must not be oversimplified. In this review, we identify the principal forms of precipitation near and over mountains and how the existence of the terrain influences the precipitation mechanisms. Grasping these fundamental facts will facilitate evaluation of the performance of increasingly detailed models, which are being used both to assess changes in climate and to forecast hazardous conditions accompanying heavy precipitation in populated,

mountainous regions [e.g., Houze *et al.*, 2011]. In addition to mountains affecting when and where precipitation falls, precipitation in turn affects the terrain itself, especially through erosion. Understanding the fundamental processes that occur when precipitation occurs near and over complex terrain is therefore prerequisite for understanding even longer term changes in the Earth system such as mountain building and degradation that occurs on time scales of tens of thousands of years or more [e.g., Roe *et al.*, 2003; Barros *et al.*, 2004, 2006].

[3] Traditionally, “orographic precipitation” is the term used to describe the rain and snow resulting from flow over terrain. But this term imbues the terrain with causation, which is misleading because on the time scale of the weather events producing precipitation, the Earth’s topography is inactive and therefore cannot ever be the proximate cause of atmospheric precipitation. Most precipitation in the atmosphere is instead attributable to one of three major categories of storms: convective clouds, frontal systems, or tropical cyclones. These storms exist for reasons fundamentally unrelated to underlying terrain: Convective storms draw their energy from the vertical stratification of atmospheric temperature and water vapor, frontal systems draw their

¹Department of Atmospheric Sciences, University of Washington, Seattle, Washington, USA.

energy from the horizontal variation of atmospheric temperature, and tropical cyclones draw theirs from latent heat stored in the upper ocean. Occasionally precipitation may also be caused by wind blowing over rugged terrain apart from the occurrence of one of these three storm categories, for example, moist trade winds blowing over the mountains of Hawaii. But most often what is called “orographic precipitation” is the alteration or reorganization of one of the three major storm types when it encounters topographic features.

[4] Because of this, the title of this review uses the somewhat more precise terminology “orographic effects on precipitating clouds.” The specific objective of the paper is to provide a comprehensive overview of all the known ways that the precipitation-producing processes in the three major storm types are affected when they occur in regions of hills and mountains. When *Smith* [1979] classic review, “The influence of mountains on the atmosphere,” and even later when the book *Cloud Dynamics* was written [see *Houze*, 1993, chapter 12], relatively little was known about the effects of topography on precipitating cloud systems. In the latter, this author had to resort to a few largely imagined conceptual drawings to illustrate the likely mechanisms of mountain effects on precipitating clouds. Since the early 1990s, however, knowledge of the effects of flow over topography on precipitation has exploded. Field experiments, new specialized satellites, and increasingly sophisticated numerical modeling have led to ~100 papers on different aspects of this problem. Up to now, review papers have been limited in scope. For example, *Barros and Lettenmaier* [1994] reviewed early progress only on the modeling and prediction of certain types of precipitation over mountains and associated surface runoff. *Lin et al.* [2001] identified certain generic environmental conditions that favor especially heavy rainfall events over mountainous regions. More recently, research has begun to focus on the mechanisms of precipitation enhancement by flow over complex terrain. *Smith* [2006] reviewed from a theoretical standpoint how precipitation is affected by stable moist airflow over mountains and how it may be formulated in idealized models; however, he did not delve into issues related to unstable flow over terrain. In a brief but somewhat more holistic review of precipitation mechanisms over mountains, *Roe* [2005, p. 665] noted, “Orographic precipitation is intrinsically a transient phenomenon. It tends to occur during the passage of a preexisting weather disturbance, and precipitation rates can vary substantially during the course of a single storm as synoptic conditions change....” As a consequence, he cautioned against overly simplistic explanations of mean precipitation patterns in mountainous regions: “One must be careful...about the sense in which an average pattern actually exists.” Despite this clear recognition of the breadth of the problem of orographic influences on precipitating clouds, he had to fall back onto a more restricted consideration of stable flow over mountains because “Much of the research to date on orographic precipitation has focused on storms impinging on midlatitude mountain ranges....” In other words, a lot of the orographic effects on

precipitating clouds occur near the less studied mountain ranges in the tropics and subtropics as well as midlatitudes. While it is true that *Lin et al.* [2001] touched on environmental aspects of precipitation enhancement over lower- and well as higher-latitude mountains, a broad examination and synthesis of the details of the dynamical and microphysical processes in both unstable and stable flows over terrain, i.e., a truly global synthesis of mountain effects on precipitation, has up to now not been accomplished.

[5] Since *Roe*’s [2005] review, the literature has further expanded and by now has begun to give us a picture of the effects of hills and mountains on precipitation of all types, including convective storms in lower latitudes and tropical cyclones as well as midlatitude frontal systems. The goal of the present review is to bring these diverse emerging components of how flow over, around, and near complex orography affects precipitation into a comprehensive summary of a type that will promote a better understanding of precipitation patterns over the globe. It is critical to understand precipitation on the global scale in order to determine the likely changes of precipitation patterns in a warming world. The review is organized into four parts. Section 2 discusses briefly the primary effects that hills and mountains have on precipitation mechanisms via microphysics, dynamics, and thermodynamics. Section 3 summarizes generically the ways in which airflow over and around complex terrain may affect precipitating clouds. Sections 4, 5, and 6 discuss how these processes operate to modify preexisting precipitating cloud systems, namely, convective storms, midlatitude frontal systems, and tropical cyclones, respectively. Section 7 summarizes the review.

2. FUNDAMENTAL FACTORS GOVERNING PRECIPITATION FALLOUT OVER HILLS AND MOUNTAINS

[6] The size and shape of a hill or mountain has a profound effect on the ultimate distribution of precipitation on the ground. The distribution of precipitation over and near a terrain feature of a given height and topographic shape is determined by a combination of microphysics of particle growth, the dynamical behavior of a fluid flow encountering a terrain barrier, and the thermodynamics of moist air. The essentials of these behaviors are as follows.

2.1. Microphysical Time Scale and Terrain Size

[7] Water drops and ice crystals require time to grow to precipitable size and fall out, and the height and steepness of terrain limit the locations where it is possible for the falling particles to land. Therefore, the microphysical time scales of particle growth and spatial scales of the terrain are critically and crucially linked. For example, Figure 1 [from *Hobbs et al.*, 1973] shows how the degree of growth by riming of ice particles can determine whether they fall on the windward or leeward side of a moderately sized two-dimensional (2-D) mountain barrier. Over a taller or wider mountain range, the particles shown would have no chance of being advected to the lee side. If the mountain is a 3-D

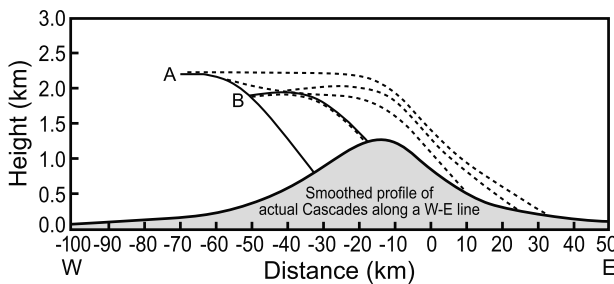


Figure 1. Ice particle trajectories starting at locations A and B show the effects of riming of snow particles embedded in the flow over the mountain barrier. Air motions were taken from a two-dimensional model of the flow over a mountain barrier similar to the Cascade Range of Washington State. The most heavily rimed particles (solid curves) fall out more quickly on the windward slope. Particles undergoing the least riming (dotted curves) are advected farthest over the crest of the mountain range by the cross-barrier flow. From Hobbs *et al.* [1973]. Copyright 1973 American Meteorological Society.

isolated peak rather than a long barrier, the particles might be carried around rather than over the mountain. Over small hills, the particles would all be carried across the peak of the terrain.

[8] Other microphysical factors crucially affect the growth rate and fallout of a precipitation particle. The concentration, size spectrum, and chemical composition of the aerosol on which the cloud drops and ice particles form in the rising air are primary among these factors. Through these factors, anthropogenic influences on precipitation in mountainous regions can become important. Such effects have only begun to be examined. Since the sources of aerosol are not connected with the mountains themselves, and since so little has yet been done to investigate aerosol sources in relation to mountain weather, this topic is beyond the scope of the present review and remains a topic ripe for urgent investigation.

[9] In considering the flow of stable air over terrain features, Jiang and Smith [2003], Smith [2003], Smith and Barstad [2004], Barstad and Smith [2005], and Roe [2005] have largely bypassed the crucial microphysical mechanisms in precipitating clouds over mountains by cleverly parameterizing them through time scales. They specify separate time scales for the microphysical processes and air motions. The microphysical time scales combined with the width and breadth of the terrain feature and the exact characteristics of the airflow over the terrain then determine where on the mountain the growing precipitation particles will ultimately land. Of course, ultimately the specific micro-physics underlying the parameterizations will need to be understood.

2.2. Dynamics of Airflow Encountering Hills and Mountains

[10] From a dynamical viewpoint, we further note that airflow encountering terrain will respond differently depending on several factors. In buoyantly unstable flow, precipitating

convection may be triggered when the oncoming air rises to pass over the obstacle. In stable flow approaching a barrier, the response of the flow to the terrain depends on three factors: the strength of the cross-barrier component of the upstream airflow, the degree of thermodynamic stability of the oncoming flow, and the height of the terrain barrier. These factors are sometime combined into a nondimensional ratio U/Nh , where U is the cross-barrier flow strength, N is the Brunt-Väisälä frequency, and h is the maximum terrain height. This ratio is a measure of the importance of nonlinear effects in the flow [Smolarkiewicz and Rotunno, 1989]. (Sometimes U/Nh is loosely referred to as a Froude number in the context of orographic precipitation. However, Baines [1995] has suggested that Froude number should be reserved for fluid dynamics problems in which it refers to the ratio of a fluid speed divided by a wave speed.) When U/Nh is large, the airflow easily rises over the terrain, and when U/Nh is small, the oncoming airflow may be blocked or dammed, and air does not easily rise over the terrain. In these cases the flow approaching the terrain may turn to flow parallel to a barrier or around an isolated hill or mountain.

2.3. Thermodynamics of Air Rising Over Complex Topography

[11] Another factor affecting precipitation fallout from clouds over mountains is that the saturation vapor pressure of the atmosphere decreases exponentially with temperature, and hence with height. Precipitation generated as a result of upward air motion and microphysical growth processes on the windward side of a barrier is most robust at lower levels. Consequently, for a high mountain, the precipitation is likely to be greater on the lower slopes of the terrain. This humidity factor often combines with one or more of the aforementioned microphysical and dynamical trends to make the upper reaches of higher mountains drier than their lower slopes. Figure 2 [from Frei and Schär, 1998] shows how the

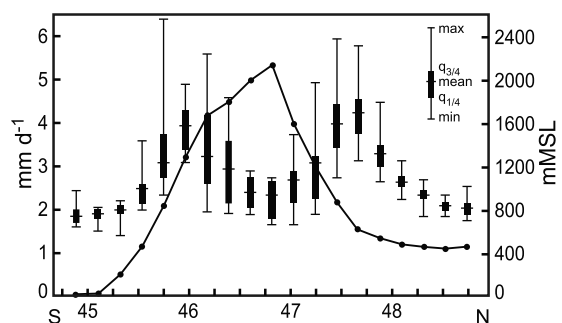


Figure 2. Mean annual precipitation (symbols) and topographic height (solid line) along a north-south section across the eastern Alps. The data represent the zonal mean of the analysis between 10.2°E and 12.6°E . The symbols (see legend) depict the interquartile range and the minima and maxima of the distribution of mean annual precipitation at stations in the corresponding latitude belts. The number of stations considered for each of the statistics is between 45 and 80 north of 47°N and between 10 and 30 south of 47°N . From Frei and Schär [1998]. Reprinted with permission from John Wiley.

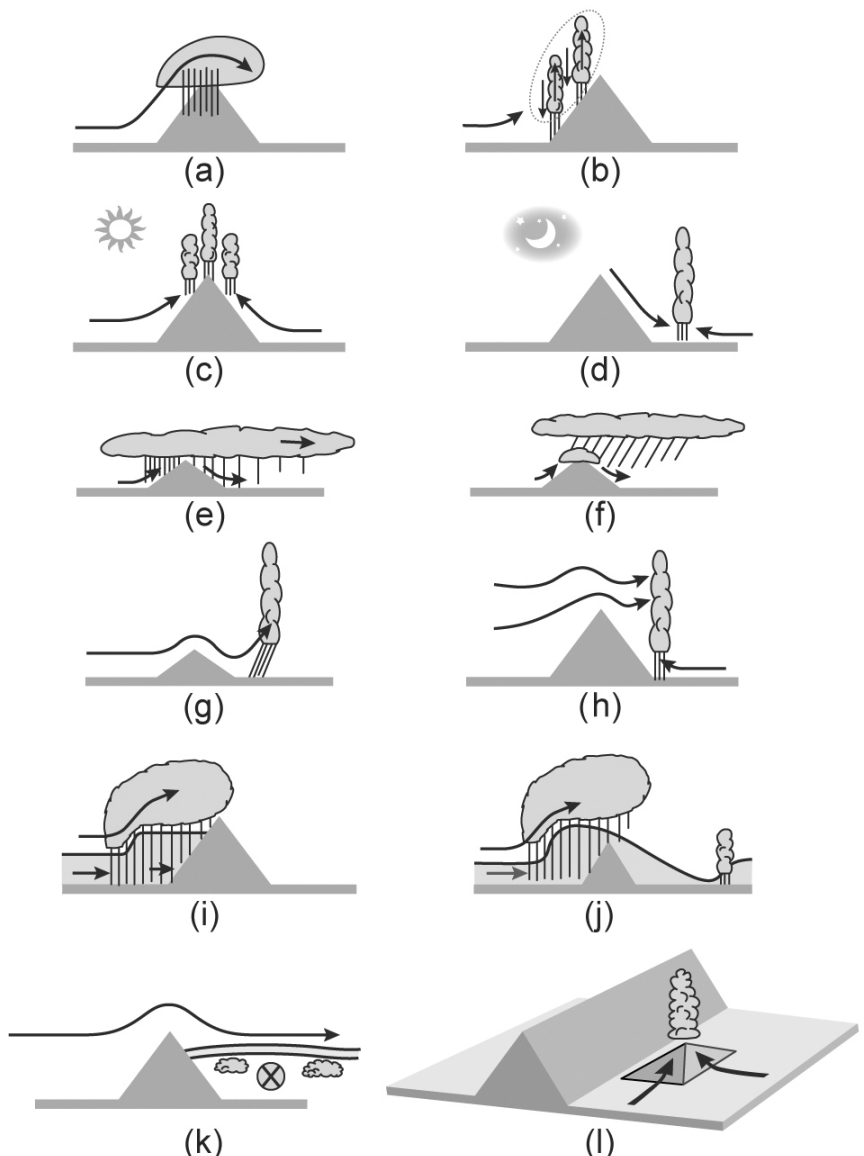


Figure 3. Mechanisms by which mountains and hills affect precipitating clouds.

climatological maximum precipitation over the European Alps occurs midway up the slope. It might be noted in this regard that schemes that automatically make mean climatological precipitation amount proportional to terrain height are likely to be in error in regions of high terrain.

3. BASIC MECHANISMS BY WHICH HILLS AND MOUNTAINS AFFECT PRECIPITATING CLOUDS

[12] From section 2 it is evident that microphysics, dynamics, and thermodynamics of the airflow in the vicinity of a hill or mountain can combine with the geometry of the terrain to affect the growth and fallout of precipitation over a topographic feature. The many degrees of freedom inherent in wind, temperature, humidity, latitude, proximity to ocean, and shape of terrain and the nonlinear nature of the atmosphere make it difficult to identify absolute analogies from

one area of complex terrain to another. However, extensive research in different topographical settings is leading to identification of several recognizable mechanisms, which are summarized schematically in Figure 3, which illustrates schematically various ways that air flowing over and around hills and mountains is known to affect precipitating clouds.

3.1. Upslope Flow, Laminar, and Overturning

[13] Figures 3a and 3b illustrate two scenarios for what may happen if air flows over a terrain feature. These processes apply to terrain features of any size. Figure 3a refers to the case in which the air approaching a barrier is stable and generally follows the terrain upward, and the vertical component of the motion produces or strengthens a cloud on the windward. On the lee side the cloud is evaporated. This effect may occur in isolation, but more commonly it is

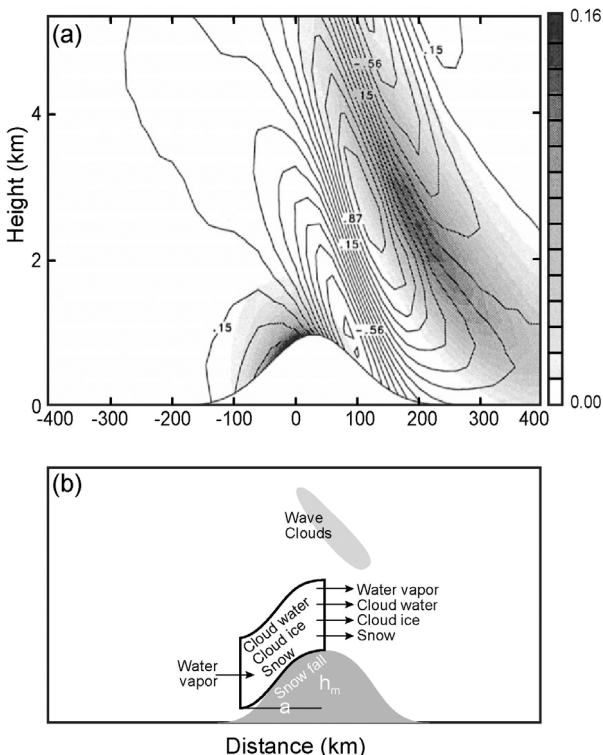


Figure 4. (a) Vertical cross section of model vertical velocity and snow mixing ratio in a steady stable flow from left to right across an idealized mountain barrier. The vertical velocity is contoured at intervals of 0.086 m s^{-1} , and the mixing ratio of snow is shaded at intervals of 0.01 g kg^{-1} . (b) Schematic of the disposition of water species. From *Jiang and Smith [2003]*. Copyright 2003 American Meteorological Society.

embedded within and modifies a larger cloud entity such as might be associated with a frontal system.

[14] Actually, the stable airflow in Figure 3 is not as simple as indicated; rather, the cross-barrier flow of stable air sets off gravity wave motions, e.g., as shown in Figure 4a from idealized model calculations carried out by *Jiang and Smith [2003]*. Two regions of upward motion occur. A layer of relatively simple upslope flow occurs over the windward slope, and a vertically propagating gravity wave occurs on the lee side and over the crest, sloping upward against the cross-barrier airflow, where it may produce cloud aloft. *Jiang and Smith [2003]* showed how the precipitation on the ground is a delicate combination of the gravity wave dynamics and microphysical processes. They used specified time scales of microphysical growth (τ_m), particle fallout (τ_f), and advection (τ_a) by the cross-barrier flow. They found the generation of snow to be controlled by the ratio τ_m/τ_a and the fraction that falls to the ground to be controlled by τ_f/τ_a . Figure 4b illustrates conceptually how these processes lead to the distribution of fallout on the windward and leeward slopes. Figure 1 shows the effect of how growth of particles by riming, which makes larger and heavier particles and shortens the time scale of growth and or fallout, can lead to more precipitation on the windward slope.

Obviously, the geometry of the mountain plays a major role. The higher or wider the mountain, the less likely any of the particles fall out on the lee side, regardless. However, the shorter the microphysical time scale, the lower the precipitation will fall on the windward slope.

[15] Figure 3b refers to the situation in which the air ascending the terrain overturns on a subbarrier scale as it rises. Such overturning may occur in a variety of ways.

[16] 1. A deep layer of very unstable air may be lifted above its level of free convection by the upslope cross-barrier flow, with the result that convective clouds form and precipitate. If the instability is strong and extends through a deep layer, the resulting cumulonimbus may be intense and reach great heights. Figure 5 shows radar data of an intense cumulonimbus cloud that formed over the Mediterranean side of the European Alps when conditionally unstable air rose over the slope of the barrier. The single-Doppler velocities showed convergence at the top of the convective cell (Figure 5b) and hail and/or graupel extending to 10 km (Figure 5c). In other situations, the layer of lifted air may only be slightly unstable but embedded in a larger-scale cloud layer such as a frontal cloud system. *Lin et al. [2001]* found that extremely heavy rainfall is likely to result whenever a layer of air impinging on a steep mountain range is in the form of a moist low-level jet, the terrain is steep, and the parent flow pattern is persistent over a substantial time period. The storm illustrated in Figure 5 occurred when the warm moist jet ahead of a frontal system intersected the European Alps. Intense convection over the upslope terrain can also occur when the intense moist circulation around a tropical cyclone intersects a steep mountain range [*Witcraft et al., 2005*] (see also section 6). *C.-S. Chen et al. [2010]* found that a similar effect accounted for an extreme convective rain event in Taiwan when the circulation around a subsynoptic low was generated on a low-level shear zone and formed a low-level jet of moist unstable air intersecting the Central Mountain Range.

[17] 2. If buoyant instability is contained in a shallower layer at low levels, the lifting over the terrain may trigger a family of small clouds on the windward side of the hill or mountain. Figure 6 shows high-resolution simulated behavior of a layer of moist moderately unstable layer of air approaching a 1 km high barrier [*Kirshbaum and Smith, 2009*]. The layer is located under a trade wind inversion and is meant to represent air flowing over the warm Caribbean Sea over the modest mountains of the island of Dominica. In the case shown, small-scale patches of humid air, or preexisting small cumuli, erupt into a population of small cumulonimbi over the windward slope of the mountain as they are carried over the terrain by the prevailing wind. The moist patches or preexisting clouds gain buoyancy after saturation as they begin to cool moist adiabatically while the surrounding unsaturated air continues to cool dry adiabatically. Once formed, clouds grow more vigorously in the rising layer of air because the bulk lifting weakens the subsidence warming in the unsaturated compensating downdrafts and increases the latent heat release within the updrafts. The raindrops in the clouds grow more

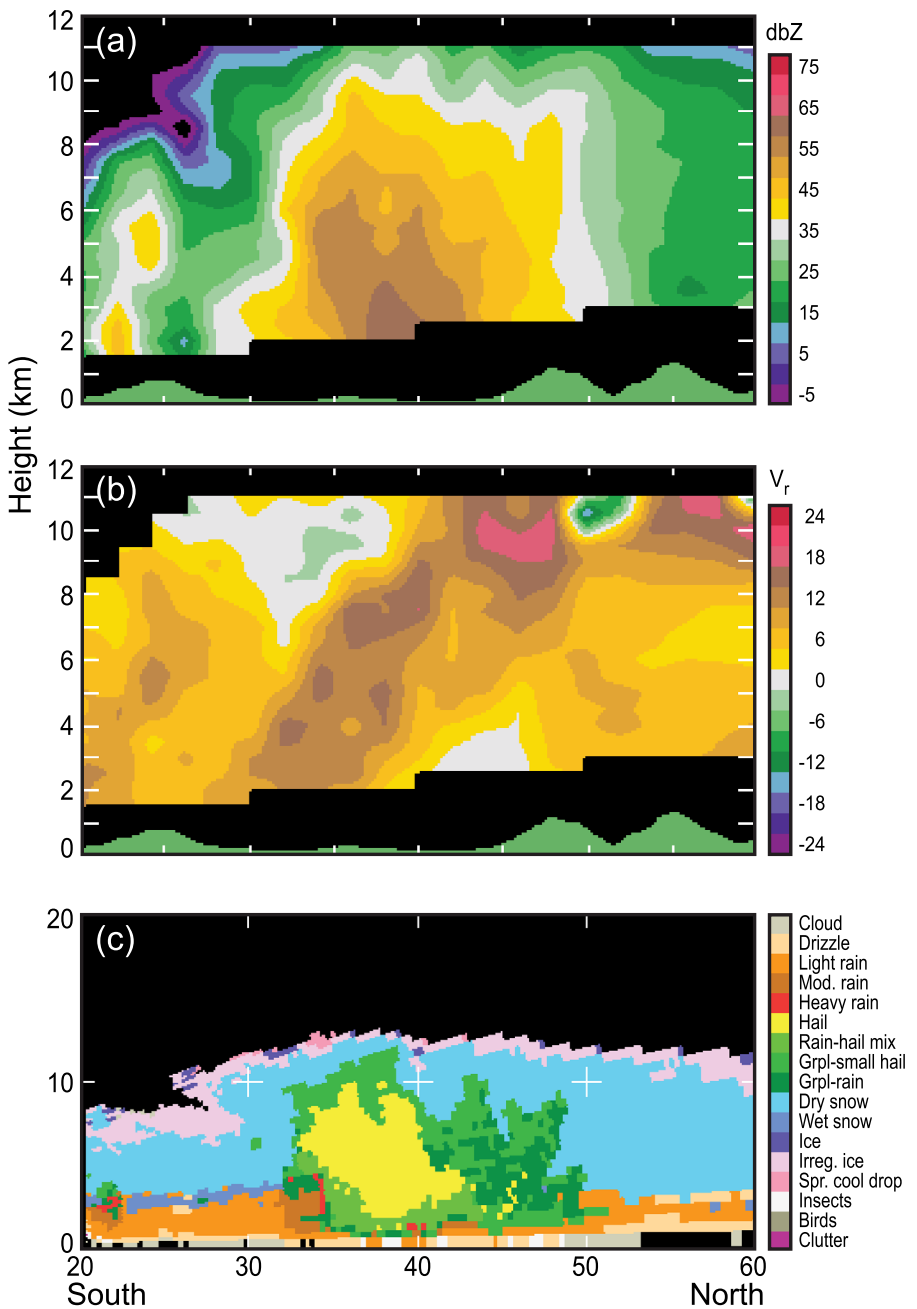


Figure 5. Data obtained during the Mesoscale Alpine Programme (MAP) over the foothills on the Mediterranean side of the Alps 18:30 UT 17 September 1999 by the National Center for Atmospheric Research S-Pol radar: (a) equivalent radar reflectivity (dBZ); (b) Doppler radial velocity (m s^{-1}); (c) particle type inferred from dual-polarimetric radar data. For further description of this storm, refer to the summary at http://www.atmos.washington.edu/gcg/MG/MAP/iop_summ.html and to Seity *et al.* [2003].

vigorously by collection of cloud water since the latter is enhanced by the more buoyant updrafts. In addition, sub-cloud evaporation is minimized as the cloud base lies close to the surface.

[18] 3. If a slightly potentially unstable layer is embedded in a preexisting widespread cloud system, such as a front, or the stratiform region of a mesoscale convective system (MCS [Houze, 2004]), convective cells may be triggered within the preexisting cloud system as it passes over sloping

terrain. The side of a mountain range is usually jagged. Radar observations show that moderately intense convective cells can occur over the upslope side of each peak of terrain [Medina and Houze, 2003; Rotunno and Houze, 2007]. Figure 7 illustrates this behavior schematically. The first sharp rise in terrain activates the cloud processes at the lowest altitudes with the most moisture available, and the cells on the peaks located at the foot of the main barrier are the loci of very robust cells. Cells of lesser intensity can

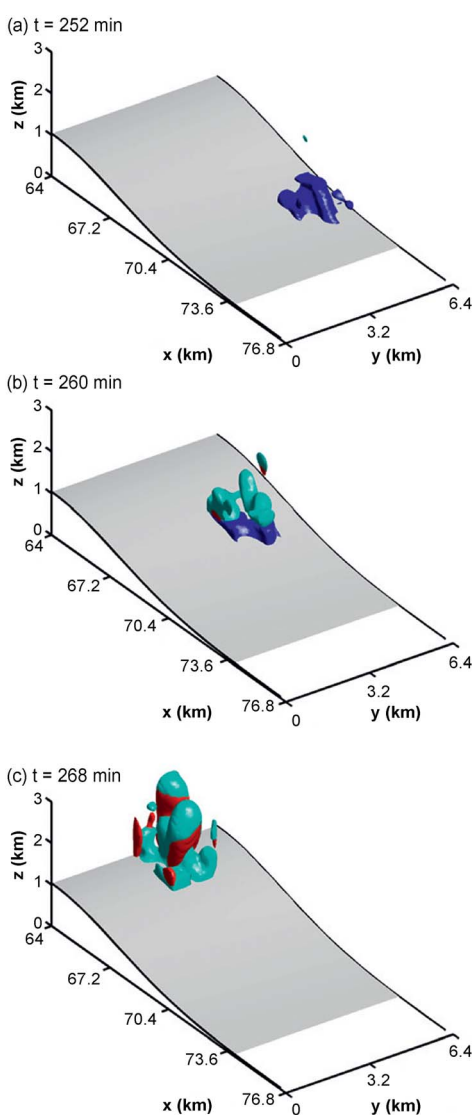


Figure 6. Isosurfaces of perturbation mixing ratios of water vapor (1 g kg^{-1} , blue), cloud liquid water (0.2 g kg^{-1} , cyan), and rainwater (0.02 g kg^{-1} , red) depicting the transition from a moist subcloud anomaly into a precipitating cell. A small moving box of data is shown to isolate a single feature of interest. From Kirshbaum and Smith [2009]. Copyright 2009 American Meteorological Society.

occur on subsequent, higher-elevation peaks. These intermittent convective cells in the upslope flow embedded within the larger-scale cloud system favor strong precipitation particle growth by coalescence below the 0°C level and riming above that level. The locally enhanced upward motion is thought to produce small-scale pockets of higher liquid water content, which in turn is accreted by precipitation particles in the preexisting cloud layer, thus making it locally more productive of precipitation. Observations by polarimetric radar data [Medina and Houze, 2003], triple Doppler radar [Georgis *et al.*, 2003], and microphysical calculations [Yuter and Houze, 2003] support this view.

[19] 4. When a layer of strong shear is present in the air flowing over the terrain, such as in a case where air is blocked or dammed at lower levels and overridden by strong cross barrier flow (Figure 7b), turbulent overturning may occur in association with the shear. This overturning occurs in statically neutral or stable conditions and is due to dynamical instability. Figure 8 illustrates schematically what may occur in that type of situation. As in the case of buoyant convective overturning, updrafts in the shear layer may produce pockets of locally higher liquid water content, which can be readily accreted by precipitation particles in a preexisting cloud layer. Such situations have been observed over both the European Alps and the mountain ranges of the West Coast of North America [Houze and Medina, 2005; Medina *et al.*, 2005, 2007].

3.2. Diurnal Forcing

[20] Figures 3c and 3d indicate how the diurnal heating cycle affects convection over hills and mountains of any scale. Figure 3c indicates the well-understood fact that solar heating of elevated terrain draws air upward to converge at mountaintop, causing air parcels to rise above the level of free convection. The surface heating at the upper level also increases the potential buoyancy of the rising parcels. These effects lead to a maximum of convective precipitation in the warm part of the day. The heating over the high terrain during the day may trigger gravity waves that propagate away from the mountains and trigger deep convective clouds at a distance from the mountain range later in the day [Mapes *et al.*, 2003]. Houze [2004] and Romatschke and Houze [2011a] have speculated that similar diurnally generated wave propagation occurs in response to intense daytime heating over moderately high terrain along the east coast of India, thus explaining the strongly diurnal propagation of MCSs southward over the Bay of Bengal during the premonsoon season, as described by Webster *et al.* [2002, Figure 4] and Zuidema [2003, Figure 12].

[21] Figure 3d illustrates schematically how nighttime cooling over the higher terrain suppresses convection at mountaintop. However, if the downslope motion resulting from the cooling at night converges with a low-level moist unstable air current, then a nocturnal maximum of precipitating convection may occur at the base of the mountain. Another way a nocturnal maximum of convection can occur at lower elevations near but away from the mountain is if a propagating wave response to the daytime heating at mountaintop occurs such that the upward motion phase of the wave moves away from the mountain. In that case, nocturnal convection again is triggered near the base of the mountain but in addition may become long lasting and propagate away from the mountain in a synergistic relationship with the wave.

3.3. Cloud Layers Moving Over Small Terrain Features and the “Seeder-Feeder” Mechanism

[22] Figures 3e and 3f refer to a small terrain feature: a hill or small mountain. In Figure 3e, a preexisting cloud passing over a hill or small mountain is enhanced to produce a

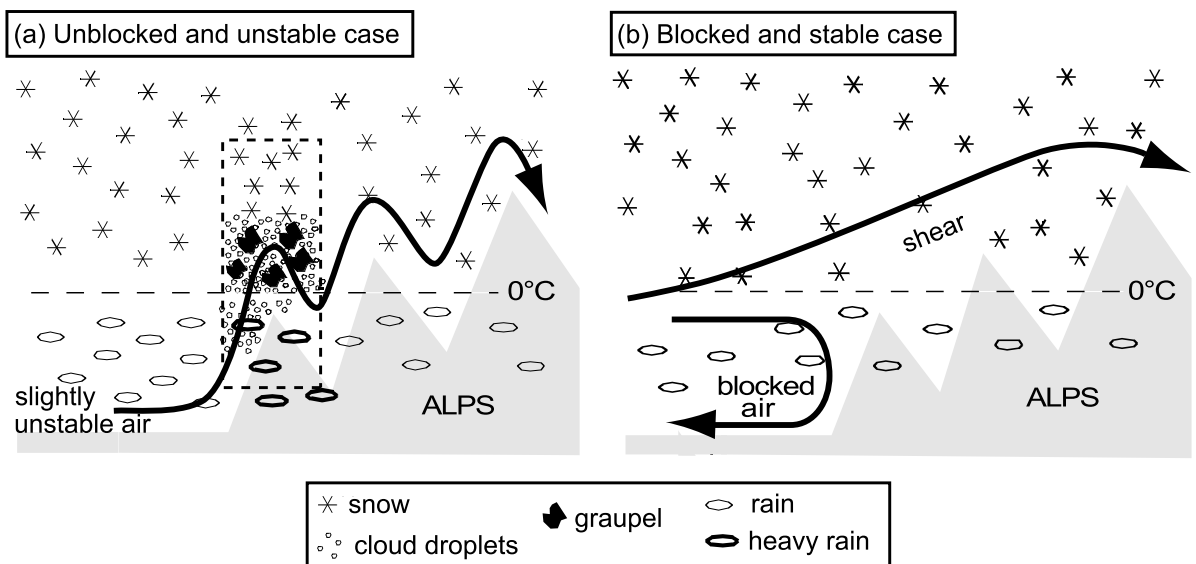


Figure 7. Conceptual model of the airflow and microphysics of orographic precipitation mechanisms in MAP cases of (a) unstable unblocked low-level flow and (b) stable blocked low-level flow. Adapted from Medina and Houze [2003]. Reprinted with permission from John Wiley.

maximum of precipitation on the upwind side of the barrier, but the hill is low enough in altitude that the precipitating cloud is advected over to the lee side, where its precipitating capacity is weakened by the downslope air motion. In contrast to Figure 3a, the hill is small enough that the precipitating cloud is advected over the hilltop and is not evaporated by lee side downslope flow. Figure 9 [from Browning *et al.*, 1974] illustrates a case in which preexisting clouds passing over a 300 m hill in Wales produced enhanced rainfall directly over the hill and streamers of rain downwind of the hill. Figure 3f illustrates a somewhat similar situation, but one in which the process occurs in vertically separated layers. A preexisting precipitating cloud

is being advected over the hill at an elevated level, while directly over the hill a shallow orographic cloud forms in the low-level upslope flow. The precipitation particles from the upper cloud grow by accretion of cloud water in the lower cloud, thus enhancing precipitation on the windward side of the mountain. Bergeron [1965] identified this layered process in investigation of rainfall over small hills in Sweden, and he called the upper cloud the “seeder” cloud and the lower cloud the “feeder” cloud. Passarelli and Boehme [1983] enhancement of precipitation over small hills in the New England region of the United States during warm frontal conditions was consistent with the Bergeron’s seeder-feeder mechanism.

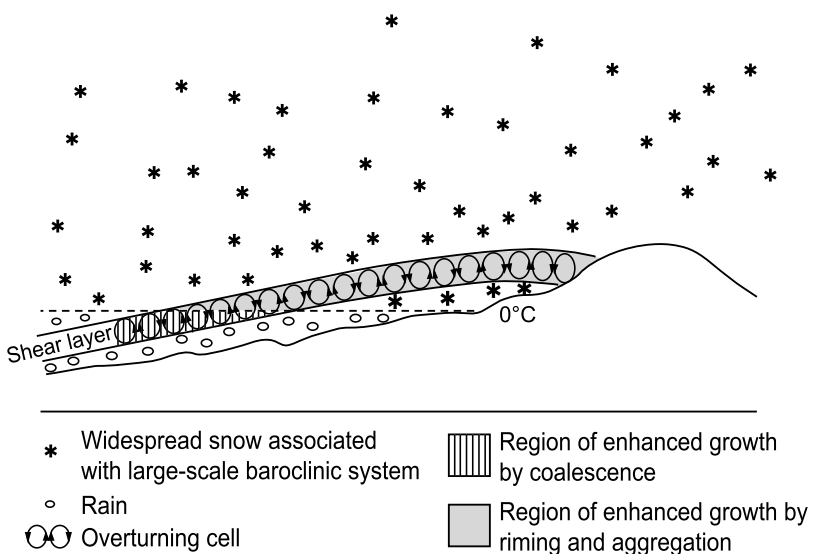


Figure 8. Conceptual model of the dynamical and microphysical mechanisms responsible for the orographic enhancement of precipitation during storms with stable stratification. From Houze and Medina [2005]. Copyright 2005 American Meteorological Society.

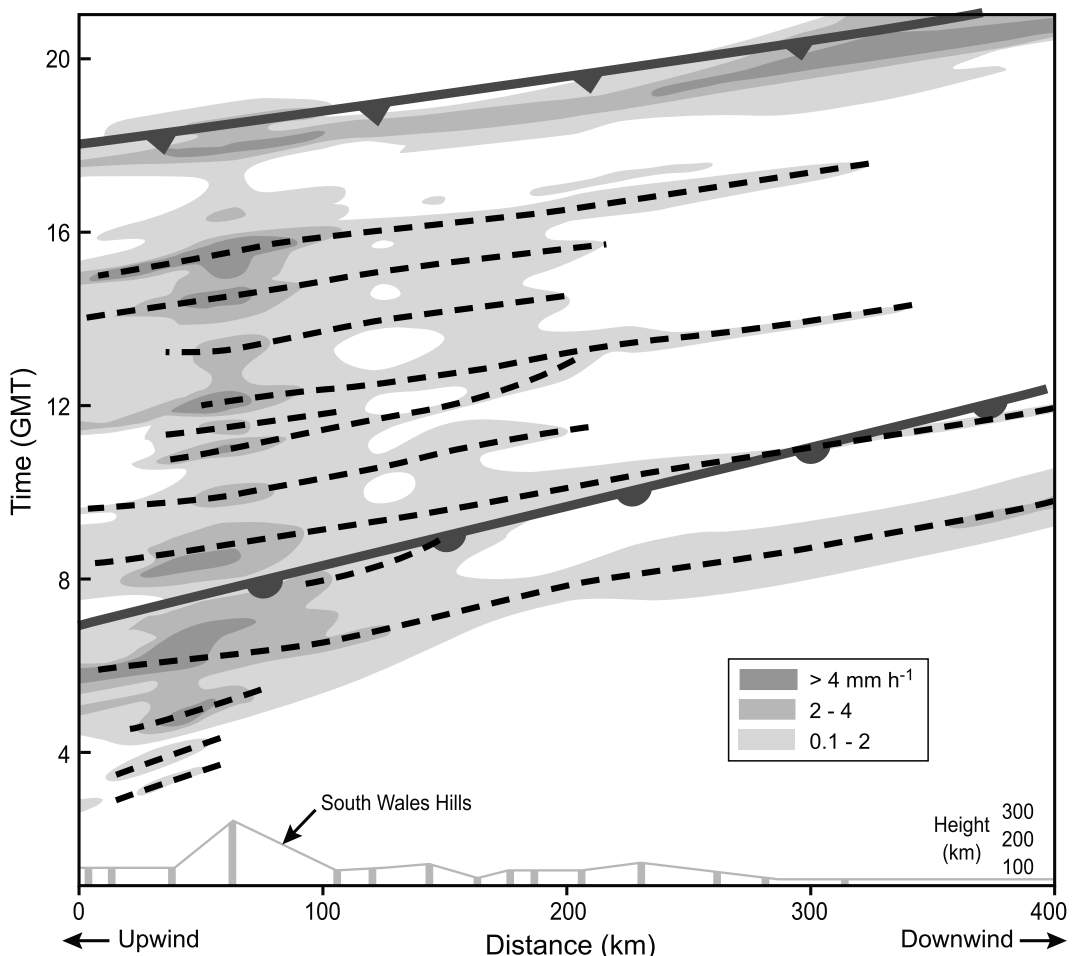


Figure 9. Time-distance diagram showing the rainfall rates (mm h^{-1}) and the movement of mesoscale precipitation areas over the hills of South Wales. The rainfall begins ahead of the cold front and continues in the warm sector. The rainfall rate over the hills is continuous but variable and closely associated with the passage of convective clouds aloft. Adapted from Smith [1979] after Browning *et al.* [1974]. Reprinted with permission from John Wiley.

3.4. Convection Associated With Wave Motions in the Wake of a Hill

[23] Figure 3g indicates how lee waves generated by a hill or small mountain may lead to a series of small convective clouds downstream of the hill. Figure 10, based on observations and high-resolution modeling, further illustrates that if the terrain in the lee of the hill has a general upward slope and other environmental conditions are met, the lee wave upward motion may trigger persistent precipitating convective clouds advected downwind to produce leeward side rainbands parallel to the flow over the hill [Kirshbaum *et al.*, 2007].

[24] Figure 3h indicates a situation in which vertically propagating wave motion initiated over high mountains induces wave motions tilting upward and upstream. On the lee side of the mountain, the upward motion phase of the propagating wave favors and/or interacts with precipitating convective cloud systems fed by low-level moist flow. Such waves may be triggered by diurnal heating over the mountainous terrain [Mapes *et al.*, 2003] or by gravity wave motions induced by the airflow over the terrain [Tripoli and Cotton, 1989].

3.5. Blocking Effects on Precipitation

[25] When the air upstream of a mountain barrier is especially stable or has a weak cross-barrier flow component, the air is dammed or blocked, i.e., it does not rise over the terrain (see Houze [1993, pp. 512–520] for a discussion of the nonlinear dynamics of blocking). Figure 3i is a simplified illustration of blocking. When air flowing toward a terrain barrier is sufficiently slow moving and/or statically stable (i.e., low Froude number), the air does not easily rise over the terrain. In the case of a 2-D barrier (extending infinitely into and out of the page of Figure 3i), the stable or slow moving air tends to pile up like water behind a dam instead of rising over the terrain. One result is that the mountain range is effectively moved upstream so that air above the blocked layer is lifted well ahead of the mountain barrier. This kind of blocking can affect both convective storms and frontal systems. Reeves and Lin [2007] found that propagating mesoscale convective systems can stall at the edge of a blocked layer in front of a mountain range. Houze *et al.* [2001] found that frontal systems passing over the European Alps have a climatological precipitation radar

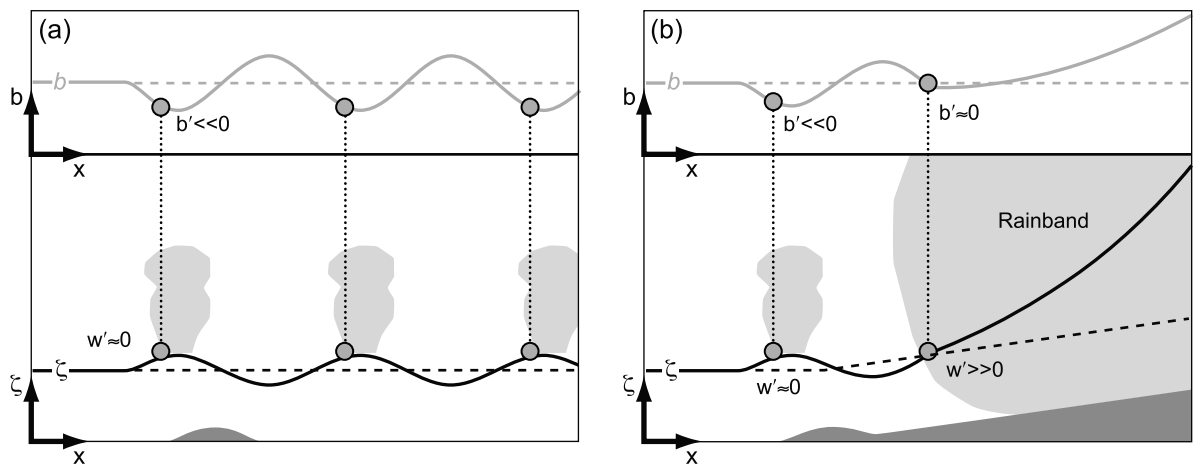


Figure 10. Schematic of the differences in cloud formation between (a) nonsloping and (b) upward-sloping terrain in marginally conditionally unstable flow over a small-scale hill. From Kirshbaum *et al.* [2007]. Copyright 2007 American Meteorological Society.

echo maximum over the Po Valley upstream of the mountain range in low Froude number flow patterns. Since unsaturated air behaves with dry static stability, the airstream approaching a mountain range is more likely to be blocked. Rotunno and Ferretti [2001] and Reeves *et al.* [2008] show how different patterns of humidity in the airflow ahead of fronts affect the degree to which the air is decelerated and turns, or does not, as it approaches a barrier. Reeves and Rotunno [2008] show that even if the air is saturated, cooling by melting of precipitation particles can increase stability and decelerate flow toward a mountain range.

[26] Sometimes the blocking is partial, as shown in Figure 3j, with a lee side supercritical flow accelerating down the mountain, and the return to equilibrium in the form of a hydraulic jump may produce a precipitating cloud downstream of the barrier. Frame and Markowski [2006] found that the cold pool of a squall line system passing over a relatively low mountain range can undergo this effect, producing a leeward side regeneration of the squall line at the location of the hydraulic jump (Figure 11). Studying conditions in the Sierra Madre in Mexico, Bhushan and Barros [2007] showed how a hydraulic jump associated with synoptic-scale flow over a region of larger mountains can produce a line of moisture convergence and trigger convection in a valley.

3.6. Capping and Triggering of Intense Deep Convection

[27] Figures 3k and 3l refer to the occurrence of very severe convection near major mountain barriers, especially the Rockies, Andes, and Himalayas. Figure 3k indicates downslope flow on the lee side producing a capping inversion and layer of dry air that allows potential instability to build up by the accumulation of sensible and latent heating below the cap. Extremely intense cumulonimbus can result when the cap is broken and deep convection erupts [Carlson *et al.*, 1983; Houze *et al.*, 2007a; Medina *et al.*, 2010; Rasmussen and Houze, 2011]. Figure 3l illustrates one important way that the instability built up in the boundary

layer can be released: by the low-level warm moist air encountering and rising over a foothill ahead of the main barrier, which may be enough to allow parcels to rise past their levels of free convection. In other cases, the cap may be broken by convergence at a front, outflow boundary, or dry line.

4. CONVECTIVE PRECIPITATION AND OROGRAPHY

[28] This section and sections 5 and 6 will address how the processes represented in simplified form in Figure 3 affect preexisting precipitating cloud systems of all the

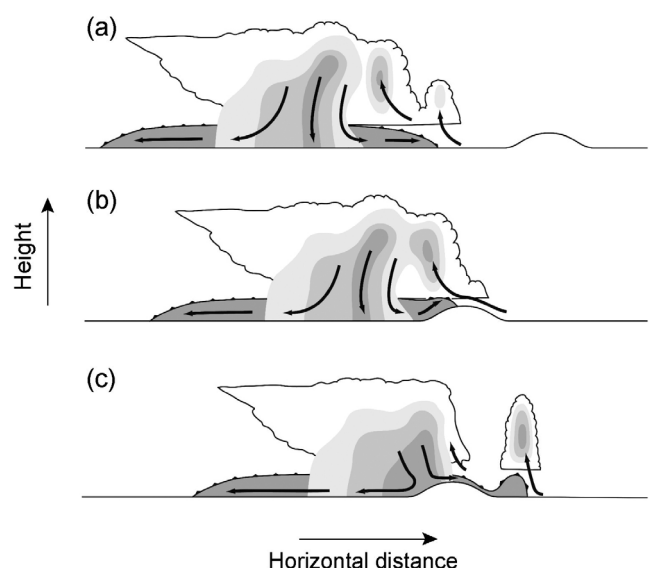


Figure 11. Schematic of a squall line passing over a terrain barrier. The downdraft cold pool is partially blocked by the ridge. A hydraulic jump exists at the bottom of the slope, resulting in enhanced lift at the gust front and the generation of a new convective line as the original line weakens. From Frame and Markowski [2006]. Copyright 2006 American Meteorological Society.

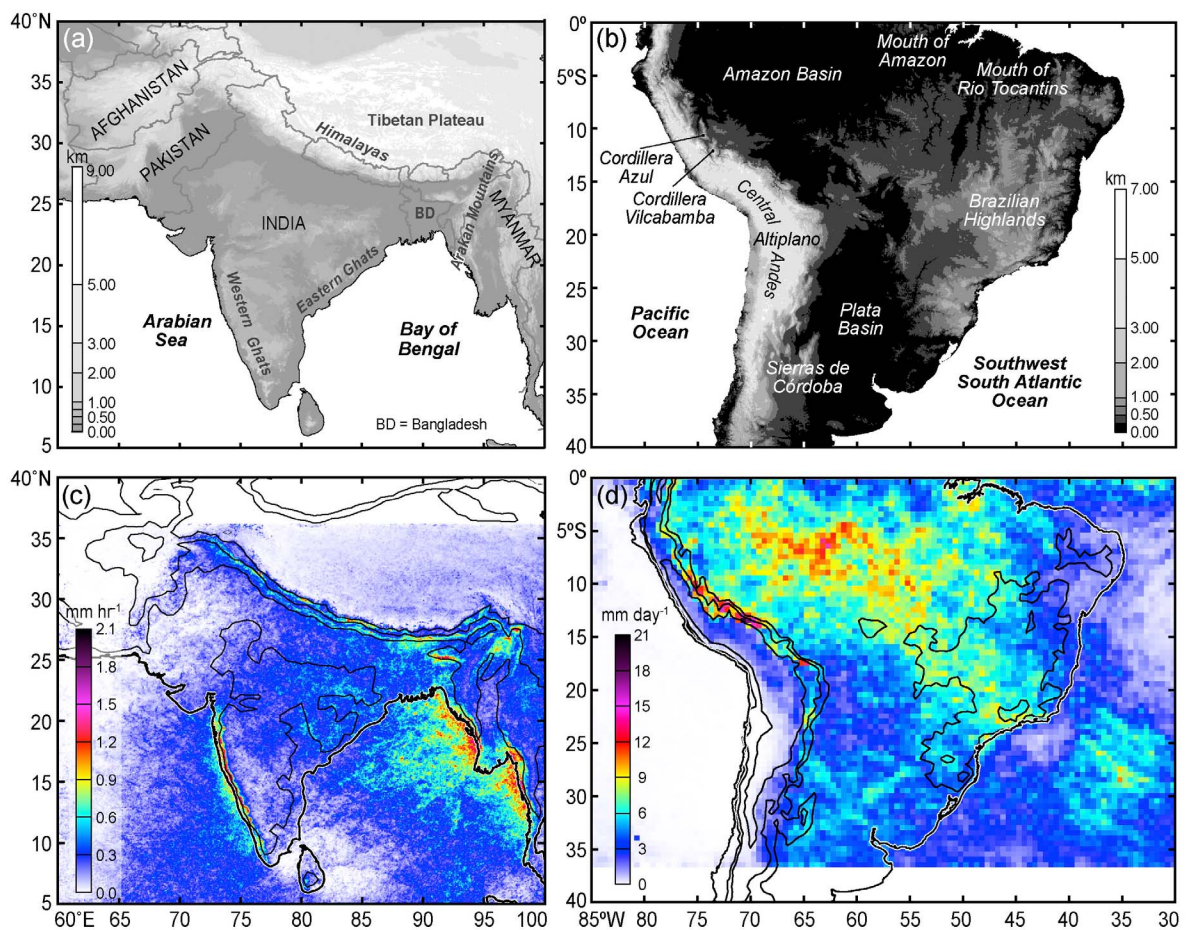


Figure 12. Geography of (a) South Asia and (b) South America. (c and d) Tropical Rainfall Measuring Mission (TRMM) summertime rainfall climatology of both regions based on 8 and 10 years, respectively, of TRMM data. From Romatschke *et al.* [2010] and Romatschke and Houze [2011a, 2011b]. Copyright 2010, 2011 American Meteorological Society.

major types: deep convection, frontal systems, and tropical cyclones. In this section, we consider orographic effects on deep convective precipitation systems.

4.1. Extreme Convective Event Distribution

[29] Deep convective events can produce extreme local rainfall and flooding when they occur near mountain ranges. When warm, moist air from the Gulf of Mexico encounters the Rocky Mountains, quasi-stationary deep convection with highly efficient warm-rain coalescence processes producing efficient fallout of rain can produce sudden torrential rain and flash floods [e.g., Caracena *et al.*, 1979]. When warm, humid air from the Mediterranean Sea encounters the European Alps or French Central Massif, deep convection triggered directly or indirectly by the mountains leads to rainfalls of several hundred millimeters in 1–2 days [e.g., Nuissier *et al.*, 2008; Ducrocq *et al.*, 2008]. In Taiwan, extreme convective rainfall and flooding events occur in association with mesoscale convective systems that are affected by the presence of the Central Mountain range [e.g., G. T.-J. Chen *et al.*, 2003, 2005; C.-S. Chen *et al.*, 2004, 2005, 2010, 2011; Chang *et al.*, 2008; Kerns *et al.*, 2010].

In these areas, the convective events near mountains have been investigated primarily in case study mode.

[30] Recently, specialized satellite data have made it possible to study extreme convective precipitation events near mountains from a climatological perspective. A key instrument on board the Tropical Rainfall Measuring Mission (TRMM) satellite launched in 1997 is a scanning Precipitation Radar (PR) with a 2 cm wavelength [Kummerow *et al.*, 1998, 2000]. TRMM operates in an orbital pattern in which the nadir view ranges over the latitude belt of 35°N–35°S and the PR swath sampling reaches to about 37° latitude [Negri *et al.*, 2002; Romatschke *et al.*, 2010]. This geographical coverage allows for mapping the climatological frequency of occurrence of precipitating convective systems in the vicinity of the Earth's two greatest mountain ranges, the Himalayas and Andes [Barros *et al.*, 2004; Hirose and Nakamura, 2005; Kodama *et al.*, 2005; Xie *et al.*, 2006; Zipser *et al.*, 2006; Houze *et al.*, 2007a; Romatschke *et al.*, 2010; Romatschke and Houze, 2010, 2011a, 2011b]. Figure 12 shows the topography in the regions of the Himalayas and Andes covered by the TRMM satellite and the average rain rates detected by the PR.

The patterns shown are for the monsoon season in the Himalayan region (June–September) and for summertime in southern South American (December–February). For the purposes of this review, these rainfall patterns based on TRMM should be regarded as semiquantitative. Even though they are based on 8–10 years of data, the interannual variability of precipitation in these regions is significant. *Barros et al.* [2006] point out that ~20%–30% of a season's rain over the central Himalayas can come from a specific synoptic-scale event. Moreover, the TRMM PR does not obtain measurements down to the Earth's surface over mountainous terrain, and it does not resolve patterns over small-scale ridges and valleys. Nevertheless, the patterns in Figure 12 are a reasonable approximation and give a sense of the importance of different regimes. Our goal here is to use the TRMM PR's capacity to show the detailed structure of radar echoes to indicate the types of precipitation processes at work in the different regimes.

[31] The horizontal and vertical structures of radar echoes carry a wealth of information indicative of the dynamical and microphysical processes operating to produce the precipitation seen by the radar. Since the TRMM PR detects the 3-D structure of the radar echoes in high resolution (4–5 km horizontal resolution and 250 m nadir vertical resolution), it is possible to identify contiguous echo objects and hence to determine characteristics of the phenomena contributing to the mean rainfall shown in Figures 12c and 12d. In order to identify the most extreme types of convective phenomena contributing to these rainfall patterns, *Houze et al.* [2007a], *Romatschke et al.* [2010], and *Romatschke and Houze* [2010] identified contiguous 3-D echo objects contained within a 40 dBZ radar reflectivity surface. They defined three categories of extreme echo types: "deep convective cores" (contiguous 3-D convective echo >40 dBZ extending to >10 km in height), representing the most vertically penetrative convection; "wide convective cores" (contiguous convective echo >40 dBZ over a horizontal area >1000 km²), indicating wide regions of intense multicellular convection; and "broad stratiform regions" (stratiform echo contiguous over an area >50,000 km²) marking MCSs that have developed especially robust stratiform regions.

[32] Figure 13 shows the climatological distributions of the frequency of occurrence of each of these three manifestations of extreme convective systems over South Asia during the monsoon season and over South America during summer. Each category exhibits a pattern of occurrence distinct from the other two categories. Figures 13a and 13b show that radar echoes exhibiting deep convective cores almost never occur over oceans, and they are most frequent in relatively arid regions near mountains (compare Figures 12c and 12d). *Zipser et al.* [2006] also pointed out that the deepest convective towers seen by TRMM occur in relatively arid regions. In the Himalayan case, echoes are most frequent in the indentation of the high terrain, where the far western end of the Himalayas intersects the Afghan Plateau. This lowland region between the two ranges is a desert and centered on Pakistan. In South America, the

echoes with deep convective cores are most frequent on the eastern edge of the Andes in southern South America, mainly Argentina, which though not a desert is nonetheless a region of low rainfall compared to other parts of South America.

[33] The deep convective core echo objects may occur either as isolated convective towers or embedded in wider MCSs. To capture the behavior of the most extreme of the horizontally more expansive MCSs, *Houze et al.* [2007a], *Romatschke et al.* [2010], and *Romatschke and Houze* [2010] analyzed the frequency of occurrence of echoes with wide convective cores. Figures 13c and 13d show that the frequency of occurrence of systems containing wide convective cores (which may or may not contain deep convective cores) overlaps with the locations where deep convective cores occur, but the systems with wide convective cores occur in other areas as well. They have fairly high concentrations over the oceans, indicating that mesoscale organization of convection occurs over oceans, but generally without the deep intense cores that can occur over land (compare Figures 13a–13d). Figure 13c further shows that systems with wide convective cores occur frequently all along the edge of the Himalayas. We will see below that these systems develop at night, likely in connection with strong nocturnal downslope flow converging with monsoonal flow at the base of the mountain range.

[34] Close examination of the patterns of occurrence of systems in the Andean region in Figure 13 shows the centroid of maximum frequency of occurrence of systems with wide convective cores (Figure 13d, ~31°S, 60°W) slightly east of the centroid of the maximum frequency of occurrence of systems with deep convective cores (Figure 13b, ~30°S, 62°W). Furthermore, the centroid of maximum frequency of occurrence of broad stratiform region echoes occurs still farther to the east (Figure 13f, ~30°S, 58°W). These statistical locations suggest a systematic evolution of orogenic convective systems evolving as they move eastward. According to previous studies [e.g., *Houze*, 1982, 1989, 1993, 1997, 2004], the convective systems would be expected to first grow upscale into mesoscale convective systems with wide regions of intense convection and then into mature systems with broad stratiform regions. In the region of Argentina east of the Andes, the prevailing midlevel westerlies would favor eastward movement of orogenically triggered systems so that these stages of development should tend to be found at successively more eastward locations.

[35] In both the South Asian and South American sectors, the maximum rainfall (Figures 12c and 12d) coincides closely with the occurrence of precipitating cloud systems containing broad stratiform regions (Figures 13e and 13f), while the maximum rainfall regions do not overlap much at all with the occurrence of systems with deep convective cores. The climatology of the three categories of extreme radar echo structure identified over South Asia and South America thus suggests that MCSs containing substantial stratiform rain areas are more responsible for producing large amounts of rain over time than are systems with

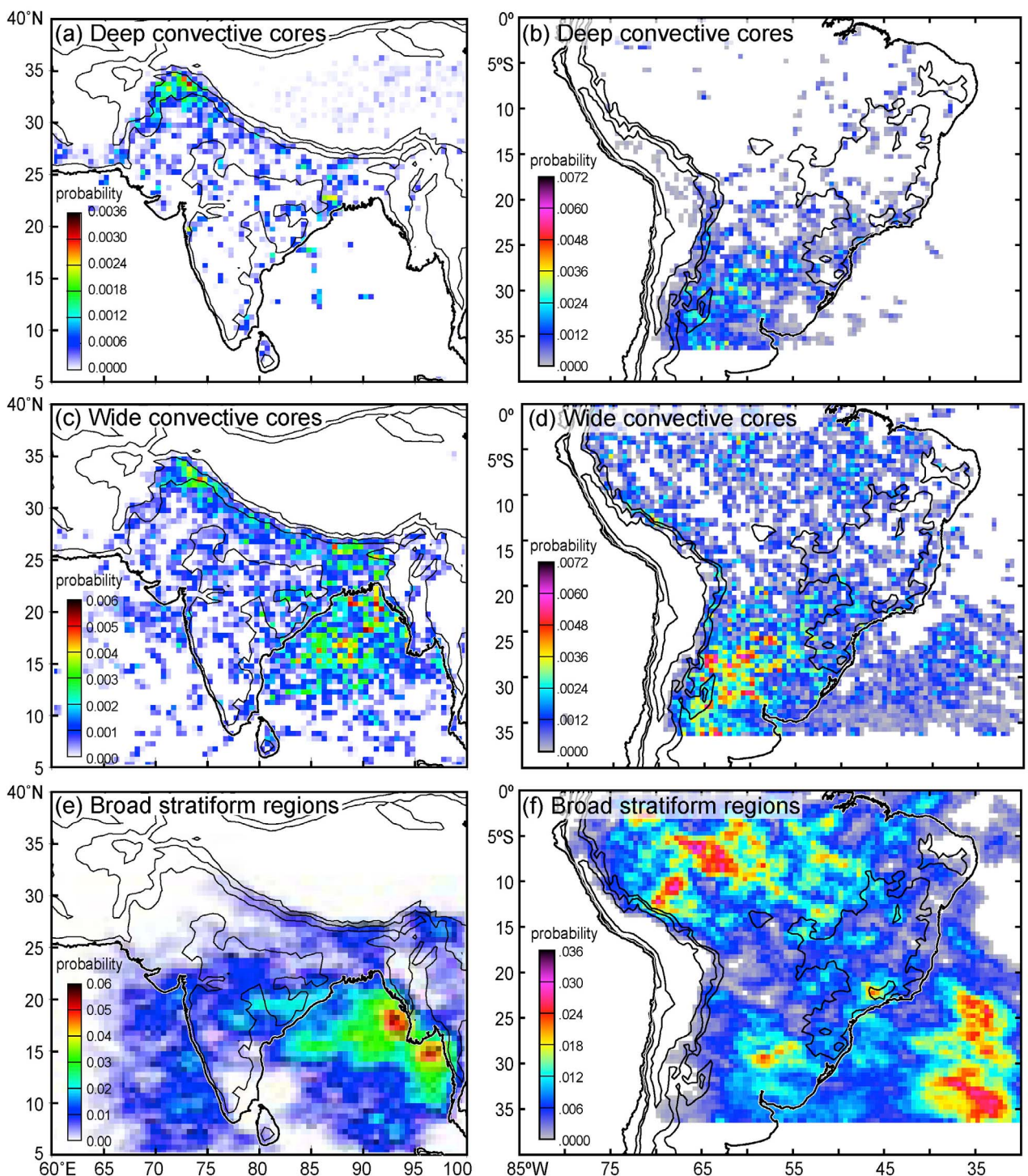


Figure 13. Geographical distribution of the probability that the TRMM Precipitation Radar will see an echo classified as a deep convective core, a wide convective core, or a broad stratiform region during the (left) Asian summer monsoon and (right) South American summer. The Asian summer monsoon (South American summer) consists of the months June–September (December–February). Topographic contours of 0.3, 1.5, and 3 km are shown in black. Note the different color scales. From Romatschke *et al.* [2010] and Romatschke and Houze [2010]. Copyright 2010 American Meteorological Society.

especially intense deep convective cores. When mesoscale systems with broad stratiform regions do rarely occur in an arid mountainous region, disastrous flooding can occur, as happened in Pakistan in 2010 [Houze *et al.*, 2011].

[36] In the South Asian sector, where both the climatological maximum of rainfall and the maximum frequency of occurrence of MCSs with broad stratiform regions occur over the Bay of Bengal and, to a lesser degree, over the

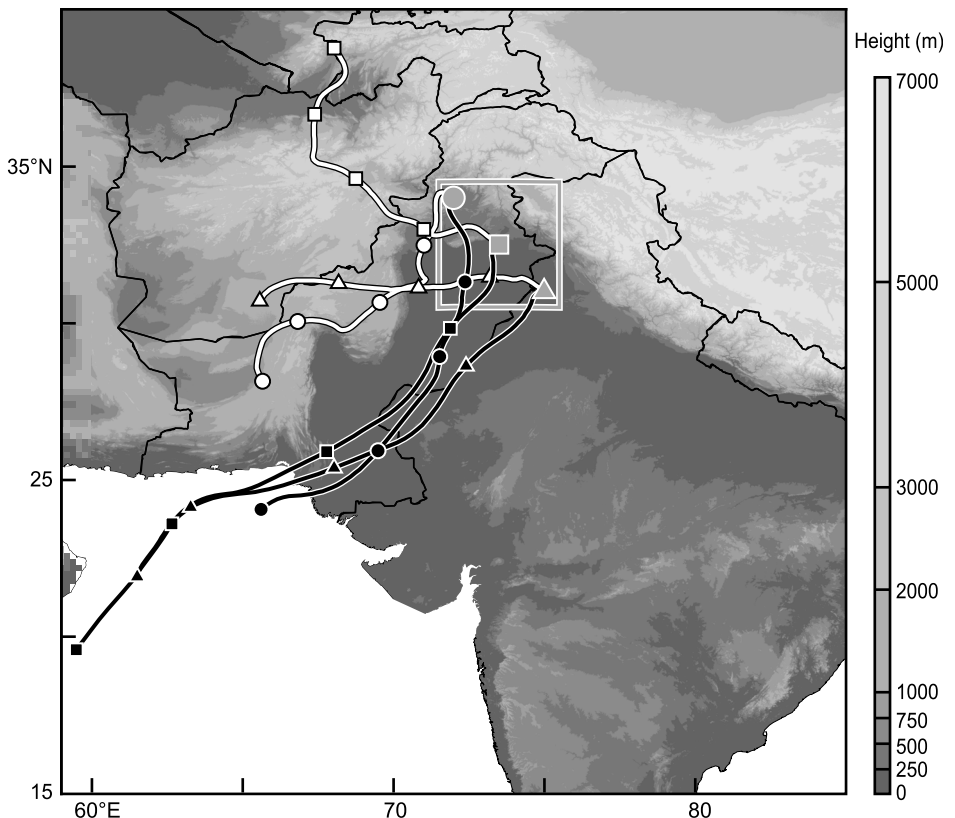


Figure 14. Backward trajectories coinciding with the occurrence of a system containing intense convective echoes. Trajectories for parcels reaching the locations indicated by the gray symbols at 18:00 UTC 3 September 2003 at 3.0 km (1.0 km) above ground level are shown in white (black). The circle, square, and triangle markers are used to identify each trajectory. The time elapsed between markers is 24 h. The box encloses the region in which convective initiation occurred. *From Medina et al. [2010]. Reprinted with permission from John Wiley.*

Arabian Sea (Figures 12c and 13e), the MCSs producing the rain are favored by the presence of a synoptic-scale Bay of Bengal monsoon depression [Koteswaram and George, 1958; Krishnamurti et al., 1975; Shukla, 1978; Das, 1987; Johnson and Houze, 1987; Houze and Churchill, 1987; Saha and Saha, 1988; Lang and Barros, 2002; Barros et al., 2006; Houze et al., 2007a; Romatschke et al., 2010; Romatschke and Houze, 2011b]. Houze and Churchill [1987] examined aircraft radar and microphysical observations from the Summer Monsoon Experiment (MONEX) of 1979 [Fein and Kuettner, 1980] and showed that the precipitation occurring in a Bay of Bengal depression was indeed located within MCSs with large stratiform precipitation regions. These systems with broad stratiform regions appear further to be susceptible to orographic enhancement when they move ashore, explaining the increased frequency of occurrence of broad stratiform radar echo toward the mountain ranges of India (Western Ghats) and Burma (Arakan Range) (Figure 13e). Medina et al. [2010] simulated a Bay of Bengal precipitation situation and showed that the stratiform precipitation regions of MCSs were strengthened when the MCSs moved inland over the mountain ranges. Houze et al. [2011] showed that the devastating

floods of Pakistan in 2010 were produced when a Bay of Bengal depression was displaced far westward and broad stratiform regions of MCSs forming in the environment of the depression became situated in upslope flow over the Himalayan terrain.

4.2. Capping and Triggering

[37] It is well known that severe convective storms occur over the United States east of the Rocky Mountains when low-level flow from the Gulf of Mexico is capped by downslope dry flow originating over the Mexican Plateau [see, e.g., Carlson et al., 1983]. The capping prevents release of the potential instability until the cap is removed by some local lifting mechanism. In the U.S. case, the cap is often removed by a mesoscale atmospheric convergent feature such as a front or dry line. Capping and triggering are also key processes near the Himalayas and Andes, in the regions where precipitating cloud systems with deep convective cores concentrate—in the Pakistan region near the western end of the Himalayas (Figure 13a) and in western Argentina just east of the Andes (Figure 13b). However, the exact nature of the capping and triggering in these three regions varies.

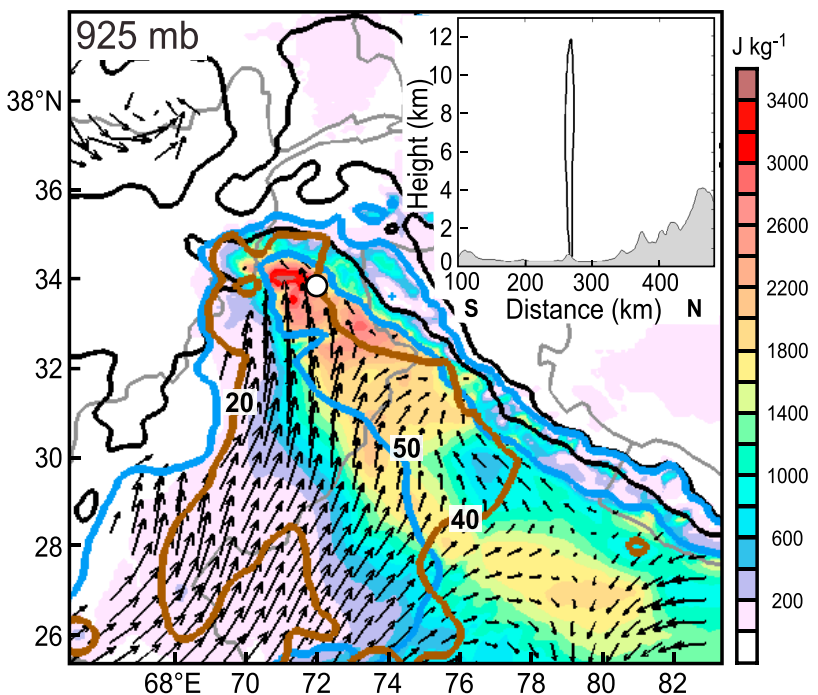


Figure 15. Model simulation of a system containing intense convective echoes at 18:00 UTC 3 September 2003: precipitable water (mm, blue contours), convective inhibition (CIN) (brown contour), convective available potential energy (color shading), and 925 hPa wind vectors. The black contours show slightly smoothed 2 and 4 km mean sea level (msl) smoothed terrain isolines. The white circle marks the location where convection eventually initiated. Inset shows a vertical cross section of model mixing ratio of precipitating hydrometeors (black contour, 1 g kg^{-1} isoline) along a south-north-oriented line crossing the location of initiation over a foothill (white circle) at the time convection was initiated (19:00 UTC 3 September 2003). The underlying terrain is shown by the grey shading in the cross section. From Medina *et al.* [2010]. Reprinted with permission from John Wiley.

[38] Figure 14 presents an example of the capping in the Himalayan region. There the low-level moist flow comes from the Arabian Sea (similar to the Gulf of Mexico in the U.S. case) and is capped by a deep layer of large-scale flow, part of which comes downslope off the Afghan Plateau (similar to flow off the Mexican Plateau in the U.S. case). As in the United States, a dry line bounds the western edge of the moist flow [Weston, 1972; Chiao and Barros, 2007]. Unlike the U.S. case, however, the triggering and release of the instability that builds up is not due to a mesoscale atmospheric feature but rather appears to be orographic. Figure 15 shows a simulation of the triggering that released the instability preserved by the capping seen in Figure 14. Low-level flow from the southeast underneath the cap increased its equivalent potential temperature first by surface sensible heating as the moist wind flowed over the desert region lying between the Himalayas and the Arabian Sea and later by surface latent heating when the air moved farther toward the Himalayas. The latter surface heating was likely associated with evapotranspiration from soil moistened by earlier precipitation systems. The convective available potential energy (CAPE) was maximum near the intersection of the Himalayas and the Afghan Plateau. In that region, the flow encountered a small foothill at the location of the white circle in Figure 14. Lifting of the flow over that hill was sufficient to produce the initial cloud

(Figure 15 inset) that blossomed into the MCS containing a wide convective echo core.

[39] In the region where deep convective cores form over Argentina, adjacent to the Andes, low-level moist flow arrives not from an ocean (as in the U.S. and the Himalayan region) but rather from the Amazon Basin. The flow is channeled southward by the Andes and is referred to as the South American Low-level Jet (SALLJ [see Nogués-Paegle and Mo, 1997; Saulo *et al.*, 2000; Vera *et al.*, 2006; Marengo *et al.*, 2004]). Rasmussen and Houze [2011] showed that this southward flow adjacent to the Andes range is capped by lee side downward motions in the mid-level westerlies crossing the mountain range (Figure 16a). When the SALLJ reaches the region of the Sierras de Córdoba (the smaller mountain range, just east of the Andes, at 32°S, 65°W in Figure 16b), the moist cap can be broken and the instability is released in the form of convective clouds with deep convective cores.

[40] To summarize, capping is produced by downslope flow from broad plateau regions to the west in the U.S. and Himalayan severe storm regions and by lee side subsidence of westerly winds crossing the narrow central Andean ridge. Triggering tends to be produced by mesoscale dynamical processes in the U.S. case but by orographic lifting over foothill terrain in the cases of the Himalayas and Andes. The occurrence of the intense convection over lower terrain is,

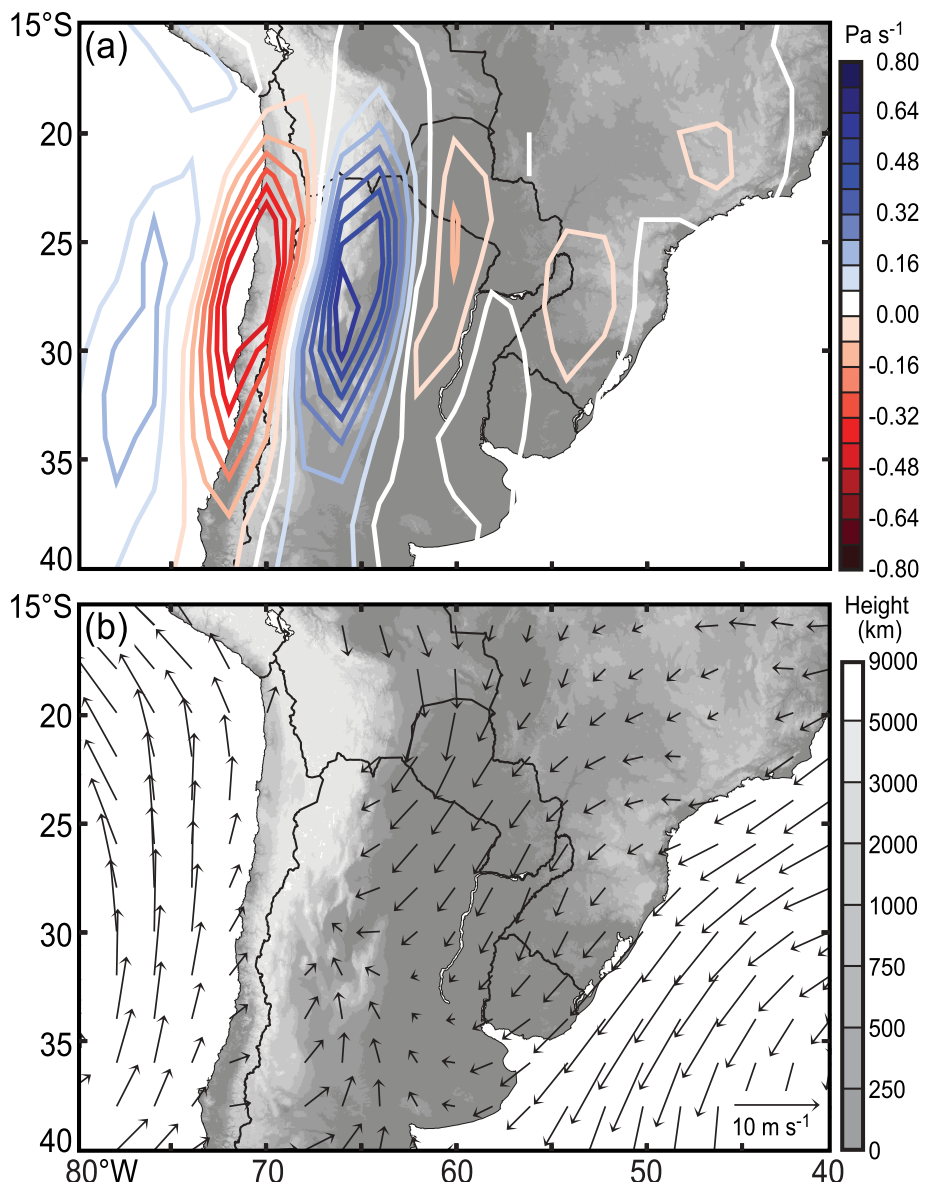


Figure 16. Climatological composite maps for days on which the TRMM Precipitation Radar showed storms containing wide convective cores over Argentina just east of the Andes. (a) Vertical motion (Pa s^{-1}) contours at 700 hPa. Negative values (red contours) indicate upward motion and positive values (blue contours) indicate downward motion. (b) Composite wind vectors at 1000 hPa. From Rasmussen and Houze [2011]. Copyright 2011 American Meteorological Society.

moreover, typical. *Houze et al.* [2007a] found that convective radar echoes seen over the Himalayan region by TRMM were systematically more intense over the lowlands and lower foothills. The greatest instability tends to be released at first opportunity, when the flow encounters relatively small hills.

4.3. MCS Stratiform Enhancement

[41] The land region lying between the eastern end of the Himalayas and the Bay of Bengal is the largely wetland region comprising the “Mouths of the Ganges.” During the monsoon season it is common for the prevailing low-level

winds to be southwesterly to southeasterly across this region. As noted in section 4.1, during active phases of the monsoon, synoptic-scale low-pressure systems (Bay of Bengal depressions) move inland from the Bay, and these episodes account for considerable portions of the rainfall that occurs in active phases of the monsoon, especially in the central and eastern Himalayas [*Lang and Barros*, 2002; *Barros et al.*, 2006; *Medina et al.*, 2010; *Romatschke and Houze*, 2011b]. As noted in section 4.1, the rain occurring in the depressions is concentrated in MCSs, which are smaller in scale than the depression but larger than convective scale [*Houze and Churchill*, 1987]. The MCSs

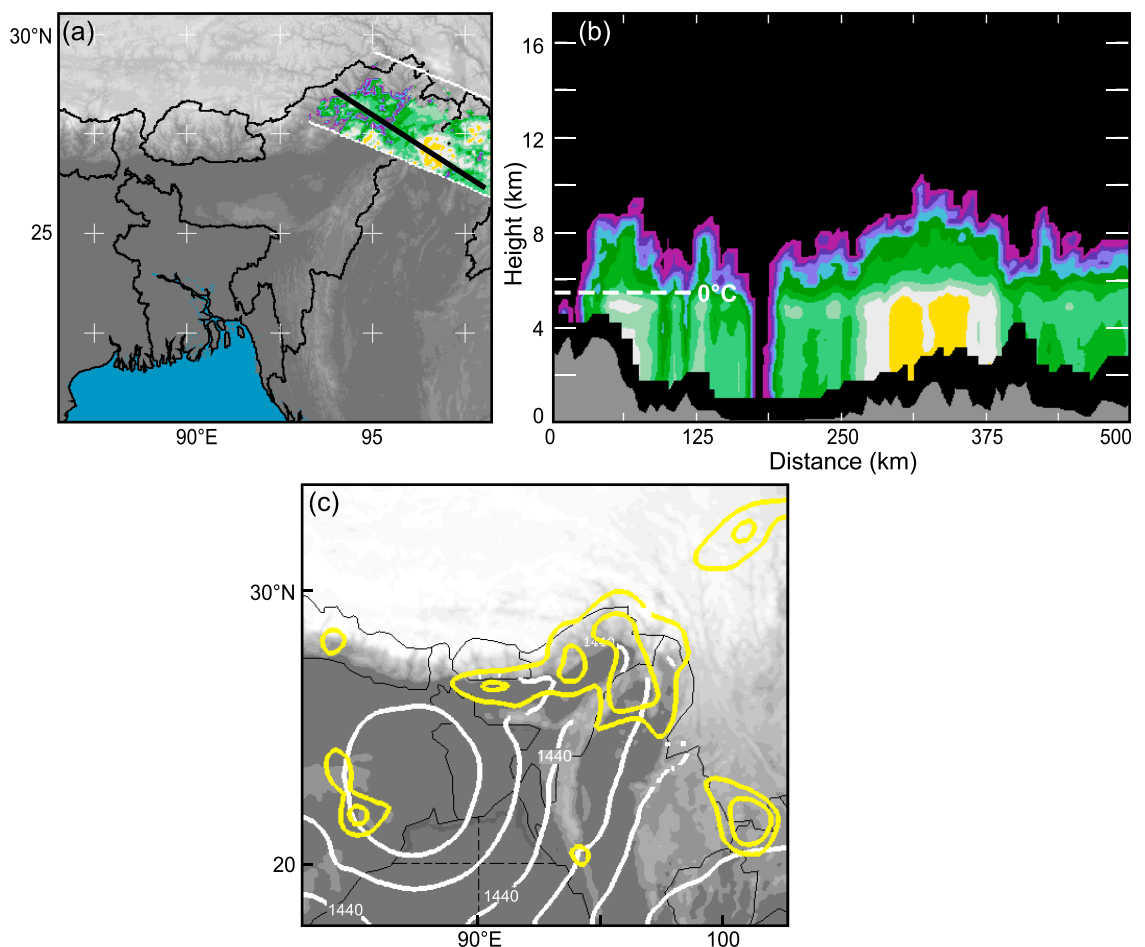


Figure 17. (a and b) TRMM observed reflectivity for a convective system containing broad stratiform echo at 02:53 UTC 11 August 2002. Figures 17a and 17c show horizontal cross sections at 4 km. Figure 17b shows a vertical cross section taken along the black line in Figure 17a. (c) Time-averaged fields during the simulation of a convective system containing broad stratiform echo: 850 hPa geopotential heights (white contours), 500 hPa vertical velocity (yellow contours, 0.05 m s^{-1} intervals). The terrain is shown in grey shading. Adapted from Houze *et al.* [2007a] and Medina *et al.* [2010]. Reprinted with permission from John Wiley.

contain embedded convection as well as broad stratiform precipitation regions [Houze *et al.*, 2007a; Romatschke *et al.*, 2010; Medina *et al.*, 2010]. When these MCSs with their broad stratiform rain regions are advected inland over the wetlands by the prevailing southwesterlies, they retain a maritime character. When they reach the mountains, they are in a mature stage dominated by stratiform precipitation. Recall from Figure 13e that the precipitation systems containing broad regions of stratiform precipitation are generally absent over the western Himalayan region and occur primarily over and upstream of the western coastal mountains of India and Burma and over the eastern portion of the Himalayas. Figure 17 shows an example in which the broad stratiform region of an MCS embedded in a Bay of Bengal depression had moved into the eastern Himalayan region. Lang and Barros [2002] and Barros *et al.* [2006] describe similar storms moving into the central Himalayas. Figures 17a and 17b show TRMM PR observations of the system. The TRMM 2A23 algorithm classified all of the

precipitation in this image as stratiform because of its lack of strong horizontal variability and the presence of a bright band in the melting layer. Despite the classification as stratiform, the data in Figure 17b indicate a cellular structure within the stratiform radar echo. The remains of previously active convective cells evidently produce this structure (as discussed by Houze [1997]). This type of stratiform precipitation is expected when the shear is weak [Houze, 1993, pp. 211–217]. The TRMM convective/stratiform separation algorithm [Awaka *et al.*, 1997] identifies such radar echoes as stratiform because they either have a bright band or lack sufficient horizontal inhomogeneity to be considered as actively convective. Thus, the MCSs in the depressions are found to consist of a combination of active convective cells, and large stratiform regions that have formed from the aging and collapsing of convective cells. This structure is consistent with the conclusions of Lang and Barros [2002], who examined MCSs in Bay of Bengal depressions encountering the east central Himalayas. The data in Figure 17b

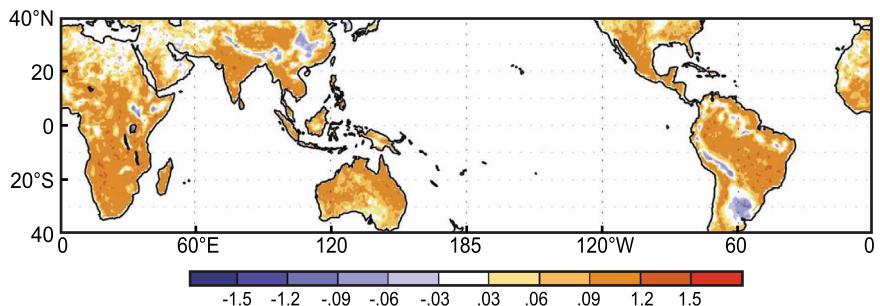


Figure 18. Horizontal distribution of empirical orthogonal function (EOF) of the annual mean diurnal cycle derived from TRMM precipitation data for the period 1998–2006 with the data normalized by the diurnal range. The EOF analysis was applied only to land areas. The horizontal resolution of the EOFs is $1.5^\circ \times 1.5^\circ$. Positive values (orange) indicate a peak frequency around 1500 solar time; negative values indicate a peak frequency at about 0600 solar time. From Kikuchi and Wang [2008]. Copyright 2008 American Meteorological Society.

further suggest that when these broad stratiform regions of MCSs encounter higher terrain, they strengthen. Figure 17c provides a more comprehensive view of the effect of the mountains on the mesoscale precipitation system. The synoptic-scale depression within which the mesoscale system was embedded is shown by the 850 hPa height contours in a realistic model simulation of the case seen by the TRMM PR. The contours of stronger upward air motion coincide with the upward sloping terrain in the location of the precipitation seen by the radar. The 850 hPa height contours indicate that the lower tropospheric flow was directed toward the Himalayan barrier. Soundings showed that the flow was mostly saturated and approximately most adiabatic where it was encountering the mountains. The low moist static stability would enable the strong impinging airflow to rise easily over the terrain without significant blocking effects. Even when unconnected with terrain, well-developed MCSs contain stratiform precipitation regions [Houze, 2004]. When such stratiform regions embedded in the moist flow impinging on the mountain barrier are advected up and over the terrain feature, they are enhanced and in effect become superbroad stratiform rain regions. While this behavior of precipitation systems occurs commonly over the eastern Himalayan region and west coastal mountain regions of India and Burma, as we have seen, it rarely occurs in the arid western Himalayan region. In the monsoon season of 2010, when air from the Bay of Bengal region invaded Pakistan from the southeast, mesoscale systems of the type illustrated in Figures 17b and 17c occurred over the eastern Himalayas. As a result, vast amounts of rainwater accumulated on the mountainsides, and the runoff flooded the Indus River [Houze et al., 2011]. An important implication of Figure 17c is that the vertical motion associated with the precipitation covers a mesoscale region corresponding primarily to the topography of the mountains. The organized synoptic-scale vertical motion associated with the depression played no apparent role other than to provide an environment in which MCSs could form and flourish and subsequently be enhanced by orographic lifting.

4.4. Diurnal Cycles

[42] The TRMM satellite has made it possible to study the diurnal cycle of precipitating convection globally over the tropics and midlatitudes. Kikuchi and Wang [2008] performed an empirical orthogonal function analysis of tropical rainfall observed by TRMM. Figure 18 [from Kikuchi and Wang, 2008] shows that the largest portion of the variance over most land areas is explained by the component of the diurnal cycle of precipitation that has a maximum in daytime (orange shading, peak occurrence around 15:00 solar time (ST)). However, Figure 18 also indicates that in regions close to or downstream of major mountain ranges, early morning maxima sometimes explain the largest portion of the variance (blue shading, peak occurrence around 06:00 ST). Mountains affect diurnal cycles of convective precipitation via the upslope/downslope wind reversal associated with the daily cycle of heating and cooling (Figures 3c and 3d) and/or by setting off remote diurnal effects through waves generated by diurnally varying heating and cooling over high terrain (Figure 3j). In addition, the timing of diurnal responses is affected by convective life cycles, which are a function of the scale of the convective systems responding to diurnal processes. We now examine each of these factors.

4.4.1. Triggering of Convective Systems by Diurnal Upslope and Downslope Winds

[43] Figure 13 showed the patterns of occurrence of three different forms of precipitating convection over the Himalayan and Andean regions. Each of these convective storm types exhibits different diurnal behavior. The broad stratiform regions are controlled diurnally primarily by nonorographic processes [Romatschke et al., 2010; Romatschke and Houze, 2010, 2011a, 2011b; Rasmussen and Houze, 2011]. However, the systems containing deep convective cores and wide convective core echoes are strongly controlled by processes near and over the mountains. Systems with deep convective cores occurring primarily in arid regions very close to the mountain ranges (Figures 13a and 13b) exhibit a maximum frequency of occurrence coinciding with the peak in daytime heating (e.g., Figure 19a).

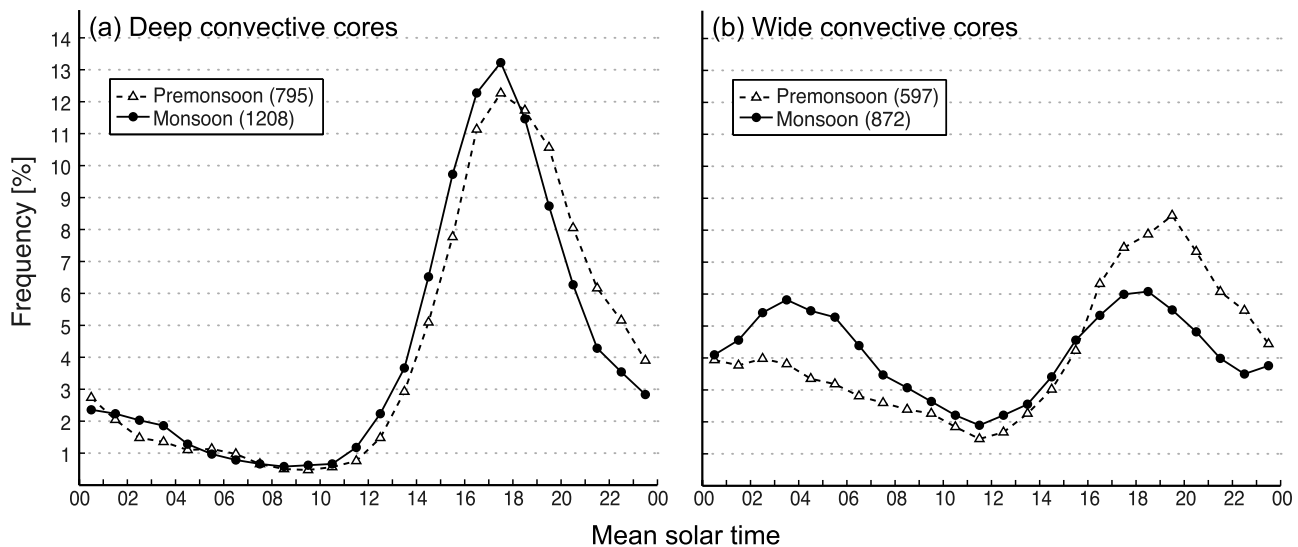


Figure 19. Diurnal cycles of the frequency of occurrence of convective systems over the landmass of South Asia observed by the TRMM Precipitation Radar during the premonsoon (March–May) and monsoon (June–September) seasons for radar echoes containing (a) deep convective cores and (b) wide convective cores. The number of radar echo structures observed in each category is shown in parentheses. The frequency was calculated separately for each category. From Romatschke *et al.* [2010]. Copyright 2010 American Meteorological Society.

In contrast, wide convective cores, which occur in a more widely distributed pattern over both land and ocean (Figures 13c and 13d), exhibit a more complex diurnal cycle. Figure 19b shows that the systems with wide convective cores in South Asia exhibit an afternoon maximum similar to the systems with deep convective cores; however, in addition, the systems with wide convective cores also have a secondary maximum frequency of occurrence in the early morning (03:00–05:00 ST for the region shown in Figure 19b). This secondary maximum is observed primarily at the foot of the Himalayas. The cooling over high elevations leads to downslope air motions. In the Himalayan region, a zone of convergence becomes located along the base of the mountains in the nighttime to early morning period, as the prevailing low-level monsoon southwesterlies encounter the downslope flow. During the daytime, powerful upslope motion changes this region to a zone of strong divergence (Figure 20).

[44] The existence of the nocturnal/early morning maximum of rainfall at the foot of the Himalayas during the monsoon has been noted in a variety of studies [Barros *et al.*, 2000; Barros and Lang, 2003; Barros *et al.*, 2004; Romatschke *et al.*, 2010; Romatschke and Houze, 2011b]. In the Himalayan monsoon case, the nocturnal maximum is not seen in smaller convective elements. Rather, the nocturnal maximum is accounted for by larger MCSs. Evidently, the moisture of the incoming low-level monsoon flow provides an environment conducive to the growth of nocturnally generated convection upscale into MCSs with wide convective cores. Nocturnal convective triggering is, however, seen in a wide variety of orographic/convective regimes and scales. For example, on Oahu in Hawaii, nocturnal convective rain clouds are systematically triggered on the

windward side of the island, where the nocturnal downslope winds meet the prevailing trade winds [Hartley and Chen, 2010]. Giovannettone and Barros [2008] have found that nocturnal downslope motions lead to convection in valleys in the Sierra Madre of Mexico.

4.4.2. Convective Lifecycle Effects on Diurnal Variability

[45] Chen and Houze [1997] found that over the open ocean (i.e., in the complete absence of orography), the diurnal cycle of tropical convective cloud systems is a function of the size attained by the convective system. Smaller convective-scale clouds seen in infrared satellite imagery were found to occur in sync with the solar heating cycle, while MCSs with cloud shields reaching approximately hundreds of kilometers in dimension were triggered in the warm part of the day but maximized in coverage around dawn. The reason for this difference is that the typical MCS lifetime (~12 h) is not small compared to the 24 h diurnal time scale. Nor is it equal to the diurnal time frame. Since MCSs often account for large portions of local climatological rainfall, the mean diurnal rain cycle may be substantially offset from the diurnal heating cycle. Moreover, if both small and large convective systems contribute significantly to local rainfall, the mean diurnal cycle may be bimodal.

[46] Over land, the life cycle effects evident in the diurnal cycle seen over oceans are superimposed on the convection-controlling effects of the pronounced diurnal heating and cooling processes over mountains. Figure 21b shows an example taken from an 8 year climatology of the TRMM PR data obtained over the central Himalayan region (CHF). Romatschke and Houze [2011a] stratified rainfall in this region according to the size of radar echo affecting the area.

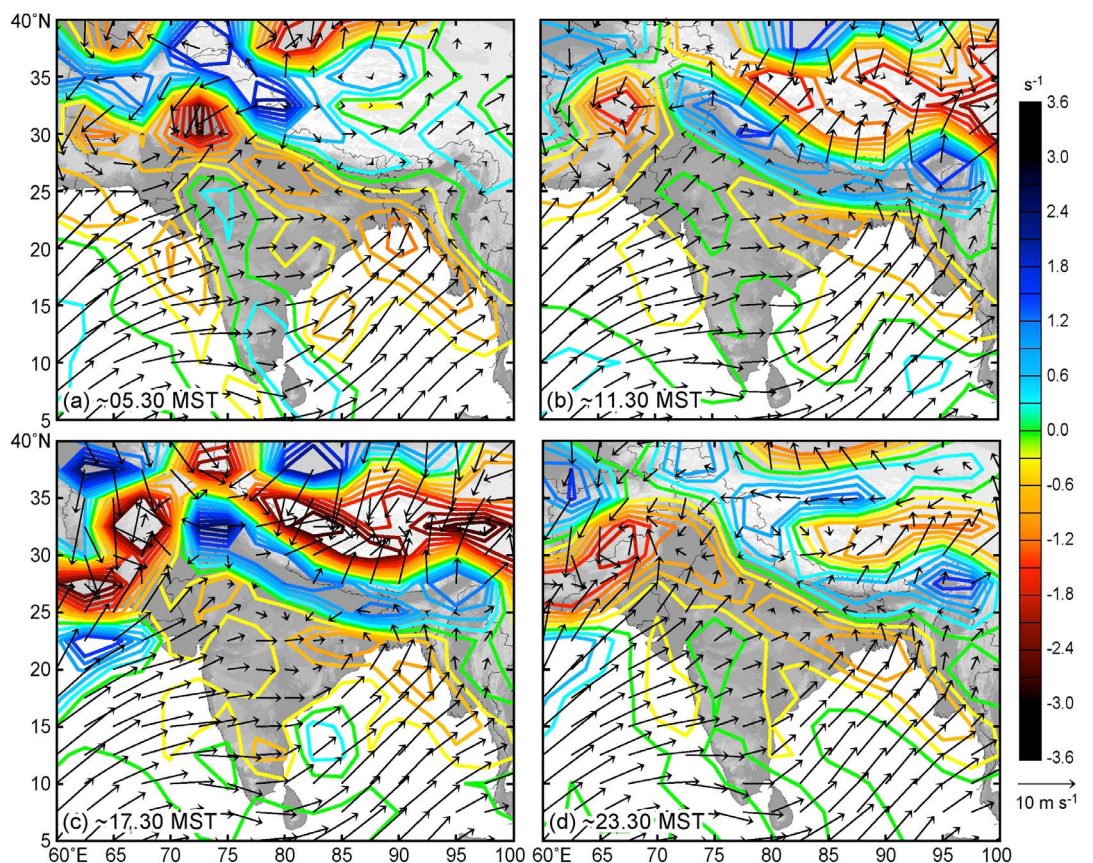


Figure 20. Climatology of surface winds (m s^{-1}) and surface divergence (s^{-1}) for June–September for (a) 00:00 UTC (~05:30 LT), (b) 06:00 UTC (~11:30 LT), (c) 12:00 UTC (~17:30 LT), and (d) 18:00 UTC (~23:30 LT). From Romatschke and Houze [2011b]. Copyright 2011 American Meteorological Society.

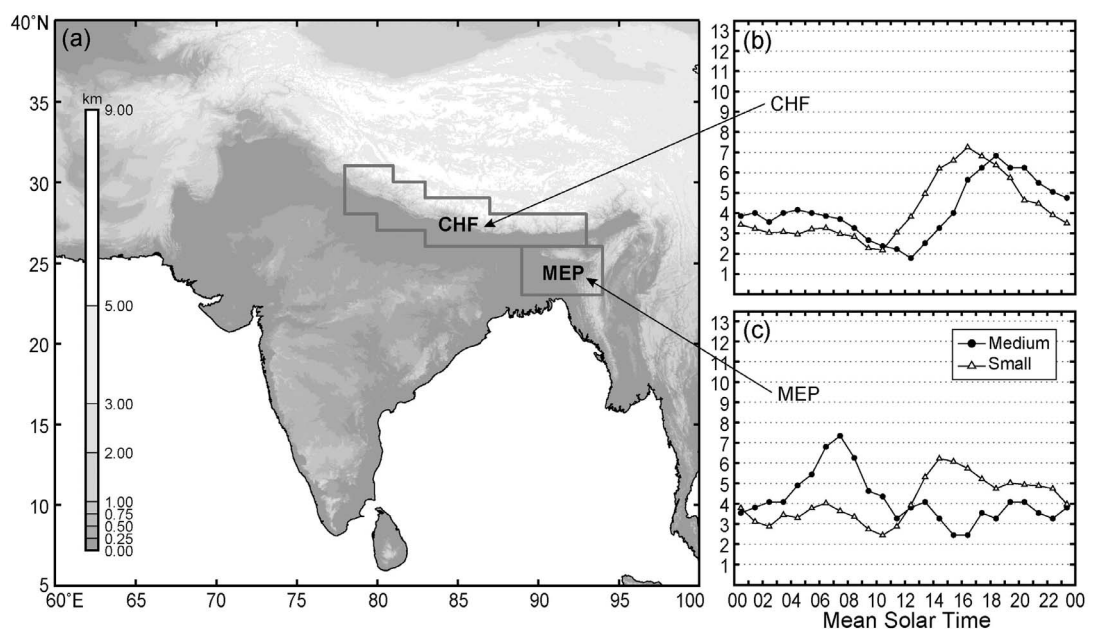


Figure 21. Topography of South Asia. CHF stands for central Himalayan foothills. MEP refers to Meghalaya Plateau (MEP). Diurnal cycles of small-sized radar echoes ($<8500 \text{ km}^2$, triangles) and medium-sized radar echoes (8500–35,000 km^2 , circles), seen by the TRMM Precipitation Radar. From Romatschke and Houze [2011a]. Copyright 2011 American Meteorological Society.

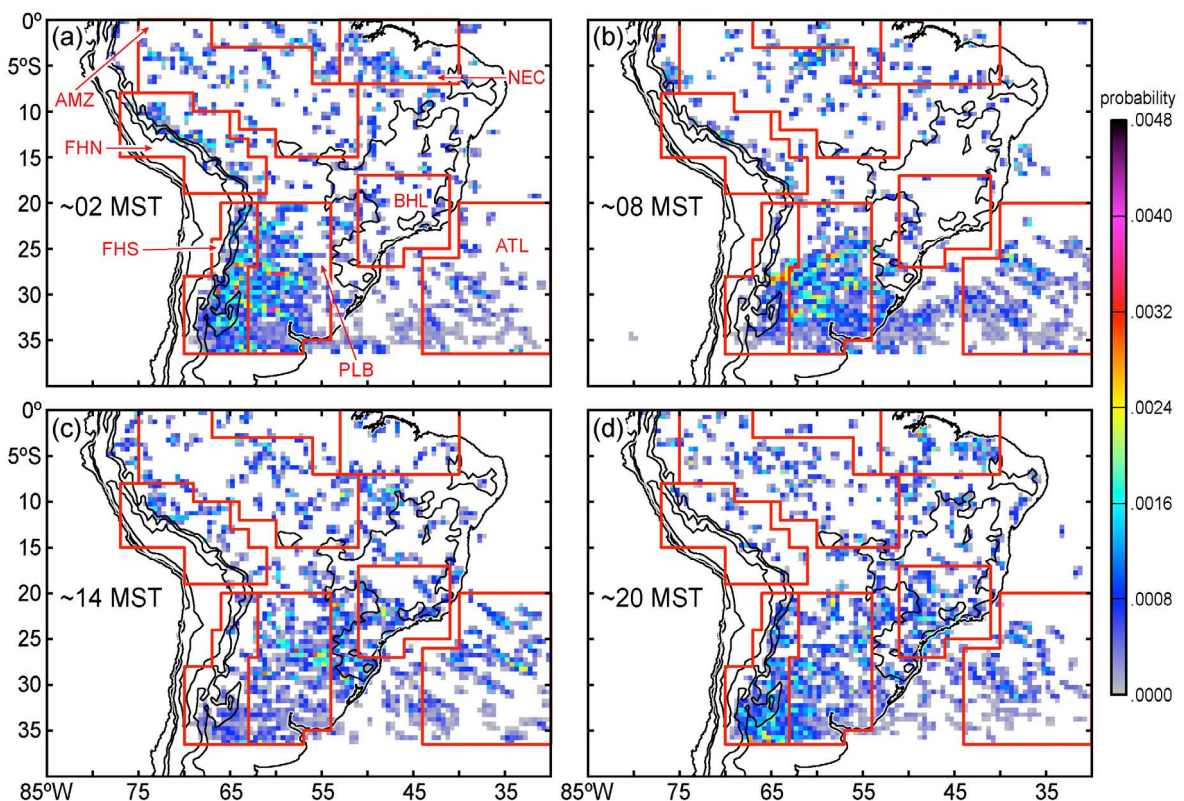


Figure 22. Geographical distribution of the probability of occurrence of the TRMM Precipitation Radar detecting a wide convective core between 3 h prior to and 3 h after (a) 06:00 UTC (~02:00 LT), (b) 12:00 UTC (~08:00 LT), (c) 18:00 UTC (~14:00 LT), and (d) 00:00 UTC (~20:00 LT). Topographic contours of 0.3, 1.5, and 3 km are shown (black). Abbreviations are defined as follows: AMZ, Amazon Basin; FHN, Foothills North; NEC, Northeast Coast; BHL, Brazilian Highlands; FHS, Foothills South; PLB, La Plata Basin; and ATL, Atlantic Ocean. From Romatschke and Houze [2010]. Copyright 2010 American Meteorological Society.

The echoes indicated as “medium” size were actually the largest radar echoes that affected this region. (Larger-sized echoes were seen mainly in regions dominated by maritime conditions.) The maximum frequency of occurrence of the medium echoes lagged the peak frequency of the smaller echoes by 2 h, which would correspond to the time likely required to grow from the smaller to the medium size.

4.4.3. Propagational Diurnal Cycles

[47] Diurnal cycles of convection downstream of mountains may occur when convective systems forced by the diurnal heating/cooling cycle over the mountains propagate away from the mountains. The propagation may be as a result of wave motion (as suggested by Figure 3j), advection, cold pool spreading, or some combination of these effects. Figure 22 [from Romatschke and Houze, 2010] shows the progression of orogenic MCSs away from the Andes. The wide convective core echoes seen by the TRMM PR (section 4.1) are a proxy for MCSs, and they are seen to appear first at about 20:00 mean solar time (MST) in the region labeled FHS near the Andes. By 02:00 MST, they are located somewhat to the east, partially in the region labeled PLB. By 08:00 MST, they are almost wholly in PLB. At 14:00 MST, they are less frequent in general but primarily eastward of PLB. Rasmussen and Houze [2011]

used geosynchronous satellite data to track systems seen by the TRMM PR and verified that they are triggered on the eastern edge of the Andes and move eastward. The eastward movement is partially due to cold pool spreading but is aided by the fact that these subtropical MCSs are embedded in midlatitude westerlies and aided by being located within baroclinic waves moving eastward across the Andes and beyond.

[48] Farther north, in the tropics, where easterly flow dominates, daytime heating over the Andes triggers gravity wave motion, and upward motion response to the heating propagates westward out over the Pacific Ocean [Mapes et al., 2003] (see Figure 23). Houze [2004] suggested that a similar behavior may occur over the Bay of Bengal during the onset of the Asian monsoon. The Eastern Ghats (Figure 12a) heat up during the day, and gravity waves excited by the heating presumably propagate out over the bay during the subsequent hours. A series of these waves was observed by an instrumented ship during the Joint Air-Sea Monsoon Interaction Experiment (JASMINE) in May 1999 [Webster et al., 2002]. Satellite infrared data plotted in time-latitude format (Figure 24) showed cold cloud tops propagating equatorward from the northern part of the bay out over the water (20–27 May). Radar data obtained at the

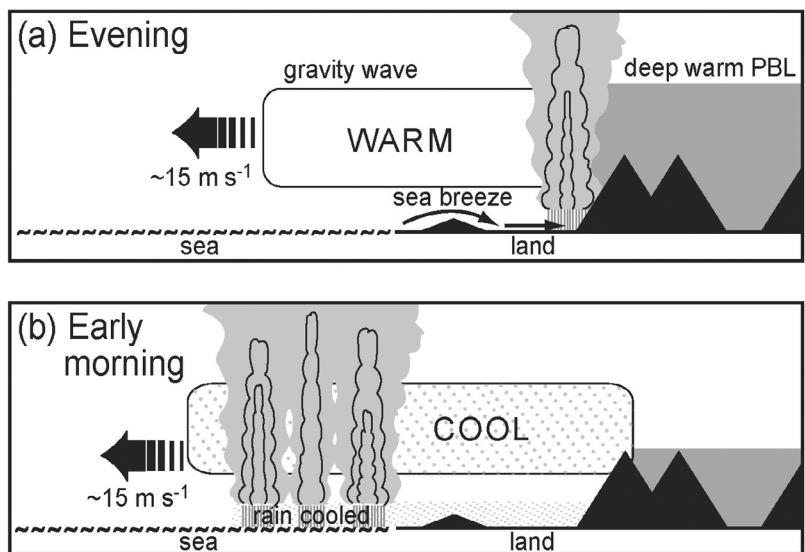


Figure 23. Schematic of diurnal gravity waves emitted as a result of daytime heating over the mountainous terrain of western tropical South America and associated deep convection: (a) evening and (b) early morning. From *Mapes et al.* [2003]. Copyright 2003 American Meteorological Society.

ship showed that the precipitation system was an MCS consisting of a convective line and a mesoscale region of trailing stratiform precipitation. See *Houze* [2004] for further discussion.

[49] *Li and Smith* [2010] have proposed another type of orographically determined propagational diurnal cycle. They found theoretical and empirical evidence suggesting that movement and systematic regeneration of MCSs downwind of the Rocky Mountains (as found by *Carbone et al.* [2002]) are related to “drifting potential vorticity anomalies.” Accord to this idea, diurnal heating over the high terrain generates potential vorticity anomalies that are advected downstream of the mountain range (Figure 25). During summer, these mid-level lows favor the development and maintenance of MCSs

moving eastward of the mountains. Because of the time it takes for the potential vorticity anomalies to move eastward, the diurnal maximum of MCS occurrence is at night over regions far to the east of the Rockies.

5. FRONTAL SYSTEMS ENCOUNTERING MOUNTAIN RANGES

5.1. Organization of Precipitation in Extratropical Cyclones Unaffected by Terrain

[50] The air motions and precipitation growth in extratropical cyclones are well known (see summary by *Houze and Hobbs* [1982] or *Houze* [1993, chapter 11]). Figure 26a [from *Browning*, 1986] shows schematically how warm, moist

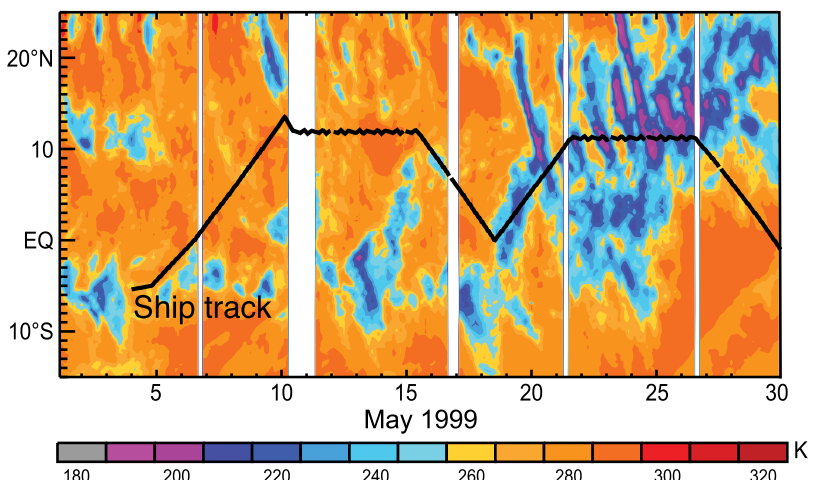


Figure 24. Time-latitude section of brightness temperature (see color-coded scale) from the European Space Agency METEOSAT 5 geostationary satellite. Data are averaged between 85°E and 90°E . Cold temperatures are indicative of high cloud tops, while relatively clear periods appear as warm temperatures representing infrared radiation emitted at the surface or the moist boundary layer or from low tropospheric clouds. From *Webster et al.* [2002].

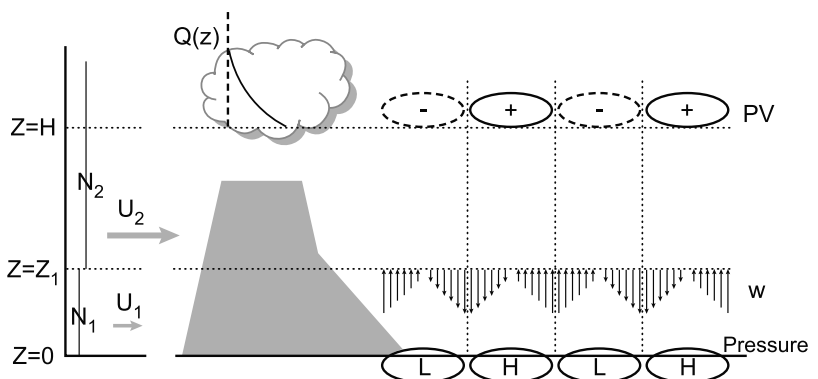


Figure 25. Schematic of mechanism of diurnal generation of potential vorticity over high terrain: U represents the background wind, N is the environmental stability, Z_1 is the shear level, $Z = H$ is the heating level, and $Q(z)$ is the vertical profile of the diurnal heating over the mountain. From Li and Smith [2010]. Copyright 2010 American Meteorological Society.

air from lower latitudes enters the storm and rises as a “conveyor belt” over the cold and warm fronts to produce clouds and precipitation. Studying cyclones moving toward the west coast of the United States, Nagle and Serebreny [1962] pointed out that the cyclonic rainfall over the ocean was concentrated in rainbands and other mesoscale and convective-scale entities and that the nature of these smaller-scale structures varied from one sector of the storm to the next (i.e., the early, middle, and late stages shown in Figure 26b). Browning [1974], Houze *et al.* [1976], and Matejka *et al.* [1980] further studied the embedded structures and identified types of mesoscale rainbands occurring in different sectors of a frontal precipitation system (Figure 26c). These basic synoptic-scale and mesoscale structures of the streams of moisture flowing into extratropical cyclones and forming clouds and precipitation have been determined largely from the study of oceanic storms or storms otherwise minimally affected by irregularities of underlying terrain. When these storms encounter hills or mountains, the cloud and precipitation processes are profoundly changed as a result of the flow of air over and around the terrain.

5.2. Atmospheric Rivers

[51] Newell *et al.* [1992] discovered that water vapor flux feeding into the extratropics tends to be concentrated into narrow filaments emanating from lower latitudes. They called these filaments “tropospheric rivers.” Later, Zhu and Newell [1994, 1998] called these filaments “atmospheric rivers” and showed their importance in feeding moisture into rapidly developing frontal cyclones. Figure 27 shows the atmospheric river water vapor flux vectors (isolated from the total vapor flux) as computed by Zhu and Newell [1998] by atmospheric rivers for a typical day. The atmospheric river flux was obtained at each point at a given latitude as the flux exceeding a background value determined for that latitude. Atmospheric rivers are especially well defined over the broad expanse of the Pacific Ocean. Ralph *et al.* [2004] analyzed atmospheric rivers over the North Pacific and found that cloud top temperatures along the atmospheric

river core decreased with increasing integrated water vapor content (IWV). They found that the core zones of the atmospheric rivers, defined as where $\text{IWV} > 2 \text{ cm}$, were $\sim 150\text{--}400 \text{ km}$ wide (depending somewhat on the satellite data set that was used). Ralph *et al.* [2005] further provide estimates of the net water vapor flux in North Pacific atmospheric rivers.

[52] The relationship of the atmospheric river relative to an extratropical cyclone is shown in a composite of data relative to the cold front in Figure 28 [from Ralph *et al.*, 2004]. The atmospheric river is closely tied to the prefrontal low-level jet that keeps a cold front in semigeostrophic balance. The filamentary structure of the river is apparently partly a result of the kinematic deformation of the flow field just ahead of the front, which extends far to the southwest and into the subtropics, where it connects with the higher water vapor content of lower latitudes.

[53] As fronts associated with Pacific cyclones fed by atmospheric rivers move over the west coastal mountains of North and South America, they are modified substantially by topography. The combination of atmospheric rivers, well-formed frontal cyclones, and steep coastal topography makes the western Pacific coasts of continents a robust venue for studying the orographic modification of extratropical cyclonic precipitation. Figure 29 [from Neiman *et al.*, 2008] illustrates the magnitude of the interaction of an atmospheric river with the coastal mountains of North America. Figure 29a is the composite structure of the IWV of atmospheric rivers of frontal systems moving into the northwestern United States. Where the atmospheric river encounters the mountainous coastal region, the water vapor content is drastically reduced while the rainfall greatly increases (Figure 29b).

[54] Ralph *et al.* [2005] analyzed dropsonde data obtained in atmospheric rivers $\sim 500 \text{ km}$ upstream of the coastal mountains of California. They found that the moist static stability of the atmospheric rivers was nearly zero from the surface to $\sim 3 \text{ km}$ altitude. As such, a nearly saturated atmospheric river has little tendency to be blocked and turn horizontally, as would be the case if the lower-level flow

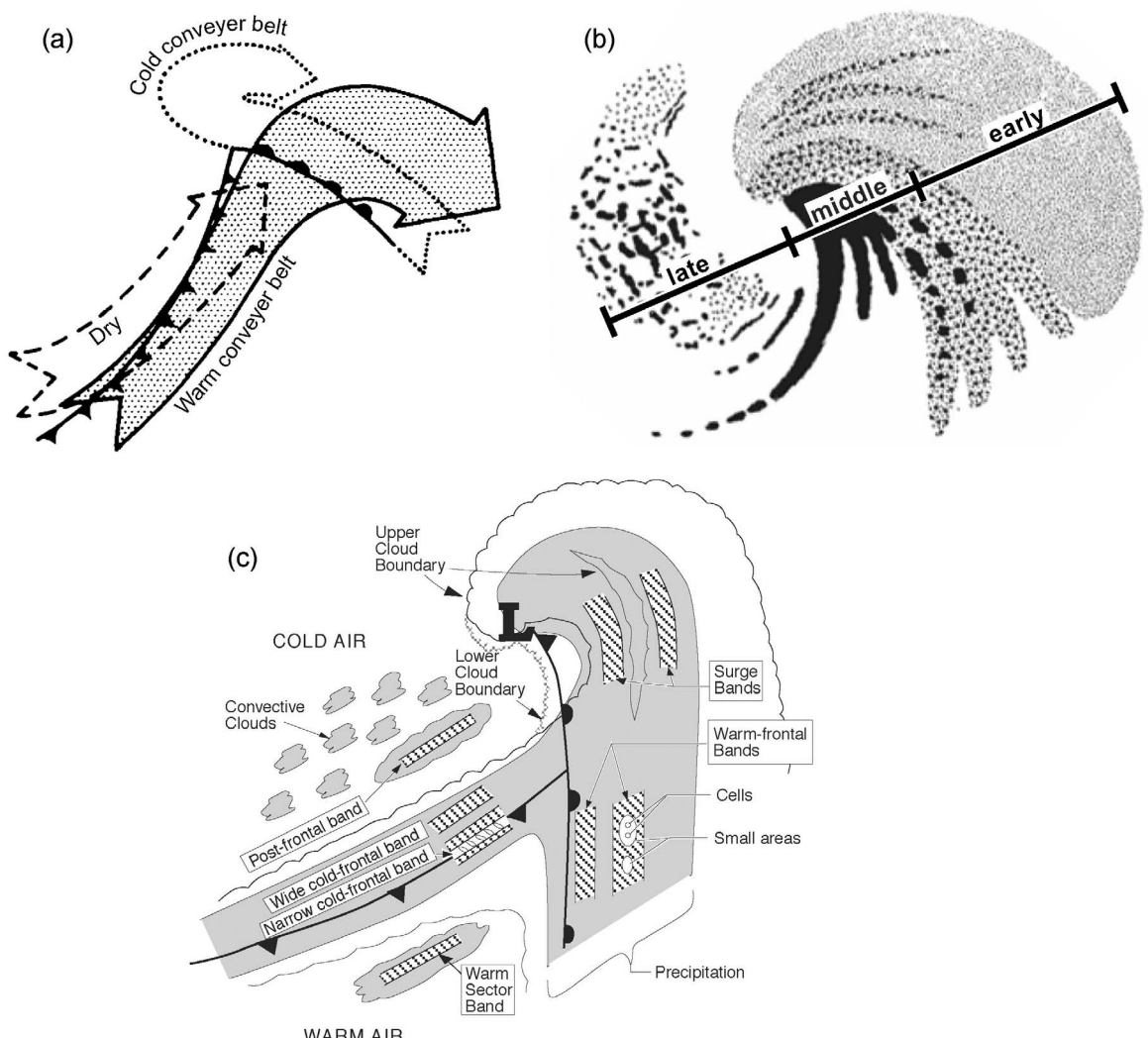


Figure 26. (a) Model depicting the main features of the large-scale flow (relative to the motion of the synoptic system) that determine the distribution of cloud and precipitation in a mature midlatitude depression in the Northern Hemisphere. The stippled arrow shows the warm conveyor belt overrunning the fronts. The dotted arrow is the low-level cold conveyor belt below the warm front. The dashed arrow indicates dry air overriding the warm conveyor belt. From Browning [1986]. (b) Idealized precipitation pattern of an eastern Pacific extratropical cyclone. The precipitation intensity is indicated by the degree of the shading. The line segments indicate the early, middle, and late sectors of the storm as they pass over the west coast of North America. Adapted from Nagle and Serebreny [1962]. (c) Idealization of the cloud and precipitation pattern associated with a mature extratropical cyclone unaffected by topography. Adapted from Matejka *et al.* [1980] and Houze [1981]. Reprinted with permission.

were unsaturated and had a high static stability [Rotunno and Ferretti, 2001]. Nearer the California coastline, Neiman *et al.* [2002] found that in some cases a shallow (~ 1 km deep) layer of flow of high stability and weak cross-barrier flow component is present just off the coast, and the atmospheric river jet must ascend this stable layer at a distance upstream of the coastal mountains (Figure 30). As a result, orographic enhancement of precipitation may occur over the ocean upstream of the coastal mountains. Analyzing a 2.5 year climatology of 3-D reflectivity data obtained by the Eureka, California, WSR-88D radar, James and Houze [2005] found that the enhancement of the precipitation in atmospheric river situations begins ~ 100 km offshore. This

enhancement could be due to lifting of the atmospheric river jet over the coastal shallow stable layer. They note, however, that the offshore enhancement could also be due to enhancement of frontogenesis, which occurs when frontal systems approach coastal topography [Yu and Smull, 2000; Colle *et al.*, 2002]. Except for the upstream enhancement, James and Houze [2005] found that the flow over the inland terrain behaved as expected for unblocked flow, with maxima of radar echo intensity over the upslope side of each small-scale ridge of the coastal mountains. Enhancement of the radar echo occurred systematically on the upstream sides of subbarrier-scale ridges.

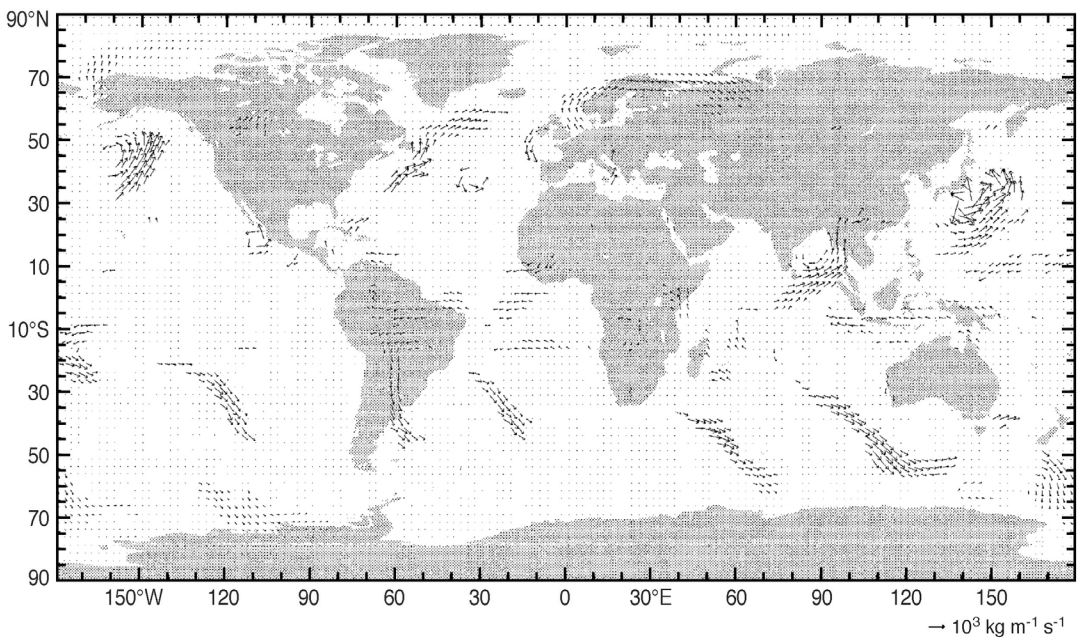


Figure 27. Moisture flux ($\text{kg m}^{-1} \text{s}^{-1}$) by atmospheric rivers, isolated from the total flux for 12:00 UTC 12 October 1991. From Zhu and Newell [1998]. Copyright 1998 American Meteorological Society.

5.3. Non-Bright Band Rain

[55] The atmospheric rivers affecting the mountainous California coast exhibit precipitation enhancement on the first ridge of the relatively low altitude coastal range. White *et al.* [2003], analyzing vertically pointing S-band radar data, deduced that much of the enhancement occurs below the 0°C level, by robust coalescence growth of drops. Although the precipitating clouds extended above this level, a radar bright band (produced by the melting of large ice particles grown at higher altitudes) is not always present. They found that this “non–bright band” precipitation accounts for 28% of the cool season rainfall at California coastal sites and that the non–bright band rain occurs generally under stably stratified conditions. Compared to other raining situations, the non–bright band rain cases are characterized by stronger low-level wind speeds, a stronger correlation between low-level upslope wind speed and coastal rain rates, and wind directions more orthogonal to the mean terrain. These factors indicate that the non–bright band rain is more likely when the low-level blocked layer is absent and the convection is at a minimum. White *et al.* [2003] further found that the relationship between radar reflectivity factor and rain rate is consistent with small drop sizes predominating in non–bright band precipitation, compared to situations of bright band rain, when melting of ice particles grown at higher levels contributes significantly to the precipitation. Kingsmill *et al.* [2006] found that in California storms, periods of non–bright band precipitation are interspersed between spells of bright band rain in the warm frontal sector of the storms, in the cool sector ahead of the warm front, and in the warm sector following the warm front. They also found that the non–bright band rain was

generally not present in the cold frontal zone or cold air mass convection following the cold front.

5.4. Precipitation Enhancement in Blocked and Unblocked Flows

[56] When extratropical cyclones pass over mountain ranges, they have already developed widespread precipitating clouds (Figure 26). These clouds are deep and composed through much of their thickness of ice particles growing by deposition, riming, and aggregation. It is the fallout and melting of the larger of these ice particles that produce the ubiquitous bright band seen on radar in extratropical cyclones [e.g., Houze *et al.*, 1976]. Below the bright band lies a layer of liquid cloud droplets and rain. Orographic enhancement of the cyclonic precipitation occurs over the windward slopes of a mountain range when air motions endemic to the storm adjust to the terrain by rising and condensing out water vapor. In order to fall out as precipitation on the windward slopes, the condensed water must be quickly converted to rapidly falling precipitation. For this to happen, the microphysical time scale of growth and fallout [Smith, 2003; Roe, 2005] must be short enough that the precipitation particles fall out before they pass over the top of the terrain feature (Figure 1). The instances of non–bright band rain seen in California (section 5.3) indicate that the orographic lifting activates coalescence of water drops at low level to quickly convert cloud drops to raindrops. Yuter and Houze [2003] found that ice particles above the bright band level can also grow significantly by riming (accretion of supercooled liquid water drops) in cyclonic storms passing over the European Alps.

[57] Exactly where the growth by coalescence and riming occurs relative to the mountains being traversed by an

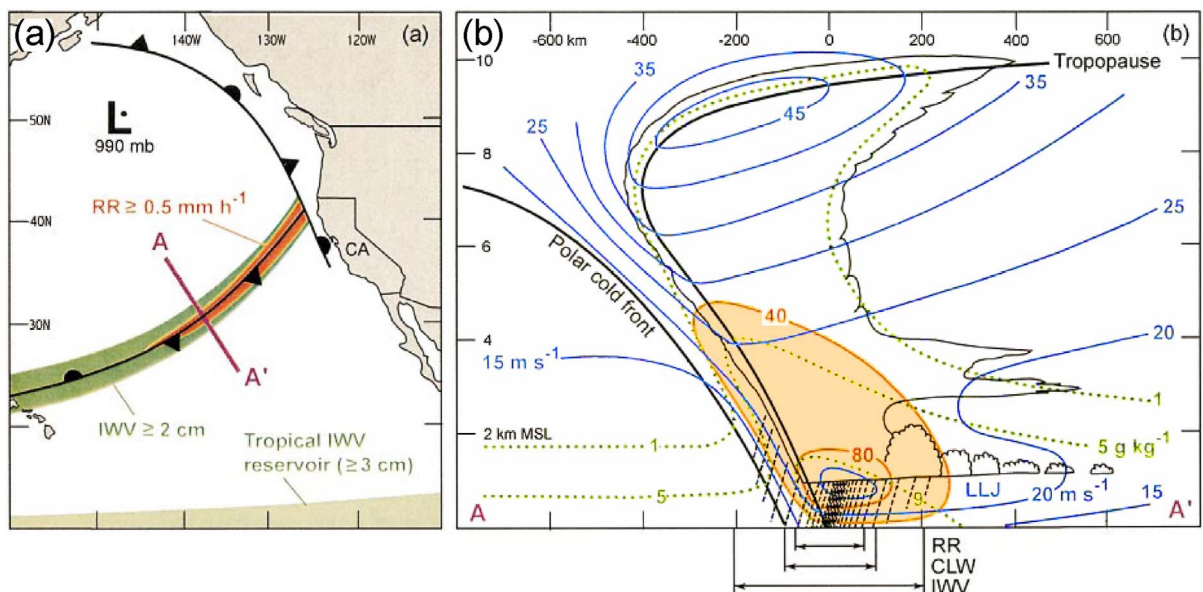


Figure 28. Conceptual representation of an atmospheric river over the northeastern Pacific Ocean. (a) Plan view schematic of concentrated integrated water vapor (IWV) along a cold front (values $\geq 2 \text{ cm}$ indicated by dark green shading). The tropical integrated water vapor reservoir ($\geq 3 \text{ cm}$; light green) is also shown. (b) Cross section along AA' highlights the vertical structure of the along-front isotach (blue contours; m s^{-1}); LLJ indicates low-level jet), water vapor specific humidity (dotted green contours; g kg^{-1}), and horizontal along-front moisture flux (orange contours and shading; 3105 kg s^{-1}). Schematic clouds and precipitation are also shown, as are the locations of the mean width scales of the 75% cumulative fraction of perturbation IWV (widest), cloud liquid water content (CLW), and rainfall rate (RR, narrowest) across the 1500 km cross-section baseline. From Ralph *et al.* [2004]. Copyright 2004 American Meteorological Society.

extratropical cyclone depends on the manner by which the air in a storm does or does not ascend the terrain. Peterson *et al.* [1991] identified two modes of ascent, which they referred to as “coupled” and “decoupled” but which correspond to the conditions that are now more commonly referred to as unblocked and blocked, as discussed in section 2.2. Unblocked conditions are illustrated in Figures 3a, 7a, and 30b; blocked conditions are illustrated by Figures 3i, 3j, 7b, and 30c.

[58] Neiman *et al.* [2002] identified unblocked and blocked regimes within frontal systems passing over the coastal mountain range of California. From wind profiler data they calculated vertical profiles of the correlation coefficient between upstream cross-barrier wind and rain rate on the windward slopes. When the low-level flow is unblocked, the rain rate at a windward slope site was highly correlated with the low-level cross-barrier flow measured just upstream. The correlation between the windward rain rate and the cross-barrier upstream flow was high from the surface up to $\sim 2 \text{ km}$ and decreased sharply above. Thus, the low-level flow was concluded to be effective in producing orographic enhancement of precipitation for unblocked cases. For blocked cases, the correlation coefficient between near-surface cross-barrier upstream flow and windward rain rate was almost zero at low levels but increased near mountaintop, which they attributed to upslope precipitation

occurring when the flow at higher levels rose over the low-level blocked flow and over the terrain.

[59] Medina and Houze [2003] examined several cyclonic storms passing over the Alps during the Mesoscale Alpine Programme (MAP) of autumn 1999 and proposed the model in Figure 7 to explain the enhancement of the deep layer of precipitation passing over the Alps in situations of both unblocked and blocked flow. In the blocked flow case, the enhancement is moved upstream of the mountain barrier, with the layer of blocked flow forced to rise before arriving at the mountains. Houze *et al.* [2001] examined radar data obtained on the Mediterranean side of the Alps in all the extratropical cyclones affecting the region over two autumn seasons and found that the precipitation on the windward slopes is enhanced in both unblocked and blocked flow patterns; with the latter, the enhancement begins well upstream of the mountain slopes.

[60] Figure 7 addresses both the unblocked and blocked cases as seen in the Alpine region during MAP. In unblocked cases, the moist static stability is near neutral or slightly unstable, allowing the cross-barrier flow component to rise over the terrain with little resistance. The flow may occasionally release convective cells over the terrain if it is slightly unstable. Whether or not the flow is unstable, the rapid upslope flow over the first significant ridge in the terrain leads to enhanced localized formation of cloud liquid water particles. Above the melting level, the snow particles

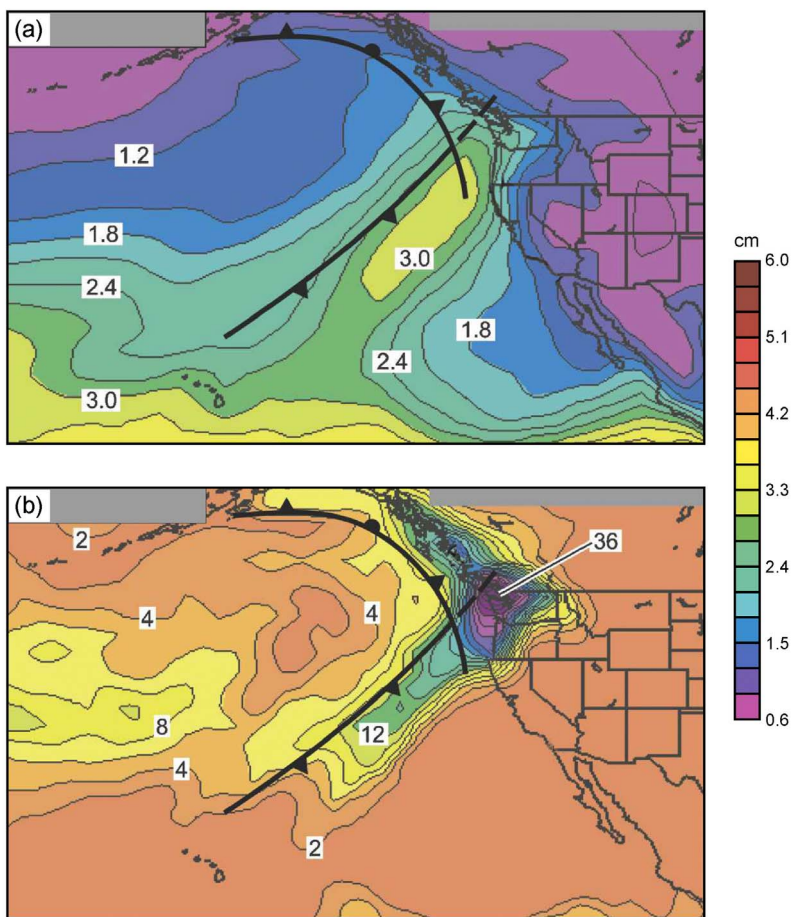


Figure 29. Composite mean (a) integrated water vapor (cm; see color scale) and (b) daily rainfall (in mm) for wintertime moisture plumes intersecting the northwestern coast of the United States. From Neiman *et al.* [2008]. Copyright 2008 American Meteorological Society.

in the preexisting widespread cyclonic storm cloud are provided with a local zone of enhanced liquid water, which can be collected by ice particles, which can then fall quickly as graupel particles into the warm layer of rain below the 0°C level and ultimately to the ground on the windward slope of the ridge. Figures 31a–31c show an example of an unblocked case seen by polarimetric Doppler radar in MAP. The data are a time composite for a 3 h period. Figure 31a shows that the cross-barrier upslope flow is maximum at low levels as it rises over the first ridge of the Alpine barrier. Figure 31b shows the intensified reflectivity cell over the windward slope of the ridge. Figure 31c shows the frequency of occurrence of particle type inferred from the polarimetric signal (using the technique of Vivekanandan *et al.* [1999]). Graupel particles are shown to be contributing to the reflectivity cell over the first ridge. The MAP radar data documented primarily the first ridge of the Alpine barrier since the low levels ahead of the second and third ridges were obscured from the view of the radar by the first ridge. In their examination of the Eureka, California, radar data, James and Houze [2005] found reflectivity maxima over the secondary and tertiary ridges as well as the first ridge encountered by the cross-barrier flow.

[61] Figures 31d–31f show an example of a blocked case. The cross-barrier flow shown in Figure 31d contrasts sharply with that in Figure 31a. The observations in Figure 31d were obtained by airborne radar, which (unlike the ground-based radar of the other plots) had a view unobstructed by intervening terrain. The aircraft radar showed a layer of retarded flow hugging the barrier at low levels. The retarded layer was bounded at its top by a strong shear layer separating it from unblocked cross-barrier flow at higher levels. The airflow in this case was generally stable, and the radar data in Figure 31e show a well-defined radar bright band where the ice particles forming at higher levels were falling and melting. Interestingly, in Figure 31f, the polarimetric retrieval indicates graupel at the top of the bright band layer. Data from a vertically pointing X-band Doppler radar located on the windward slope of the Alps in this storm showed vertical velocity updrafts $\sim 1\text{--}3 \text{ m s}^{-1}$ located at regularly spaced intervals of a few kilometers in a 2 km deep layer just above the bright band in the same storm. These observations indicate that in and just above the layer of shear, the air was undergoing turbulent overturning. This cellularity would make it more likely for precipitation particles to collide and grow by aggregation or riming. The

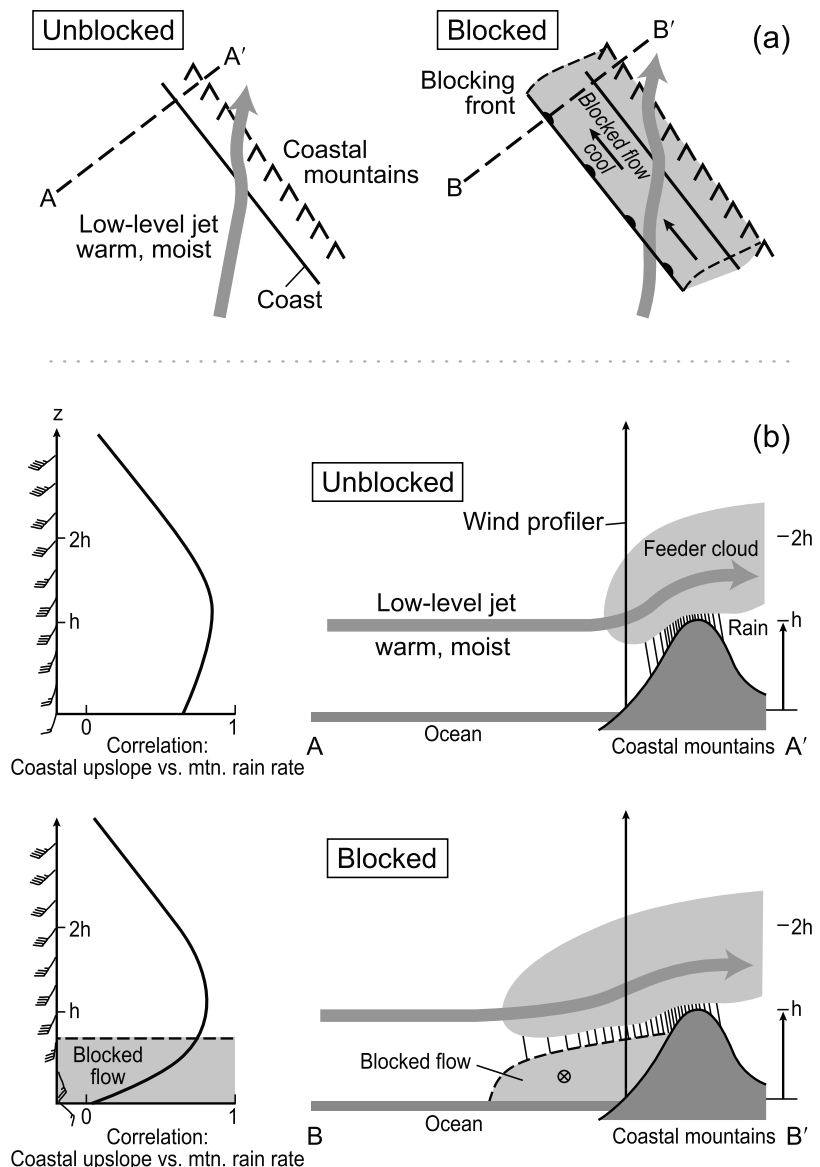


Figure 30. Conceptual representation of orographic rainfall distribution in California's coastal mountains and the impact of terrain-blocked flow on this distribution: (a) plan view and (b) cross-section perspective, with representative coastal profiles of wind velocity (flags = 25 m s^{-1} , full barbs = 5 m s^{-1} , half barbs = 2.5 m s^{-1}) and correlation coefficient (based on the magnitude of the upslope flow at the coast versus the rain rate in the coastal mountains) shown on the left. The variable h in Figure 30b is the scale height of the mountain barrier. The spacing between the rain streaks in Figure 30b is proportional to rain intensity. The circled cross within the blocked flow in Figure 30b portrays a terrain-parallel barrier jet. From Neiman *et al.* [2002]. Copyright 2002 American Meteorological Society.

turbulent updrafts produce pockets of elevated supercooled water content so that the snow particles present in the cloud layer above the bright band (also shown by the polarimetric radar data in Figure 31f) can collect this water and grow by riming into graupel particles such as were detected by polarimetric radar.

[62] Houze and Medina [2005] found similar behavior in frontal systems passing over the Cascade Mountains of central Oregon in the United States. In a sequence of Pacific storms, the cross-barrier flow at lower levels was retarded (though not completely blocked). The retarded low-level flow was bounded above by strong shear (similar to that

seen in the Alpine case), separating the lower layer from the strong westerlies at higher levels. Medina *et al.* [2005] conducted 2-D idealized simulations and found that in the presence of sufficient upstream static stability, orographic effects alone are sufficient to support development of the upward-sloping shear layer in the windward side of the barrier. Furthermore, they found that if there is preexisting vertical shear in the incident upstream flow, this shear is strengthened by the orography and by surface friction. Upstream soundings indicated stability through the layer of precipitating cloud, yet in every storm passage a layer of cellular overturning was centered on the shear layer and

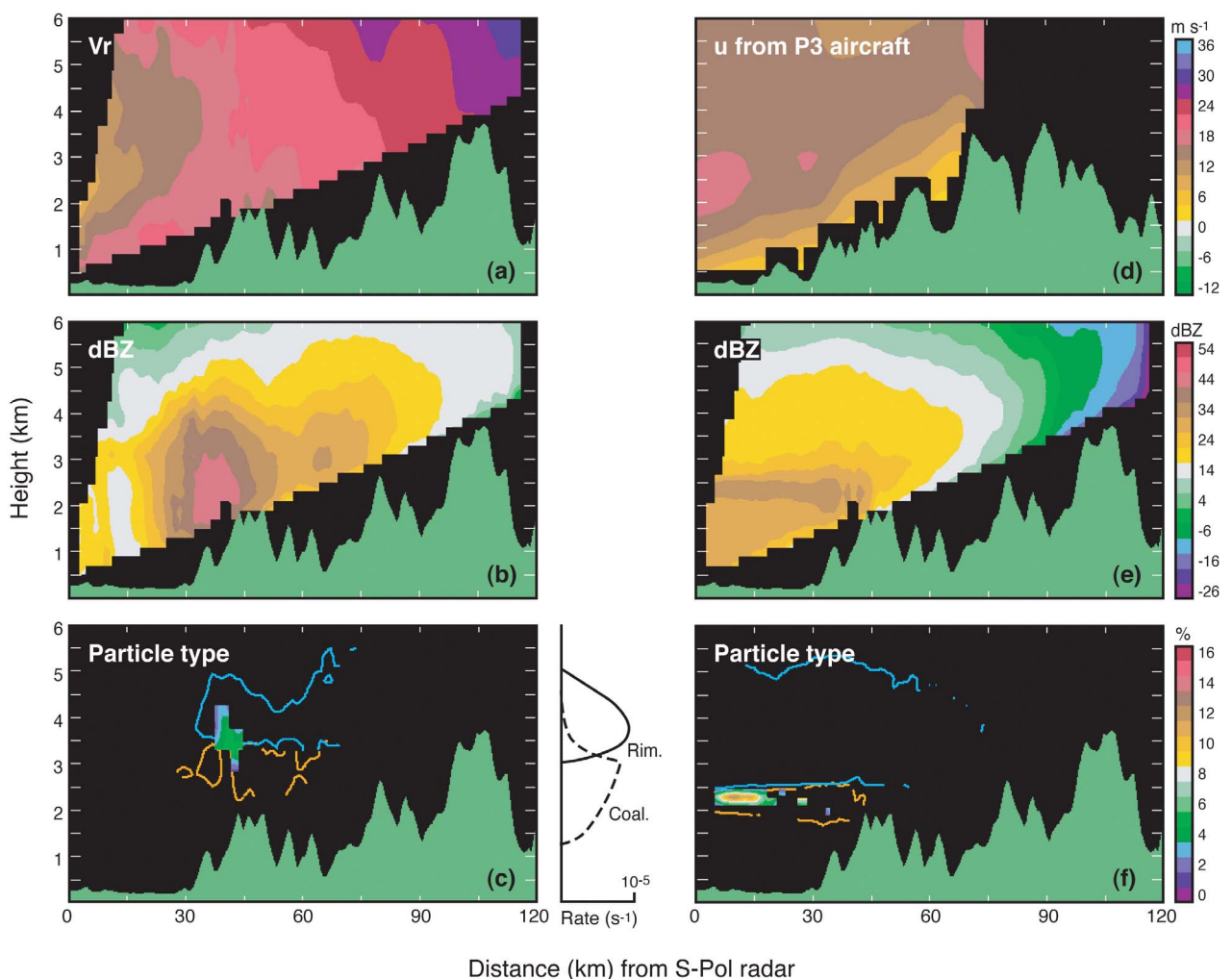


Figure 31. Three hour composite vertical cross sections of radar data (a–c) in MAP Intensive Observation Period (IOP) 2b and (d–f) in IOP 8. All data except those in Figure 31d are from the S-Pol radar, and all of the cross sections extend from the S-Pol radar location toward the northwest. The IOP 2b data are from 07:00–10:00 UTC on 20 September 1999, and the IOP 8 data are from 08:00–11:00 UTC on 21 October 1999, except for Figure 31d. Figure 31a shows 3 h mean radial velocity from the S-Pol radar. Figure 31d shows the wind component in the plane of the cross section indicated by airborne dual-Doppler radar measurements averaged over 09:00–10:00 UTC 21 October 1999. Figures 31b and 31e show 3 h mean radar reflectivity from S-Pol radar, and Figures 31c and 31f show 3 h accumulated frequency of occurrence of particle types identified by S-Pol polarimetric variables. Color shading indicates frequency of occurrence of graupel and/or dry aggregates during the 3 h of observations. Cyan (orange) contours surround the region in which dry snow (wet snow) was present 50% (30%) or more of the time. The diagram to the right of Figure 31c shows the rates of particle growth by coalescence and riming calculated by Yuter and Houze [2003]. All of the cross sections are adapted from Medina [2005] and Rotunno and Houze [2007]. Reprinted with permission from John Wiley.

extended up into the layer of snow of the preexisting widespread frontal cloud system passing over the mountains. These observations led to the conceptual model in Figure 8. Aircraft samples of ice particles in the snow layer were consistent with this interpretation, as they showed evidence of enhanced riming and/or aggregation of snow in the layer where the turbulent motions were located. Because of the static stability of the layer and the fact that in the shear layer the Richardson number was <0.25 , it was concluded that the precipitation growth and fallout are aided by small-scale

cellularity over the windward slope, whether the air being forced over the slope is statically unstable (as in Figure 7a) or statically stable (as in Figures 7b and 8).

[63] The results and inferences of Houze and Medina [2005] and Medina *et al.* [2005] are supported by a little-known but comprehensive master's thesis by Farber [1972]. Some of Farber's results were included in the Cascade Project overview paper of Hobbs [1975], but many important results lie buried in that obscure thesis. The Cascade Project examined some 100 extratropical cyclone passages over the

Cascade Mountains from 1969 to 1971. Farber subdivided the storms into prefrontal, transitional, and postfrontal sectors and analyzed microphysical and turbulence measurements. In the transitional sector, he noted a high degree of turbulence and high concentrations of both ice crystals and water droplets. He found that the degree of irregularity of the ice particle shapes was large and proportional to the turbulence. The concentration of aggregates had a high degree of variability, and the liquid water content and degree of riming were large in this sector of the storm. Similar to *Houze and Medina* [2005], he concluded that the “turbulent nature of the air enhanced collisions between crystals” and “pockets of moisture were observed in the liquid water content meter.” He further noted that the turbulence appeared to be originating from a combination of the air movement over local topographic features as well as strong vertical wind shears.

5.5. Low-Level Stable Flow Modification Ahead of Frontal Systems Approaching Mountains

[64] From the foregoing it is evident that stable or stagnant air may lie at the foot of a mountain range unable to ascend the barrier and that the air at slightly higher levels rises over this stable layer, producing clouds and precipitation upstream of the range, as if the mountains were effectively extended upwind (e.g., Figures 7, 8, and 30). The manner in which the low-level flow is blocked or retarded depends on the exact juxtaposition of the storm, its fronts, and the mountain range it is approaching or passing over. Sometimes low-level winds are blocked and turn parallel to the mountains (i.e., air tries to go around rather than over the mountains) so that air piles up between the approaching front and the mountain barrier. At other times, low-level stable air enters the region between the approaching storm and the mountain barrier from another region and becomes trapped between the oncoming storm and the mountains. In yet other situations, stable air is dammed against the mountains on the side of the barrier opposite to the approaching storm, creating an effective extension of the mountain range over which the warm moist “conveyor belt” (Figure 26a) must rise before it gets to either the approaching front or the intervening mountain range. All of these effects—blocking, retardation, trapping, and damming of low-level stable air ahead of approaching fronts—interfere with the basic organization of the extratropical cyclone, as would exist in the absence of topography (Figures 26a–26c). Although it is impossible to examine every conceivable combination of frontal structure, mountain range, and low-level airflow, several illuminating analyses have been done that illustrate how these low-level flow configurations modify the clouds and precipitation of an extratropical cyclone.

5.5.1. Approach of a Warm Front

[65] As noted in section 3.3, *Passarelli and Boehme* [1983] examined unblocked moist flow associated with warm frontal passages in the New England region of the United States and found that the observed enhancement of precipitation over small hills was consistent with the *Bergeron* [1965] seeder-feeder mechanism. *Doyle and Bond*

[2001] examined a Pacific warm front approaching the steep coastal mountain range of Vancouver Island (Figure 32). They analyzed aircraft data and modeled the low-level flow ahead of the warm front and found that the low-level winds ahead of the surface warm front formed a low-level jet squeezed into the wedge-shaped region between the front and the mountainous coast. The jet did not form as a barrier jet due to blocking but rather was a southeasterly cold stable flow emanating from the Strait of Juan de Fuca, a narrow gap between the Olympic Mountains to the south and the Vancouver Island range to the north. Although radar data (not shown) were limited, it appeared that in connection with the low-level flow modification between Vancouver Island and the warm front, the band of precipitation separated from the surface front and moved across the island with the midlevel flow.

5.5.2. Cold Fronts Approaching and Passing Over Mountains

[66] Cold fronts approaching the Appalachian Mountains are a good combination for examining how a front is affected when terrain lies in its path because the Appalachians are a long quasi 2-D barrier having a length and orientation (southwest-northeast) that are similar to those of the fronts typically approaching the mountain range. *Schumacher et al.* [1996] analyzed cold fronts oriented parallel to and approaching the Appalachians and found that over 55% of the fronts slowed down as they approached the barrier (Figure 33). The unretarded fronts were associated with stronger synoptic-scale baroclinic circulations at middle and upper levels, while the Froude number of the flow was not a strong indicator of retardation. They suggest (pp. 2465–2466) that “a stronger upper-level short-wave trough forces a stronger ageostrophic cross-frontal circulation and that this dynamically induced circulation overwhelms the mountain circulation and allows the front to propagate over the mountains.” *Chen and Hui* [1990] and *Gross* [1994] found that the mountains block colder air at low levels after retardation occurs. *Schumacher et al.* [1996] conjecture that such blocking behavior occurs between the Appalachians and the oncoming retarded front, but they did not investigate effects of blocking on precipitation formation processes. *Dickinson and Knight* [1999] confirmed and extended these interpretations with a simple 2-D model, which showed that when a mountain barrier retards and blocks the approaching front at the surface, the associated upper level PV anomaly sometimes moves across the domain unaffected. They found that when the upstream blocking is strong, frontal propagation is discontinuous across the ridge. This behavior occurs for tall mountains, narrow mountains, and weak fronts. For low mountains, wide mountains, and strong fronts, only weak retardation occurs on the windward slope, the surface front remains coupled with the upper level PV anomaly, and the front moves continuously across the mountain.

[67] *Parish* [1982] and *Marwitz* [1983, 1987] studied precipitation events over the Sierra Nevada Range in California. The relationship to fronts approaching from the Pacific Ocean is not very clear from their analyses and

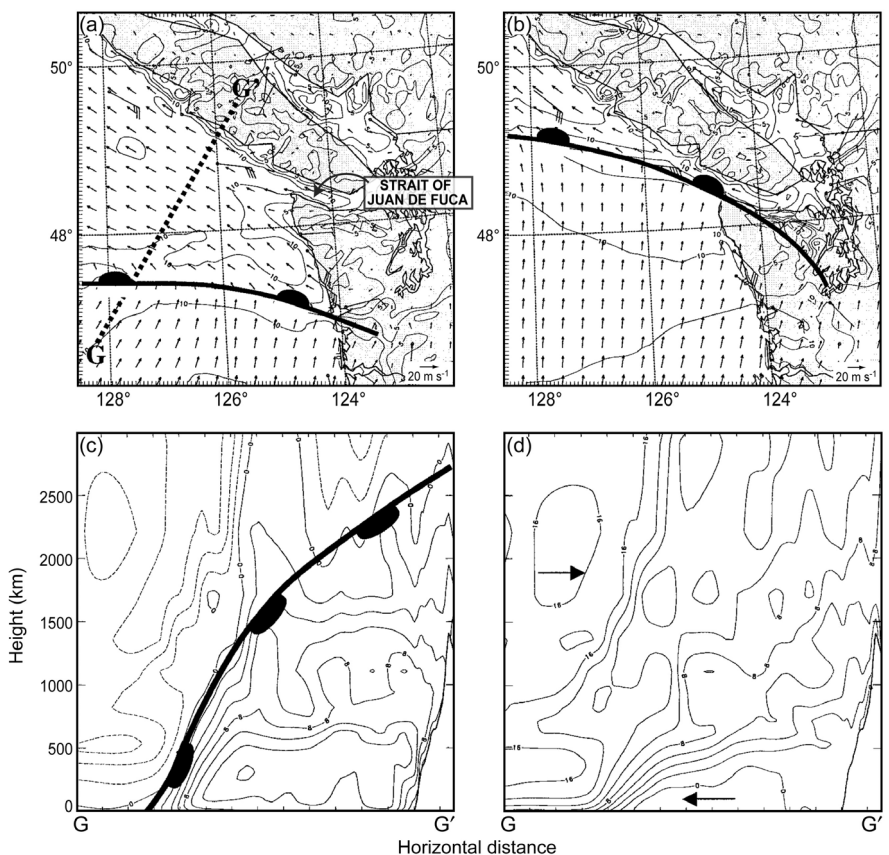


Figure 32. Horizontal maps show model-simulated 10 m winds for (a) 21:00 UTC 9 December 1995 and (b) 03:00 UTC 10 December 1995 with an isotach interval of 2.5 m s^{-1} . Selected surface wind observations are displayed with one full barb representing 5 m s^{-1} . Vertical cross sections show (c) coast-parallel (section normal) and (d) coast-normal (section parallel) model wind components along line GG' for 21:00 UTC 9 December 1995 with an isotach interval of 2.5 m s^{-1} , and wind maxima are denoted by the maximum speed labels in Figures 32b and 32c. From Doyle and Bond [2001]. Copyright 2001 American Meteorological Society.

modeling. However, in the situations that they studied, the low-level stable flow turned cyclonically to form a barrier jet, with air damming up against the Sierra Nevada barrier. These early findings are consistent with studies such as that of Braun *et al.* [1999a, 1999b], who used an idealized model to analyze a cold front approaching a plateau and found that the front was retarded and that the Coriolis force leads to a barrier jet, but that the barrier jet's strength is reduced in the presence of frictional forces. The results of Braun *et al.* [1999a, 1999b] further showed that frontogenesis is enhanced upstream of the upward sloping terrain. Examining airborne Doppler radar obtained in a front approaching the mountainous Oregon coast, Yu and Smull [2000] studied the zone of enhanced frontogenesis in the retarded frontal zone. They found that the shear in this zone favored upright convection [Rotunno *et al.*, 1988] and that the modification of the precipitation processes along the orographically retarded front led to the genesis of a narrow cold frontal rainband (Figure 26c). Analyzing airborne Doppler radar observations of a cold front approaching the Oregon coast, Braun *et al.* [1997] also found that the

convective clouds along the front were organized in a narrow cold frontal rainband and that as the front approached to within 20 km of the Oregon coast, deformation of the frontal zone appeared to cause the dissipation of precipitation cores along the front.

[68] Barrett *et al.* [2009] used the Weather Research and Forecasting (WRF) model to study changes in low-level flow and precipitation patterns when a cold front approaches the Andes from the South Pacific Ocean. Figure 34 shows three physically distinct precipitation zones. A Pacific precipitation zone (PPZ), located over the southeastern Pacific west of the Chilean coast; a coastal precipitation zone (CPZ), extending from the eastern edge of the PPZ along the Chilean coast eastward to the Andes Cordillera; and a windward precipitation zone (WPZ), located over the high Andean terrain. Each precipitation feature was directly related to the lower- and middle-tropospheric wind field, including a barrier jet. At the start of the simulation, the PPZ was located over the southeastern Pacific west of Chile and oriented from southeast to northwest (Figure 34a). The CPZ, in contrast, was located along the central Chilean coast with

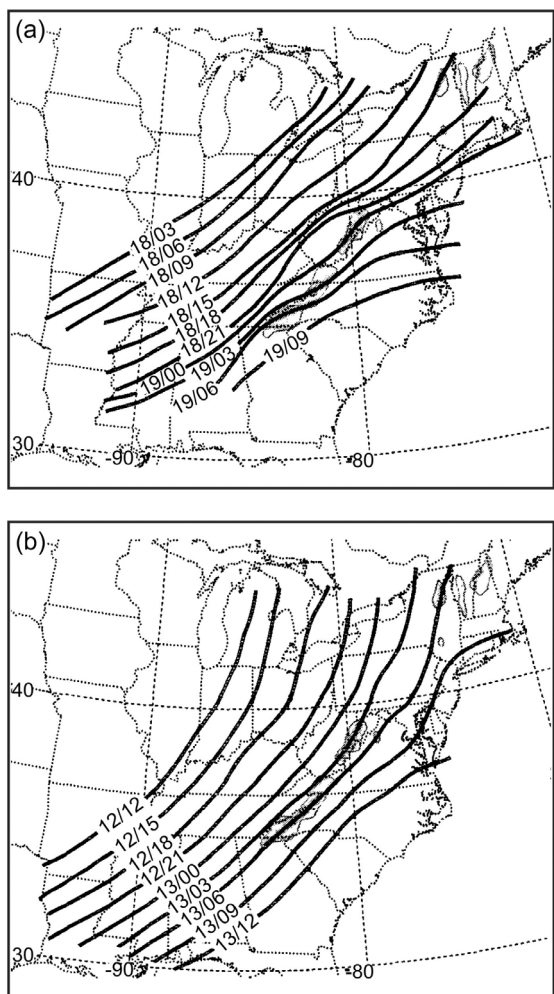


Figure 33. Isochrones of frontal position at 3 h intervals (UTC) for (a) a retarded front on 18–19 January 1990 and (b) an unretarded front on 12–13 January 1989. From Schumacher *et al.* [1996]. Copyright 1996 American Meteorological Society.

a more meridional orientation. The PPZ joined the CPZ 50 km west of the coast. Over time, the PPZ maintained its southeast to northwest orientation while advancing steadily equatorward (Figures 34b–34d). The CPZ advanced equatorward slowly and stalled over central Chile and became oriented nearly parallel to the coast. This change in orientation has also been seen in cold front–terrain interactions off the California coast [Doyle, 1997; James and Houze, 2005]. The WPZ formed in advance of the front and was well developed over the Chilean cordillera as zonal wind speeds increased and static stability decreased ahead of the approaching upper level trough; that is, the Froude number in this region became high enough to allow the flow to cross the barrier. Similar to the coastal CPZ, the WPZ did not advance northward as rapidly as the PPZ. The turning of the low-level flow to form the barrier jet is evident in Figure 35a. The air at slightly higher levels was not turning, and in Figure 35b it can be seen to have been rising over the blocked flow as shown conceptually in Figures 7 and 30.

The shading in Figure 34 indicates the precipitation enhancement in response to the lifting upstream of the mountain barrier. Analyzing a somewhat similar frontal system passing over the Cascade Mountains of Oregon, Garvert *et al.* [2007] showed, from fifth-generation Pennsylvania State University–National Center for Atmospheric Research (PSU–NCAR) Mesoscale Model (MM5) simulations plus airborne Doppler radar and other field experiment data, how the low-level flow parallel to the mountain barrier responded to the higher wave number ridges and valleys of the mountain range, while the cross-barrier flow rising over the lower layer of barrier-parallel flow was more responsive to the low-wave number, barrier-scale structure of the range (Figure 36). Minder *et al.* [2008] examined the subbarrier scale of the Olympic Mountains of Washington State and found that the rainfall maxima occur over ridges and minima in valleys (Figure 37). This result is consistent with the findings of Medina and Houze [2003], who found the radar echo maxima occurred over the first sharp rise of terrain on the Mediterranean side of the Alps. James and Houze [2005] found radar echo maxima over each individual ridge of the coastal mountains of California as well as a broader response on the scale of the larger mountain barrier.

5.6. Cold-Air Damming and Down-Valley Flow

[69] Sometimes a major mountain range is located between an approaching baroclinic wave and frontal system, so that the conveyor belt that rises to produce much of the storm's precipitation must first rise over the intervening mountain range. This situation is further complicated if a layer of cold air lies adjacent to the mountain range and the approaching storm so that the conveyor belt air must first rise over the pool of cold air before it reaches the intervening mountain range. This type of situation occurs on the Mediterranean side of the Alps ahead of baroclinic troughs approaching the Alps from the west. Houze *et al.* [2001] showed that the precipitation maximum associated with the Alps occurred upstream of the mountains in low Froude number situations. A well-documented case occurred in October 1999 during the Mesoscale Alpine Programme. Figure 38a [from Medina and Houze, 2003] and Figure 38b [from Bousquet and Smull, 2003] show easterly flow across the Po Valley, upstream of the Alps. Much of this cold stable air was coming into the region from eastern Europe. The conveyor belt air from the southwest was shown by radar data obtained in this case to be rising over the low-level air layer of weak cross-barrier flow in Figures 31d–31f. The cyclonic turning of the winds in Figure 38a suggest that the low-level easterly flow in the Po Valley was in part due to blocking by the Alps. Certainly the low-level air was not rising over the Alps, and in the individual river valleys the low-level flow was in the down-valley direction (Figure 38b). The down-valley flow was documented by the Doppler on Wheels (DOW) radar. Steiner *et al.* [2003] analyzed the DOW data together with wind profiler observations and sounding data and suggested that the down-valley flow occurred below the melting level (Figure 39), which is consistent with the hypothesis that the down-valley flow is in part driven by

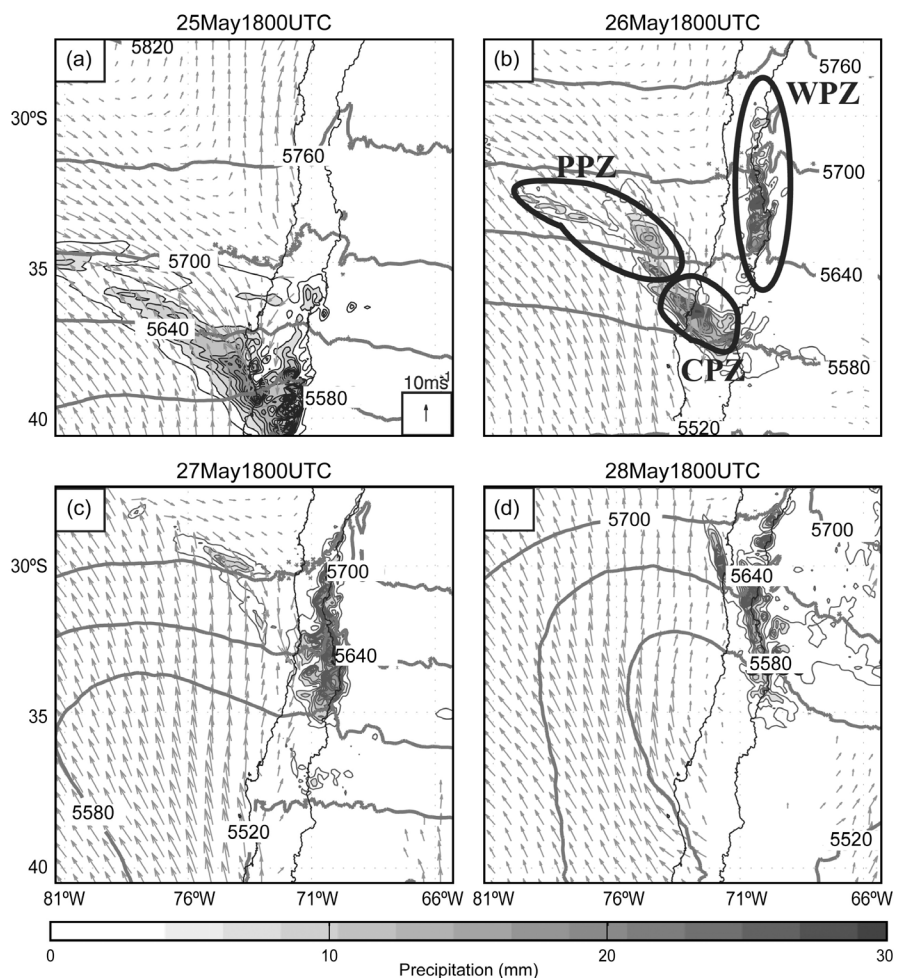


Figure 34. Model output of 3 h precipitation totals, 975 hPa wind, and 500 hPa geopotential height. Wind speed is scaled to 10 m s^{-1} , and geopotential height is contoured every 60 m. The three precipitation features identified in Figure 34b are the Pacific precipitation zone (PPZ) located over the southeastern Pacific Ocean, the coastal precipitation zone (CPZ) located over the Chilean coast and central valley, and the windward precipitation zone (WPZ) located over the high cordillera along the Chile–Argentina border. From *Barrett et al. [2009]*. Copyright 2009 American Meteorological Society.

melting and evaporational cooling at low levels, much as would be a downdraft in the trailing stratiform region of a squall line [Zipser, 1977; Houze, 1977]. These results were confirmed in a model simulation by *Asencio and Stein* [2006]. However, they also found that down-valley flow can sometimes be produced by the dynamics of blocking rather than diabatic effects.

[70] Another prime location for low-level cold-air damming occurs on the Atlantic side of the Appalachian Mountains. As described by *Keeter et al. [1995]*, it is common for cold air from the northeastern United States to flow south-southwestward along the edge of the Appalachians, while warm moist subtropical air from the Gulf of Mexico and Atlantic Ocean approaches from the lower latitudes (Figure 40). As shown by *Bell and Bosart* [1988], this warm air first ascends over the dammed cold air and then the mountains before it can rise over any front that might be approaching from the west (Figure 41). *Barros and Kuligowski* [1998] described how this process could lead to precipitation on the Atlantic side of the Appalachians.

5.7. Vertical Structure Changes of an Extratropical Cyclone Traversing a Mountain Range

[71] In sections 5.1–5.6 we have examined specific ways that mountains can interfere with and modify the horizontal and vertical air motions of a frontal system approaching mountains. The effects can be so strong that the basic structure of the clouds and precipitation of an extratropical cyclone can be completely overwhelmed and changed. In the absence of terrain the different sectors have recognizable mesoscale horizontal patterns of clouds and precipitation (e.g., the rainbands and convective elements evident depicted in Figures 26b and 26c). When the air motions are strongly modified by mountains, the different sectors of the storm are more recognizable by changes in the vertical profiles of the cloud and precipitation processes. The kinematic and stability properties of the air vary between the leading, middle, and trailing portions of the extratropical cyclone, and the orographically modified motions produce different effects in each part of the storm. *Medina et al.*

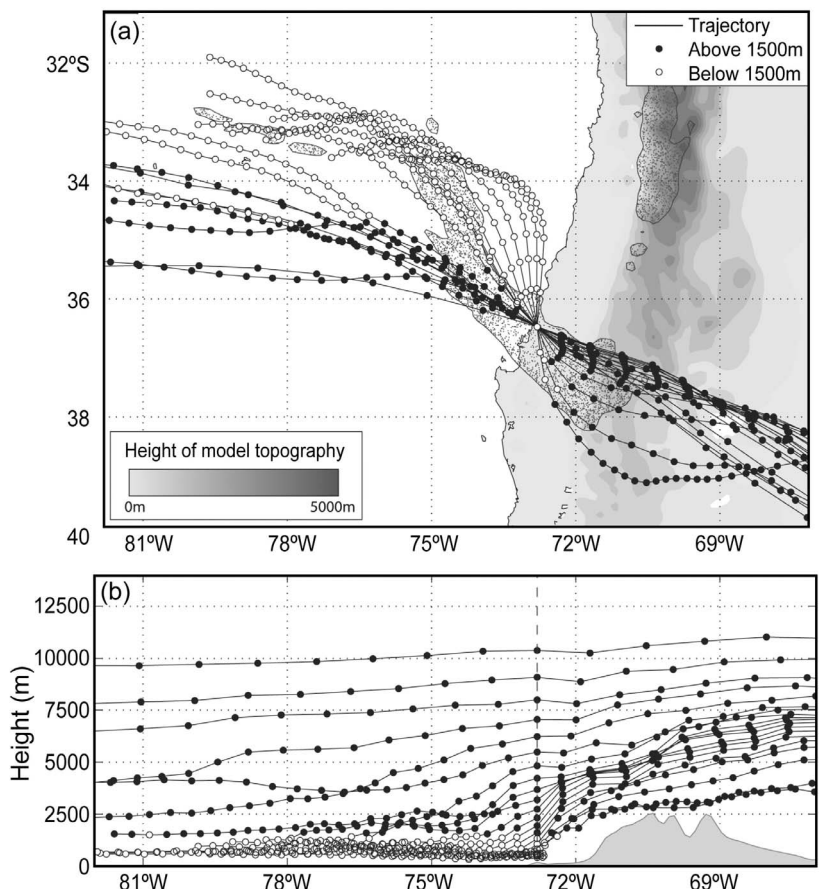


Figure 35. Trajectories of parcels passing through a point located just north of a cold front crossing the west coast of South America. Open (solid) circles represent hourly parcel locations below (above) 1500 m. In Figure 35a, model 3 h rainfall is stippled and terrain height is shaded. The cluster of below 1500 m parcels arriving at the cold front from the north represents the barrier jet. From *Barrett et al. [2009]*. Copyright 2009 American Meteorological Society.

[2007] examined the passage of occluded frontal systems over the Cascade Mountains of Oregon as observed by vertically pointing S-band radar. They divided the storms into early, middle, and late sections, as indicated in Figure 26b. These three sectors and their observed behavior as described by *Medina et al. [2007]* are consistent with *Farber [1972]* (see also section 5.4). The vertical structure of the storm varied as shown in Figures 42a–42c, respectively.

[72] In the early sector of a cyclone, a “leading edge echo” appears aloft and descends toward the surface, gradually at first and then more abruptly, until a deep stratiform echo period extends from the surface to approximately 6–7 km. It begins as an elevated echo and tends to consist of relatively uniform snow. Updraft cells inferred from the vertically pointing Doppler radial velocity are sometimes embedded in the leading edge echo at upper levels. When cold air arrived aloft in this sector, the cells in the leading edge echo layer were numerous, but in most cases cells were infrequent, weak, or absent. The early period of the storm passage seen by *Medina et al. [2007]* over the Cascades was similar to the warm frontal radar echo seen in cloud radar data by *Locatelli and Hobbs [1987]* as storms first moved over the

Pacific Northwest coast, before the storms reached the mountains. By comparison with that study, the leading edge echoes over the mountains do not appear to have been qualitatively altered by the orography. However, over the Cascades the leading edge echo over the mountains is typically weakened at lower levels by lower level easterly downslope flow.

[73] In the middle sector, the radar echo consists of a thick, vertically continuous layer extending from the mountainside up to a height of approximately 5–6 km. When the middle sector passed over the windward slope of the Cascades, the vertical structure of the radar reflectivity exhibited a “double maximum echo.” One maximum was the radar reflectivity bright band. The second reflectivity maximum was located ~1–2.5 km above the bright band. This upper maximum was also seen in California storms approaching the Sierra Nevada Range by *Kingsmill et al. [2006]*. There is some debate as to whether this secondary maximum is associated with modification of the storm by its passage over the mountain range. *Medina et al. [2007]* found that this maximum did not appear in the Cascades cases until the middle sector was passing over the windward slope

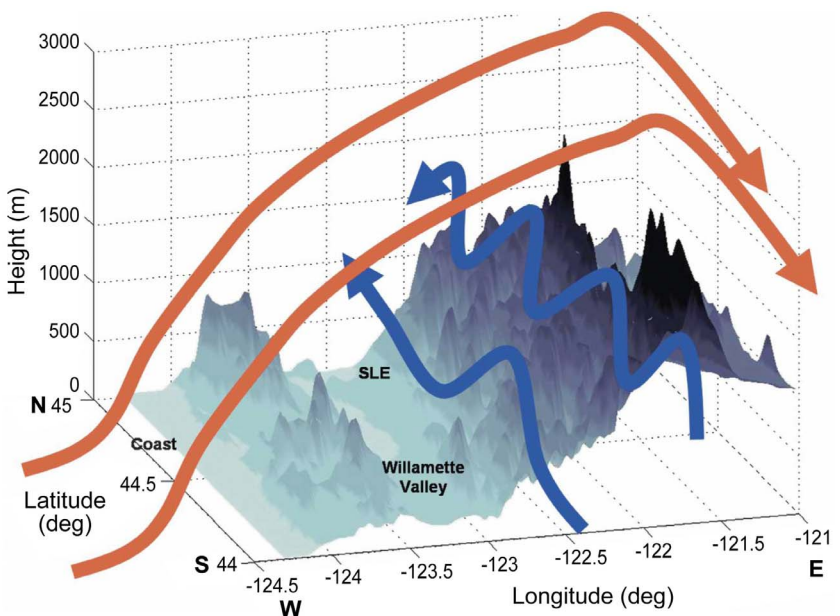


Figure 36. Three-dimensional schematic of topography and wind flow over a portion of the Oregon Cascade Mountains as observed from 23:00 to 01:00 UTC 13–14 December 2001. Blue arrows show strong southerly low equivalent potential temperature airflow at low levels along the windward (west facing) slopes. Red arrows show the high equivalent potential temperature airflow that surmounted the low equivalent potential temperature airflow and exhibited a vertically propagating mountain wave structure anchored to the mean north-south Cascade crest. From *Garvert et al. [2007]*. Copyright 2007 American Meteorological Society.

of the Cascades, suggesting that it resulted from or was enhanced by the interaction of the baroclinic system with the terrain. In the intervening region between the two reflectivity maxima, there was a turbulent layer with updraft cells ($>0.5 \text{ m s}^{-1}$), spaced $\sim 1\text{--}3 \text{ km}$ apart. This turbulent layer is thought to be crucial for enhancing the growth of precipitation particles and thus speeding up their fallout over the windward slope of the Cascades.

[74] In the late sector of the Cascade storms, the precipitation consisted of generally isolated shallow convection echoes, with low echo tops and, in some cases, upward motion near the tops of the cells. The shallow convection echoes became broader upon interacting with the windward slope of the Cascade Range, suggesting that orographic uplift enhances the convective cells, perhaps by the mechanism depicted in Figure 6 and described by *Kirshbaum and Smith [2009]*. In the period of shallow convection echoes, the precipitation decreases very sharply on the lee slope of the Cascades.

6. TROPICAL CYCLONES ENCOUNTERING MOUNTAINS

[75] Much is known about the cloud and precipitation structure of tropical cyclones. *Houze* [2010] categorized the rainfall features of a tropical cyclone as primary eyewall, secondary eyewall, principal rainband, secondary rainbands, and distant rainbands. Despite this detailed knowledge of storm structure derived from observations and models, relatively little research has been done on the interaction of

these elements of tropical cyclones with topography, yet some of the greatest tropical cyclone disasters occur when a cyclone passes over mountainous terrain. For example, Hurricane Mitch (1998) caused over 9000 deaths when the storm encountered the complex terrain of Central America (<http://www.nhc.noaa.gov/1998mitch.html>). *Lin et al. [2001, p. 633]* found that four common ingredients for especially heavy local rain and flooding over mountainous

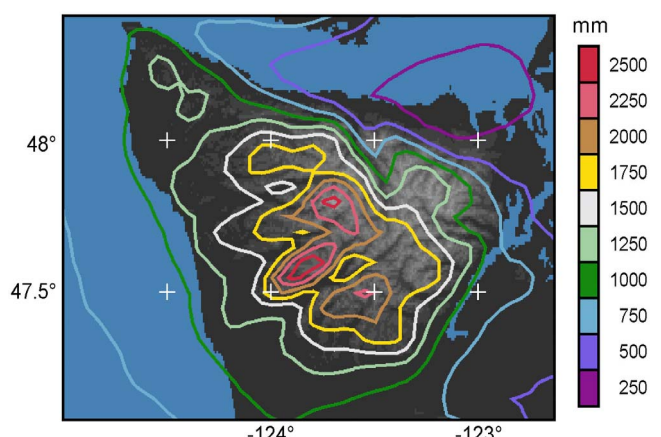


Figure 37. Five year average November–January rainfall (mm) over the Olympic Mountains produced by a high-resolution model simulation and verified against rain gauge data by *Minder et al. [2008]*. The model output shown by Minder et al. has been replotted here. From *Minder et al. [2008]*. Reprinted with permission.

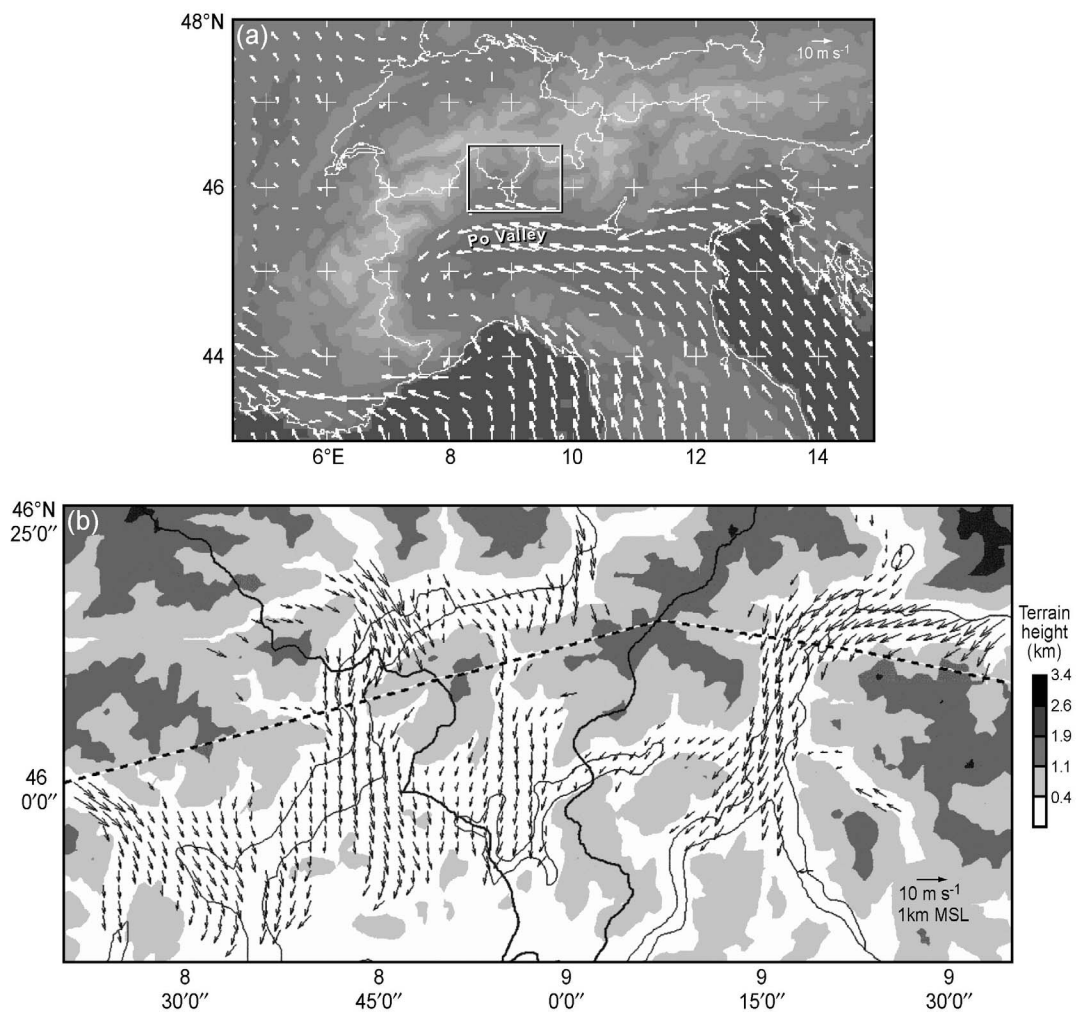


Figure 38. (a) Mean wind at 940 hPa near the Alps as computed from the atmospheric Mesoscale Compressible Community numerical forecast model (MC2) topography and storm mean wind field around the Alps at 940 hPa for the time period 12:00 UTC 20 October to 22:00 UTC 21 October 1999. (b) Airborne dual-Doppler synthesis of airflow at a height of 1 km msl based upon data collected during the interval 12:55–13:10 UTC 21 October 1999. Dashed line indicates aircraft flight track. Figure 38a from *Medina and Houze* [2003] and Figure 38b from *Bousquet and Smull* [2003]. Reprinted with permission from John Wiley.

regions were “1) a conditionally or potentially unstable airstream impinging on the mountains, 2) a very moist low-level jet, 3) a steep mountain, and 4) a quasi-stationary synoptic system to slow the convective system over the threat area.” Since these conditions are all met when the circulation around a tropical cyclone intersects a mountain range, it is not surprising that flooding and associated disasters occur. Yet the details of what happens when such an intersection occurs have not yet been thoroughly investigated. Here we summarize what is known at this time about orographic effects on the clouds of tropical cyclones.

[76] *Smith et al.* [2009] studied a rainband (probably a principal rainband) of a tropical cyclone positioned over the small mountainous Caribbean island of Dominica (Figure 43). They found that the precipitation was well described by linear wave dynamics and particle growth mechanisms such as those illustrated in Figure 4. These

idealized 2-D linear dynamics combined with assumed microphysical time scales for growth and fallout of particles accounted for enhanced precipitation on the windward slope of the island and decreased rainfall on the leeward ocean side (Figure 43a). Their results were consistent with radar observations and are summarized conceptually in Figure 43b. *Yu and Cheng* [2008] arrived at similar conclusions regarding the fallout of rain in relation to orographic upslope and downslope flow superimposed on rainbands of Typhoon Xangsane (2000) and further showed how the height of the mountains determines whether the rainfall maximum will be on the windward or leeward slope of the mountain (Figure 44). It is not surprising that the linear gravity wave dynamics work well in describing the response of the tropical cyclone winds impinging on a terrain barrier because a tropical cyclone is largely a conditionally symmetrically neutral circulation [*Emanuel*, 1986;

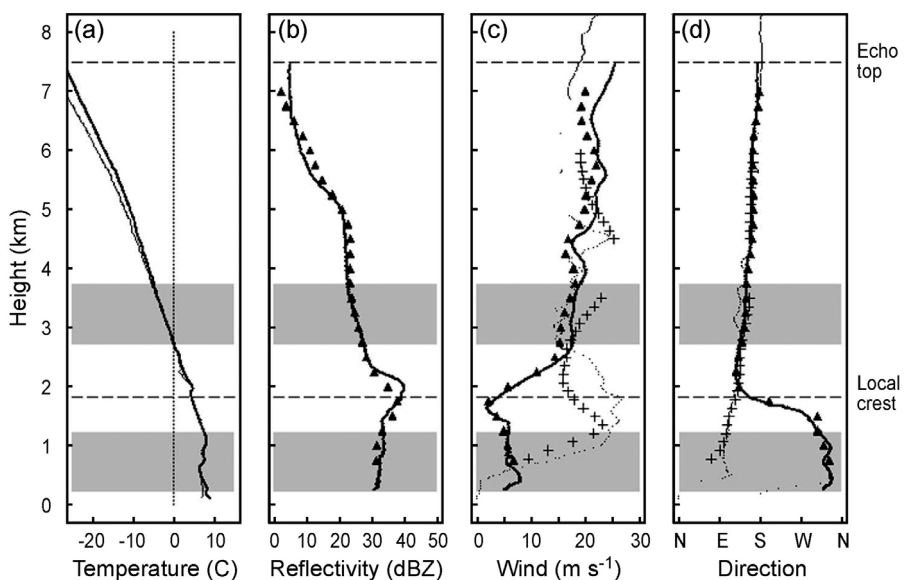


Figure 39. Vertical profiles of temperature, precipitation, and wind as recorded by a rawinsonde launched at 12:00 UTC from Milano-Linate airport (dotted lines); a UHF wind profiler at Lonate Pozzolo (crosses); a ground-based mobile X-band Doppler radar deployed within the Toce River valley (solid lines); and an airborne X-band Doppler radar above the Toce River valley (solid triangles). All locations are in Italy on the Mediterranean side of the Alps. Measurements were made at about 09:50 UTC 21 October 1999. Temperature and dewpoint temperature from the sounding are in Figure 39a. Radar reflectivities from the ground-based and airborne radars are in Figure 39b. Wind speed and direction are in Figures 39c and 39d, respectively, from the ground-based and airborne radars, UHF profiler, and sounding. From Steiner *et al.* [2003]. Reprinted with permission from John Wiley.

Houze, 2010]; that is, the strong winds in the cyclone are not for the most part buoyantly unstable. The strong and nearly moist-neutral flow is not blocked but rather easily rises over the terrain, and the flow does not need to respond by triggering buoyant convection. Witcraft *et al.* [2005] found that heavy rain over the slope of a mountain encountered by the moist airflow of a tropical cyclone is enhanced by the convective available potential energy of the airstream. Although the airstream in the cyclone tends to be moist neutral the warm oceanic boundary layer keeps the air slightly unstable, and as pointed out by Houze [2010], buoyant convective cells are often superimposed on the generally slantwise overturning of the balanced vortex. The lifting over the mountainside releases this instability. Tang *et al.* [2011] have explored these effects further and found both convective triggering and gravity wave dynamics to be active in the tropical cyclone flow over the Central Mountain Range of Taiwan. When a rainband of Typhoon Nari (2001) and the associated strong azimuthal wind flow intersected the mountain range, convective cells were triggered on the upwind side (as suggested by Witcraft *et al.*'s [2005] analysis) while a gravity wave developed on the leeside (more or less as described by Smith *et al.* [2009]) where the thermodynamic and moisture stratification was stable. In addition, the convective cells triggered on the windward side were advected over to the leeside and interacted with the gravity wave.

[77] Geerts *et al.* [2000] examined the passage of Hurricane Georges (1998) over the island of Hispaniola. As the

storm passed over the island, measurements were made with a nadir-pointing X-band Doppler radar mounted on an ER-2 aircraft flying above the top of the storm. This data set captured the passage of the eye of the storm over the mountainous island, and the radar showed that intense convection broke out within the eye. Updrafts were over 20 m s^{-1} , and 35 dBZ echoes reached 12 km. The structure of one of these convective cells over the Cordillera Central is shown in Figure 45. Convection of such intensity was found to be consistent with the potential instability of a sounding within the eye of the storm prior to its passage over the island. Tropical cyclones are noted for subsidence in the eye producing a stable layer atop a highly mixed and energetically rich boundary layer [Willoughby, 1998; Houze *et al.*, 2007b; Houze, 2010]. The subsidence and stable layer prevent the outbreak of convection in the eye while the storm is over the ocean. This capping is like that seen east of major mountain ranges (Figure 31) preceding the outbreak of severe convection over the U.S. Great Plains [Carlson *et al.*, 1983], the Himalayas [Houze *et al.*, 2007b; Medina *et al.*, 2010], and Argentina [Rasmussen and Houze, 2011]. In this case, the capping is produced by the downward motion required by the balanced vortex dynamics of the tropical cyclone [Shapiro and Willoughby, 1982] rather than large-scale flow over an upstream mountain range. When Georges moved over the mountains of Hispaniola, the cap was evidently broken so that intense convection could be released.

[78] Finally, an area not yet adequately investigated is the passage of remnants of tropical cyclones, after they have lost

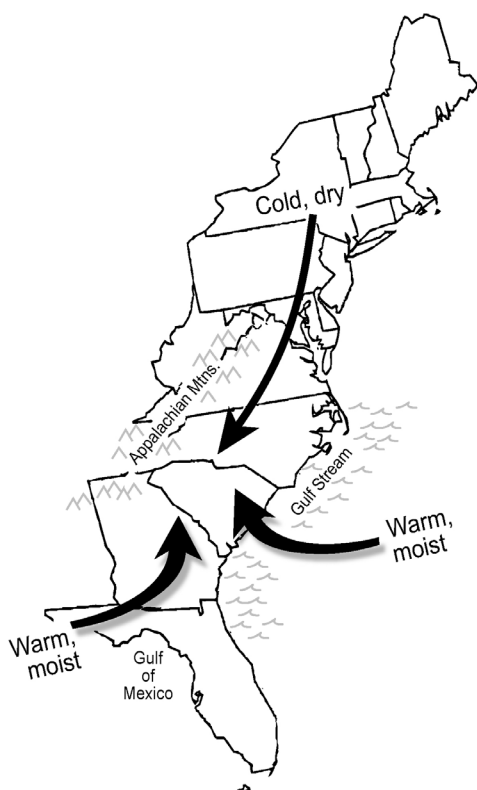


Figure 40. Typical flow pattern associated with cold-air damming on the east side of the Appalachian Mountains. From Keeter *et al.* [1995]. Copyright 1995 American Meteorological Society.

their connection with the ocean, with major mountain ranges. It is well known that these systems are climatologically important rain producers over land. It is likely that the remnant storms with their high moisture content, low static

stability, and still-strong winds have most of the characteristics enumerated by Lin *et al.* [2001]. They may in fact behave similar to Bay of Bengal lows in producing heavy rain upon encountering mountains [Barros *et al.*, 2006; Medina *et al.*, 2010; Houze *et al.*, 2011]. But the exact mechanisms in the case of former tropical cyclones remain to be determined.

7. CONCLUSIONS

[79] Mountains and hills have both direct and indirect effects on the formation of precipitation within clouds. By far the bulk of orographically affected precipitation comes from cloud systems that owe their existence to fundamental instabilities of the atmosphere but happen to form near or pass over uneven terrain. In this review, we have identified the direct and indirect effects of surface topography on the three major precipitating storm types: deep convective clouds, extratropical cyclones, and tropical cyclones.

7.1. Deep Convection

[80] Deep convective clouds arise from and derive their energy from buoyant instability associated with the temperature and moisture stratification of the large-scale atmosphere. Mountains and hills affect occurrence of precipitation due to deep convection by the following.

7.1.1. Triggering

[81] Potentially unstable flow striking even a small rise in terrain can allow convection otherwise capped by a stable layer to erupt. Foothills and small mountains near the bases of the Himalayas and Andes are especially effective in triggering some of the deepest and most intense convection on Earth.

7.1.2. Channeling and Capping

[82] Midlevel flow descending from higher terrain can cap convection and thus allow instability to build up. Capping is

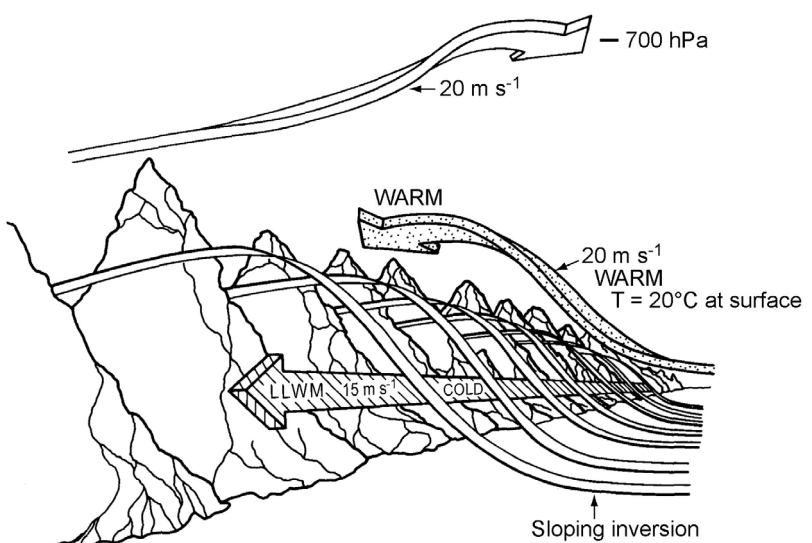


Figure 41. Conceptual model of cold-air damming east of the Appalachian Mountains. A strong low-level wind maximum (LLWM) lies within the cold dome. Easterly flow just above the cold dome advects warm air across the barrier. Southwesterlies at 700 hPa are associated with an advancing short-wave trough west of the mountains. From Bell and Bosart [1988]. Copyright 1988 American Meteorological Society.

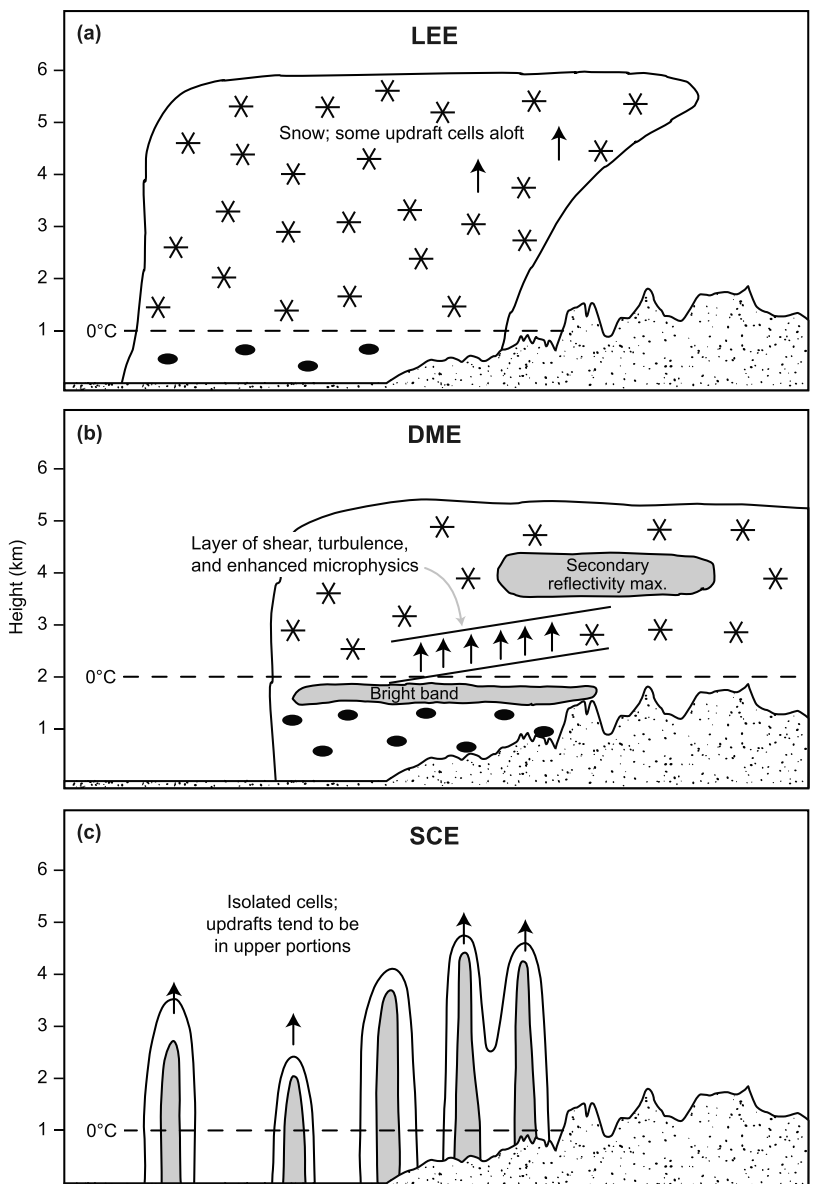


Figure 42. Schematic of the typical reflectivity structures observed in the (a) leading, (b) middle, and (c) trailing periods of midlatitude Pacific cyclones as they progress toward the terrain of the Cascade Mountains. The solid contours enclose areas of moderate reflectivity, while the shading indicates areas of increased reflectivity. The stars indicate snow, and the ellipses indicate rain. The speckled area shows the orography. The arrows represent updrafts. From *Medina et al. [2007]*. Copyright 2007 American Meteorological Society.

pronounced where flow descends the Afghan Plateau in South Asia and the Rocky Mountains in the U.S. Great Plains. Low-level moist airstreams from the Arabian Sea and Gulf of Mexico, respectively, are capped in these regions. The capping works in concert with channeling of the low-level moist flow. In the Himalayan region the flow from the Arabian Sea is confined by the Afghan Plateau to the west and the Himalayas to the north. Over the Great Plains of the United States, the low-level flow from the Gulf of Mexico is to some extent confined to flow northward east of the Rockies. Over South America, low-level moist flow from the Amazon is strongly channeled just east of

the Andes, while it is capped by midlevel flow crossing the Andes until the cap can be broken by the low-level flow encountering small mountains or foothills on the eastern edge of the Andes, usually in the latitude range of Argentina.

7.1.3. Enhancement of Mesoscale Stratiform Precipitation

[83] Mesoscale convective systems rich with moisture develop stratiform precipitation regions. The mesoscale upward motion in the stratiform regions is nearly moist-neutral and is easily enhanced by lifting over terrain when mesoscale convective systems move over mountain ranges.

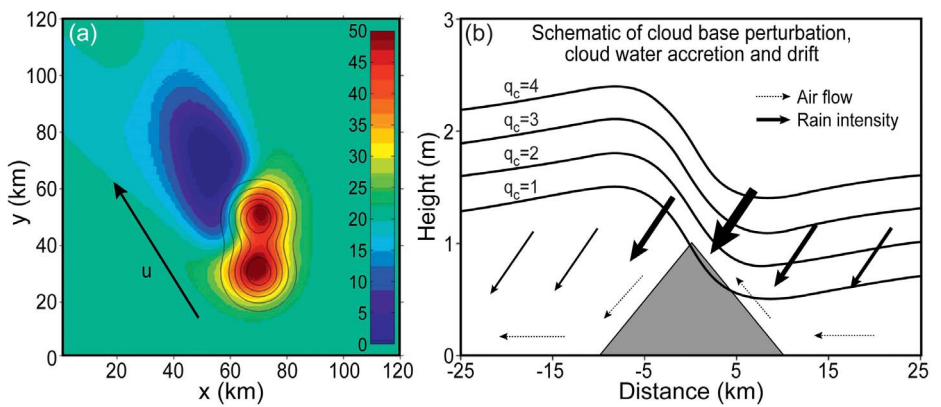


Figure 43. (a) Idealized linear model simulation of the precipitation (color coded in mm^{-1}) over the island of Dominica (contours showing the idealized topography) and surrounding ocean. The colors show the wet-dry dipole caused by the flow over the topography. (b) Schematic of the orographically affected precipitation process accounting for the wet-dry dipole. Curves are the contours of cloud water concentration (increasing aloft) as disturbed by forced ascent and descent. Thin arrows are the airflow. Heavy arrows represent falling rain. From *Smith et al. [2009]*. Copyright 2009 American Meteorological Society.

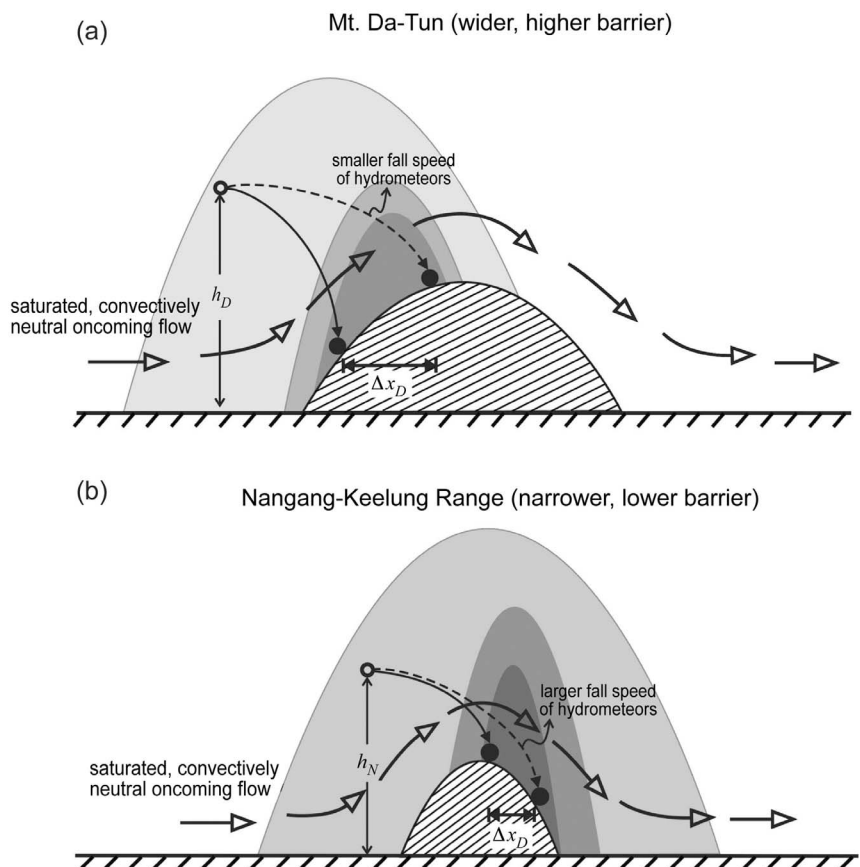


Figure 44. Schematic of precipitation fallout when rainbands of Typhoon Xangsane (2000) lay over mountains in the northern region of Taiwan. The diagrams illustrate the downstream shift of hydrometeors over mountains of different heights. Shading denotes the main region of heavy precipitation, with darker shading representing stronger precipitation intensity. Solid (dashed) arrows indicate the trajectory of hydrometeors in the weak (strong) oncoming flow condition. Open arrows denote airflow patterns over mountains. The h_D and h_N represent the altitude for hydrometeors starting their descent to the ground. The x_D and x_N represent the distance of downstream shift of hydrometeors. From *Yu and Cheng [2008]*. Copyright 2008 American Meteorological Society.

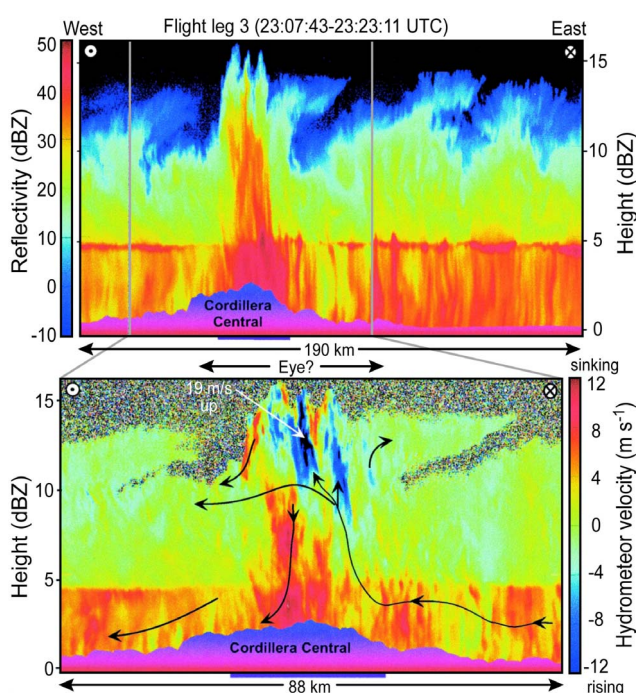


Figure 45. East-west cross section of (top) radar reflectivity and (bottom) Doppler radial velocity from an airborne nadir pointing Doppler radar aboard the NASA ER-2 flying over the Caribbean Sea and Hispaniola. The black lines with arrows are streamlines estimated from the radial velocities. From Geerts *et al.* [2000]. Copyright 2000 American Meteorological Society.

This type of enhancement is pronounced when mesoscale convective systems forming within Bay of Bengal depressions move over the mountains of Burma, northeastern India, and Bangladesh.

7.1.4. Diurnal Variability

[84] As is well known, daytime heating and nighttime cooling over high terrain produce convergence over mountaintop during the day and divergence at night. These effects are especially pronounced over the extreme Himalayan and Andes ranges, which are extremely high terrain located at lower latitudes where the solar insolation is direct. Convective cells are triggered over the high terrain during the day. However, mesoscale convective systems are generally not produced over the peaks but rather over the lowlands or ocean adjacent to the mountain range. Two processes are notable: (1) Where low-level moist flow impinges on the base of a mountain range—for example, the South Asian monsoon flow toward the Himalayas or the South American low-level jet—nighttime downslope flow off the mountain range often converges with the low-level flow to trigger mesoscale convective systems. (2) Mesoscale systems form as a delayed remote response at a distance from the mountain range when daytime heating and latent heat release over the high terrain either generate gravity waves propagating away from the range or potential vorticity anomalies, which are advected downstream of the mountains.

[85] Note that only one of the above effects is a direct enhancement of rainfall by condensation of water by forced lifting over terrain (enhancement of stratiform rain of mesoscale convective systems). The rest of the effects involve indirect influence of the mountains on the precipitating clouds: triggering, channeling, capping, and remote responses of the airflow's encounter with mountains.

7.2. Extratropical Cyclones

[86] In contrast, extratropical cyclones tend to be more directly affected by the flow over the terrain. Extratropical cyclones form as a result of baroclinic instability of the large-scale flow, and the cloud and precipitation patterns are determined by dynamics of the baroclinic disturbance that forms and its associated frontogenesis. When these storms pass over mountains, the clouds and precipitation undergo direct orographic modification to such a great extent that the basic baroclinic storm structure becomes barely recognizable. Orographic effects on the clouds and precipitation of extratropical cyclones include the following:

7.2.1. Atmospheric Rivers Impinging on Coastal Mountains

[87] In the general circulation of the atmosphere, especially over the great expanses of ocean, water vapor becomes concentrated into long narrow plumes flowing poleward and eastward out of the tropics into midlatitudes. The low-level jet required to keep a cold front in semigeostrophic balance helps to concentrate this moisture into an “atmospheric river” of water vapor. When the atmospheric river intersects the coastal mountain ranges of North and South America, the lifting of the atmospheric river over the mountain ranges produces a concentrated region of enhanced condensation and precipitation. This enhancement takes on various forms during the passage of a storm over the mountains.

7.2.2. Microphysical Time Scales, Air Motions, and Geometry of the Terrain

[88] No matter what configuration of extratropical cyclone and mountain range happens to occur, certain essential factors govern the response of the clouds and precipitation to the passage over the landform topography. One factor is the microphysical time scale. The mode of microphysical growth of particles (vapor diffusion, coalescence, riming, aggregation), and the resultant particle sizes and densities, and phase (liquid versus ice) can be lumped together in a microphysical time scale that describes how quickly condensed water can reach the ground. This time scale conflates with the time scale of the advective motions of air and the height and width of the terrain features to determine where the condensed water will fall to the surface. This location could be on either side of the crest and at lower or higher elevation, entirely dependent on how these factors combine in a particular case.

7.2.3. Unblocked Flow

[89] If air is saturated, as in the clouds of an extratropical cyclone, if the moist static stability is near neutral, and if the cross-barrier wind component is even moderately strong, the saturated air easily rises over terrain. In such a flow, as has been observed on the Mediterranean side of the Alps,

ahead of a frontal system passing over the mountains from the west, the condensation and precipitation are strongly enhanced where the moist low-level flow from the Mediterranean Sea ascends the first substantial rise in terrain on the lower slopes of the barrier. If the air is slightly statically unstable, the precipitation might occur in intermittent bursts as the air moves over the lower slopes, but even if stable, the air rises and the clouds respond. What is somewhat surprising is that the microphysical time scale is short; that is, the enhanced precipitation falls out nearly immediately over the first rise of terrain. Accretion processes (coalescence and/or riming) must rapidly come into play to convert the cloud water droplets created by the orographic lifting component to rapidly falling precipitation particles quickly reaching the ground.

7.2.4. Blocking and Damming

[90] If the air at low levels within an extratropical cyclone is especially stable and/or slow moving, it will be blocked as it approaches the mountain range. It might be dammed, as in the case of cold air east of the Appalachians ahead of a front approaching the west side of the Appalachians. Or it might form a barrier jet, as in the case of a cold front approaching the coastal mountains of North or South America. In the case of the European Alps, cold stable unsaturated air from eastern Europe may come westward across the Po Valley and lie in front of the Alps while a baroclinic trough at midlevels approaches from the west. Along the California coast, cold stable air may lie in the way of a frontal system approaching from the west. In all of these cases, warmer, less stable upstream cross-barrier flow often rises up and over the layer of blocked or dammed air and leads to precipitating clouds forming at a distance upstream of the mountains. For blocked flow conditions, the precipitation maximum on the Mediterranean side of the Alps extends well upstream of the mountains.

7.2.5. Shear and Turbulence

[91] When a layer of strong unblocked cross-barrier flow lies over a layer of slower moving (e.g., blocked) air, the vertical shear of the cross-barrier flow is conducive to turbulent overturning, even if the flow is statically stable. Such a shear layer often occurs when an extratropical cyclone passes over a mountain range. In these cases, the shear layer and overturning occur within the broader precipitating cloud of the extratropical cyclone. The shear-induced overturning can produce small pockets of enhanced cloud liquid water content within the cloud layer. The snowflakes and raindrops within the cloud layer can quickly accrete the water in these pockets, thus growing more quickly by coalescence and riming than would be possible in the absence of the turbulent overturning layer. In effect, the shear-induced turbulence shortens the microphysical time scale.

7.2.6. Small-Scale Ridges and Valleys Versus Barrier-Scale Response

[92] In stable flows embedded in extratropical cyclones passing over large mountain ranges, a lower wave number gravity wave response to the mean barrier scale occurs through a deep layer, while at lower levels the vertical air

motions and precipitation have a higher wave number response, producing maxima of precipitation on the ridges and minima in valleys.

7.2.7. Variation of Vertical Structure Within an Extratropical Cyclone

[93] When an extratropical cyclone passes over a mountain range, the horizontal organization of its precipitation pattern becomes obscured by the orographic effects of blocking and forced ascent. At the same time, the vertical structure of the precipitating clouds takes on a systematic variation that changes from the early to middle to late stages of the passage of the storm system over the mountains. In the case of Pacific storms passing over the coastal mountains of the United States, the middle stage is marked by a turbulent shear layer that seems to increase the efficiency of fallout of precipitation over the windward slopes of the mountains.

7.3. Tropical Cyclones

[94] Tropical cyclones passing over complex terrain have not been studied nearly as much as other types of orographically affected cloud systems, despite the fact that passage of tropical cyclones over mountains produce some of the worst weather disasters. The few studies so far conducted have found the following results:

7.3.1. Tangential Winds in Rainbands and Eyewall Force Strong Upslope Flow

[95] When the strong conditionally symmetrically neutral tangential winds of a tropical cyclone impinge on mountains, enhanced upslope motion occurs as a part of a gravity wave response. Extremely concentrated rains can thus occur over slopes susceptible to runoff and flooding. The height of the mountains together with the microphysical and advective time scales determine whether the maximum rains will occur on the windward or lee side of the mountain.

7.3.2. Release of Capped Potential Instability in the Eye

[96] The eye of a tropical cyclone contains very high moist static energy (air with high equivalent potential temperature) in a boundary layer capped by subsidence in the eye of the storm. When the eye moves over mountainous terrain, the cap can be broken and intense convection can occur.

7.4. Final Comment

[97] This review has shown the variety of orographic effects that profoundly modify the structure of major precipitating cloud systems through combinations of dynamical response, terrain shape and size, and alteration of microphysical time scales. Although every orographic and storm combination is unique, this holistic examination of the principal storm types in the context of the major topographic features on Earth has revealed the primary processes that must be accounted for in the ever more detailed output of global and regional models tasked with weather forecasting and climate projections. As the Earth's climate fluctuates and trends toward warmer conditions, precipitation patterns affected will certainly change. The knowledge summarized

here provides a starting point for evaluating how these changes will manifest.

[98] **ACKNOWLEDGMENTS.** Socorro Medina, Ulrike Romatschke, and Kristen Rasmussen have been invaluable colleagues in the research leading to this paper and have provided numerous valuable comments on the manuscript. Ana Barros provided an especially helpful review. Stacy Brodzik's technical support has made the research possible. Beth Tully is responsible for the excellent graphics and editing of the text. This research was sponsored by NSF grant ATM 0820586 and NASA grant NNX 10AH70G.

[99] The Editor responsible for this paper was Alan Robock. He thanks Ana Barros and two anonymous reviewers.

REFERENCES

- Asencio, N., and J. Stein (2006), Origins of the reversed flow over the windward Alpine foothills during MAP IOP3 and IOP8, *Q. J. R. Meteorol. Soc.*, **132**, 297–316, doi:10.1256/qj.04.188.
- Awaka, J., T. Iguchi, H. Kumagai, and K. Okamoto (1997), Rain type classification algorithm for TRMM precipitation radar, in *Geoscience and Remote Sensing, 1997: IGARSS '97, Remote Sensing—A Scientific Vision for Sustainable Development*, vol. 4, pp. 1633–1635, Inst. of Electr. and Electron. Eng., New York, doi:10.1109/IGARSS.1997.608993.
- Baines, P. G. (1995), *Topographic Effects in Stratified Flows*, 482 pp., Cambridge Univ. Press, New York.
- Barrett, B. S., R. D. Garreaud, and M. Falvey (2009), Effect of the Andes cordillera on precipitation from a midlatitude cold front, *Mon. Weather Rev.*, **137**, 3092–3109, doi:10.1175/2009MWR2881.1.
- Barros, A. P., and R. J. Kuligowski (1998), Orographic effects during a severe wintertime rainstorm in the Appalachian Mountains, *Mon. Weather Rev.*, **126**, 2648–2672, doi:10.1175/1520-0493(1998)126<2648:OEDASW>2.0.CO;2.
- Barros, A. P., and T. J. Lang (2003), Monitoring the monsoon in the Himalayas: Observations in central Nepal, June 2001, *Mon. Weather Rev.*, **131**(7), 1408–1427, doi:10.1175/1520-0493(2003)131<1408:MTMITH>2.0.CO;2.
- Barros, A. P., and D. P. Lettenmaier (1994), Dynamic modeling of orographically induced precipitation, *Rev. Geophys.*, **32**, 265–284, doi:10.1029/94RG00625.
- Barros, A. P., M. Joshi, J. Putkonen, and D. W. Burbank (2000), A study of the 1999 monsoon rainfall in a mountainous region in central Nepal using TRMM products and rain gauge observations, *Geophys. Res. Lett.*, **27**, 3683–3686, doi:10.1029/2000GL011827.
- Barros, A. P., G. Kim, E. Williams, and S. W. Nesbitt (2004), Probing orographic controls in the Himalayas during the monsoon using satellite imagery, *Nat. Hazards Earth Syst. Sci.*, **4**, 29–51, doi:10.5194/nhess-4-29-2004.
- Barros, A. P., S. Chiao, T. J. Lang, D. Burbank, and J. Putkonen (2006), From weather to climate—Seasonal and interannual variability of storms and implications for erosion processes in the Himalaya, *Spec. Pap. Geol. Soc. Am.*, **398**, 17–38, doi:10.1130/S2006.2398(02).
- Barstad, I., and R. B. Smith (2005), Evaluation of an orographic precipitation model, *J. Hydrometeorol.*, **6**, 85–99, doi:10.1175/JHM-404.1.
- Bell, G. D., and L. F. Bosart (1988), Appalachian cold-air damming, *Mon. Weather Rev.*, **116**, 137–161, doi:10.1175/1520-0493(1988)116<0137:ACAD>2.0.CO;2.
- Bergeron, T. (1965), On the low-level redistribution of atmospheric water caused by orography, paper presented at the International Conference on Cloud Physics, Tokyo and Sapporo, Japan, Int. Assoc. of Meteorol. and Atmos. Phys. of the Int. Union of Geod. and Geophys., 24 May to 1 June.
- Bhushan, S., and A. P. Barros (2007), A numerical study to investigate the relationship between moisture convergence patterns and orography in central Mexico, *J. Hydrometeorol.*, **8**, 1264–1284, doi:10.1175/2007JHM791.1.
- Bousquet, O., and B. Smull (2003), Airflow and precipitation fields within deep Alpine valleys observed by airborne Doppler radars, *J. Appl. Meteorol.*, **42**, 1497–1513, doi:10.1175/1520-0450(2003)042<1497:AAPFWD>2.0.CO;2.
- Braun, S. A., R. A. Houze Jr., and B. F. Smull (1997), Airborne dual-Doppler observations of an intense frontal system approaching the Pacific Northwest coast, *Mon. Weather Rev.*, **125**, 3131–3156.
- Braun, S. A., R. Rotunno, and J. B. Klemp (1999a), Effects of coastal orography on landfalling cold fronts: Part I. Dry, inviscid dynamics, *J. Atmos. Sci.*, **56**, 517–533, doi:10.1175/1520-0469(1999)056<0517:EOCOOL>2.0.CO;2.
- Braun, S. A., R. Rotunno, and J. B. Klemp (1999b), Effects of coastal orography on landfalling cold fronts: Part II. Effects of surface friction, *J. Atmos. Sci.*, **56**, 3366–3384, doi:10.1175/1520-0469(1999)056<3366:EOCOOL>2.0.CO;2.
- Browning, K. A. (1974), Mesoscale structure of rain systems in the British Isles, *J. Meteorol. Soc. Jpn.*, **50**, 314–327.
- Browning, K. A. (1986), Conceptual models of precipitation systems, *Weather Forecasting*, **1**, 23–41, doi:10.1175/1520-0434(1986)001<0023:CMOPS>2.0.CO;2.
- Browning, K. A., F. F. Hill, and C. W. Pardoe (1974), Structure and mechanism of precipitation and the effect of orography in a wintertime warm sector, *Q. J. R. Meteorol. Soc.*, **100**, 309–330, doi:10.1002/qj.49710042505.
- Caracena, F., R. A. Maddox, L. R. Hoxit, and C. F. Chappell (1979), Mesoanalysis of the Big Thompson storm, *Mon. Weather Rev.*, **107**, 1–17, doi:10.1175/1520-0493(1979)107<0001:MOTBTS>2.0.CO;2.
- Carbone, R. E., J. D. Tuttle, D. A. Ahijevych, and S. B. Trier (2002), Inferences of predictability associated with warm season precipitation episodes, *J. Atmos. Sci.*, **59**, 2033–2056, doi:10.1175/1520-0469(2002)059<2033:IOPAWW>2.0.CO;2.
- Carlson, T. N., S. G. Benjamin, G. S. Forbes, and Y. Li (1983), Elevated mixed layers in the regional severe storm environment: Conceptual model and case studies, *Mon. Weather Rev.*, **111**, 1453–1474, doi:10.1175/1520-0493(1983)111<1453:EMLITR>2.0.CO;2.
- Chang, L. T.-C., G. T.-J. Chen, and K. K. W. Cheung (2008), Mesoscale simulation and moisture budget analyses of a heavy rain event over southern Taiwan in the Meiyu season, *Meteorol. Atmos. Phys.*, **101**, 43–63, doi:10.1007/s00703-008-0286-7.
- Chen, C.-S., W.-C. Chen, and W.-K. Tao (2004), Characteristics of heavy summer rainfall in southwestern Taiwan in relation to orographic effects, *J. Meteorol. Soc. Jpn.*, **82**, 1521–1543, doi:10.2151/jmsj.82.1521.
- Chen, C.-S., W.-C. Chen, Y.-L. Chen, P.-L. Lin, and H.-C. Lai (2005), Investigation of orographic effects on two heavy rainfall events over southwestern Taiwan during the Mei-Yu season, *Atmos. Res.*, **73**, 101–130, doi:10.1016/j.atmosres.2004.07.005.
- Chen, C.-S., Y.-L. Lin, W.-C. Peng, and C.-L. Liu (2010), Investigation of a heavy rainfall event over southwestern Taiwan associated with a subsynoptic cyclone during the 2003 Mei-Yu season, *Atmos. Res.*, **95**, 235–254, doi:10.1016/j.atmosres.2009.10.003.
- Chen, C.-S., Y.-L. Lin, N.-J. Hsu, and C.-Y. Chen (2011), Orographic effects on localized heavy rainfall events over southwestern Taiwan on 27 and 28 June 2008 during the post-Mei-Yu period, *Atmos. Res.*, **101**, 595–610, doi:10.1016/j.atmosres.2011.04.004.
- Chen, G. T.-J., Z. Jiang, and M.-C. Wu (2003), Spring heavy rain events in Taiwan during warm episodes and the associated large-

- scale conditions, *Mon. Weather Rev.*, 131, 1173–1188, doi:10.1175/1520-0493(2003)131<1173:SHREIT>2.0.CO;2.
- Chen, G. T.-J., C.-C. Wang, and D. T.-W. Lin (2005), Characteristics of low-level jets over northern Taiwan in Mei-Yu season and their relationship to heavy rain events, *Mon. Weather Rev.*, 133, 20–43, doi:10.1175/MWR-2813.1.
- Chen, S. S., and R. A. Houze Jr. (1997), Diurnal variation and life cycle of deep convective systems over the tropical Pacific warm pool, *Q. J. R. Meteorol. Soc.*, 123, 357–388, doi:10.1002/qj.49712353806.
- Chen, Y., and W. Hui (1990), Analysis of a shallow cold front during the Taiwan mesoscale experiment, *Mon. Weather Rev.*, 118, 2649–2667, doi:10.1175/1520-0493(1990)118<2649:AOASFD>2.0.CO;2.
- Chiao, S., and A. P. Barros (2007), A numerical study of the hydrometeorological dryline in northwest India during the monsoon, *J. Meteorol. Soc. Jpn.*, 85A, 337–361, doi:10.2151/jmsj.85A.337.
- Colle, B. A., B. F. Smull, and M.-J. Yang (2002), Numerical simulations of a landfalling cold front observed during COAST: Rapid evolution and responsible mechanisms, *Mon. Weather Rev.*, 130, 1945–1966, doi:10.1175/1520-0493(2002)130<1945:NSOALC>2.0.CO;2.
- Das, P. K. (1987), Short and long-range monsoon prediction in India, in *Monsoons*, edited by J. S. Fein and P. L. Stephens, pp. 549–578, John Wiley, New York.
- Dickinson, M. J., and D. J. Knight (1999), Frontal interaction with mesoscale topography, *J. Atmos. Sci.*, 56, 3544–3559, doi:10.1175/1520-0469(1999)056<3544:FIWMT>2.0.CO;2.
- Doyle, J. D. (1997), The influence of mesoscale orography on a coastal jet and rainband, *Mon. Weather Rev.*, 125, 1465–1488, doi:10.1175/1520-0493(1997)125<1465:TIOMOO>2.0.CO;2.
- Doyle, J. D., and N. A. Bond (2001), Research aircraft observations and numerical simulations of a warm front approaching Vancouver Island, *Mon. Weather Rev.*, 129, 978–998, doi:10.1175/1520-0493(2001)129<0978:RAOANS>2.0.CO;2.
- Ducrocq, V., O. Nuissier, D. Ricard, C. Lebeaupin, and T. Thouvenin (2008), A numerical study of three catastrophic precipitating events over southern France, II: Mesoscale triggering and stationarity factors, *Q. J. R. Meteorol. Soc.*, 134, 131–145, doi:10.1002/qj.199.
- Emanuel, K. A. (1986), An air-sea interaction theory for tropical cyclones: Part I. Steady-state maintenance, *J. Atmos. Sci.*, 43, 585–605, doi:10.1175/1520-0469(1986)043<0585:AASITF>2.0.CO;2.
- Farber, R. J. (1972), A study of cloud particles in synoptic storms over the Pacific Northwest, M.S. thesis, 649 pp., Dep. of Atmo. Sci., Univ. of Wash., Seattle.
- Fein, J. S., and J. P. Kuettner (1980), Report on the summer MONEX field phase, *Bull. Am. Meteorol. Soc.*, 61, 461–474.
- Frame, J., and P. Markowski (2006), The interaction of simulated squall lines with idealized mountain ridges, *Mon. Weather Rev.*, 134, 1919–1941, doi:10.1175/MWR3157.1.
- Frei, C., and C. Schär (1998), A precipitation climatology of the Alps from high-resolution rain-gauge observations, *Int. J. Climatol.*, 18, 873–900, doi:10.1002/(SICI)1097-0088(19980630)18:8<873::AID-JOC255>3.0.CO;2-9.
- Garvert, M. F., B. Smull, and C. Mass (2007), Multiscale mountain waves influencing a major orographic precipitation event, *J. Atmos. Sci.*, 64, 711–737, doi:10.1175/JAS3876.1.
- Geerts, B., G. M. Heymsfield, L. Tian, J. B. Halverson, A. Guillory, and M. I. Mejia (2000), Hurricane Georges's landfall in the Dominican Republic: Detailed airborne Doppler radar imagery, *Bull. Am. Meteorol. Soc.*, 81, 999–1018, doi:10.1175/1520-0477(2000)081<0999:HGLITD>2.3.CO;2.
- Georgis, J.-F., F. Roux, M. Chong, and S. Pradier (2003), Triple-Doppler radar analysis of the heavy rain event observed in the Lago Maggiore region during MAP IOP2b, *Q. J. R. Meteorol. Soc.*, 129, 495–522, doi:10.1256/qj.02.46.
- Giovannettone, J. P., and A. P. Barros (2008), A remote sensing survey of the role of landform on the organization of orographic precipitation in central and southern Mexico, *J. Hydrometeorol.*, 9, 1267–1283, doi:10.1175/2008JHM947.1.
- Gross, B. D. (1994), Frontal interaction with isolated orography, *J. Atmos. Sci.*, 51, 1480–1496, doi:10.1175/1520-0469(1994)051<1480:FIWIO>2.0.CO;2.
- Hartley, T. M., and Y.-L. Chen (2010), Characteristics of summer trade wind rainfall over Oahu, *Weather Forecasting*, 25, 1797–1815, doi:10.1175/2010WAF2222328.1.
- Hirose, M., and K. Nakamura (2005), Spatial and diurnal variation of precipitation systems over Asia observed by the TRMM Precipitation Radar, *J. Geophys. Res.*, 110, D05106, doi:10.1029/2004JD004815.
- Hobbs, P. V. (1975), The nature of winter clouds and precipitation in the Cascade Mountains and their modification by artificial seeding: Part I. Natural conditions, *J. Appl. Meteorol.*, 14(5), 783–804, doi:10.1175/1520-0450(1975)014<0783:TNCWA>2.0.CO;2.
- Hobbs, P. V., R. C. Easter, and A. B. Fraser (1973), A theoretical study of the flow of air and fallout of solid precipitation over mountainous terrain: Part II. Microphysics, *J. Atmos. Sci.*, 30, 813–823, doi:10.1175/1520-0469(1973)030<0813:ATSOTF>2.0.CO;2.
- Houze, R. A., Jr. (1977), Structure and dynamics of a tropical squall-line system, *Mon. Weather Rev.*, 105, 1540–1567, doi:10.1175/1520-0493(1977)105<1540:SADOT>2.0.CO;2.
- Houze, R. A., Jr. (1981), Structure of atmospheric precipitation systems: A global survey, *Radio Sci.*, 16, 671–689, doi:10.1029/RS016i005p00671.
- Houze, R. A., Jr. (1982), Cloud clusters and large-scale vertical motions in the tropics, *J. Meteorol. Soc. Jpn.*, 60, 396–410.
- Houze, R. A., Jr. (1989), Observed structure of mesoscale convective systems and implications for large-scale heating, *Q. J. R. Meteorol. Soc.*, 115, 425–461, doi:10.1002/qj.49711548702.
- Houze, R. A., Jr. (1993), *Cloud Dynamics*, 337 pp., Academic, San Diego, Calif.
- Houze, R. A., Jr. (1997), Stratiform precipitation in regions of convection: A meteorological paradox?, *Bull. Am. Meteorol. Soc.*, 78, 2179–2196, doi:10.1175/1520-0477(1997)078<2179:SPIROC>2.0.CO;2.
- Houze, R. A., Jr. (2004), Mesoscale convective systems, *Rev. Geophys.*, 42, RG4003, doi:10.1029/2004RG000150.
- Houze, R. A., Jr. (2010), Clouds in tropical cyclones, *Mon. Weather Rev.*, 138, 293–344.
- Houze, R. A., Jr., and D. D. Churchill (1987), Mesoscale organization and cloud microphysics in a Bay of Bengal depression, *J. Atmos. Sci.*, 44, 1845–1868, doi:10.1175/1520-0469(1987)044<1845:MOACMI>2.0.CO;2.
- Houze, R. A., Jr., and P. V. Hobbs (1982), Organization and structure of precipitating cloud systems, *Adv. Geophys.*, 24, 225–315, doi:10.1016/S0065-2687(08)60521-X.
- Houze, R. A., Jr., and S. Medina (2005), Turbulence as a mechanism for orographic precipitation enhancement, *J. Atmos. Sci.*, 62, 3599–3623, doi:10.1175/JAS3555.1.
- Houze, R. A., Jr., P. V. Hobbs, K. R. Biswas, and W. M. Davis (1976), Mesoscale rainbands in extratropical cyclones, *Mon. Weather Rev.*, 104, 868–878, doi:10.1175/1520-0493(1976)104<0868:MRIEC>2.0.CO;2.
- Houze, R. A., Jr., C. N. James, and S. Medina (2001), Radar observations of precipitation and airflow on the Mediterranean side of the Alps: Autumn 1998 and 1999, *Q. J. R. Meteorol. Soc.*, 127, 2537–2558, doi:10.1002/qj.49712757804.
- Houze, R. A., Jr., D. C. Wilton, and B. F. Smull (2007a), Monsoon convection in the Himalayan region as seen by the TRMM Precipitation Radar, *Q. J. R. Meteorol. Soc.*, 133, 1389–1411.
- Houze, R. A., Jr., S. S. Chen, B. F. Smull, W.-C. Lee, and M. M. Bell (2007b), Hurricane intensity and eyewall replacement, *Science*, 315, 1235–1239, doi:10.1126/science.1135650.

- Houze, R. A., Jr., K. L. Rasmussen, S. Medina, S. R. Brodzik, and U. Romatschke (2011), Anomalous atmospheric events leading to the summer 2010 floods in Pakistan, *Bull. Am. Meteorol. Soc.*, 92, 291–298, doi:10.1175/2010BAMS3173.1.
- James, C. N., and R. A. Houze Jr. (2005), Modification of precipitation by coastal orography in storms crossing northern California, *Mon. Weather Rev.*, 133, 3110–3131, doi:10.1175/MWR3019.1.
- Jiang, Q., and R. B. Smith (2003), Cloud timescale and orographic precipitation, *J. Atmos. Sci.*, 60, 1543–1559, doi:10.1175/2995.1.
- Johnson, R. H., and R. A. Houze Jr. (1987), Precipitating cloud systems of the Asian monsoon, in *Monsoon Meteorology*, edited by C.-P. Chang and T. N. Krishnamurti, pp. 298–353, Oxford Univ. Press, New York.
- Keeter, K. K., S. Businger, L. G. Lee, and J. S. Waldstreicher (1995), Winter weather forecasting throughout the eastern United States: Part III. The effects of topography and the variability of winter weather in the Carolinas and Virginia, *Weather Forecasting*, 10, 42–60, doi:10.1175/1520-0434(1995)010<0042:WWFTTE>2.0.CO;2.
- Kerns, J., B. Wesley, Y.-L. Chen, and M.-Y. Chang (2010), The diurnal cycle of winds, rain, and clouds over Taiwan during the Mei-Yu, summer, and autumn rainfall regimes, *Mon. Weather Rev.*, 138, 497–516, doi:10.1175/2009MWR3031.1.
- Kikuchi, K., and B. Wang (2008), Diurnal precipitation regimes in the global tropics, *J. Clim.*, 21, 2680–2696, doi:10.1175/2007JCLI2051.1.
- Kingsmill, D. E., P. J. Neiman, F. M. Ralph, and A. B. White (2006), Synoptic and topographic variability of Northern California precipitation characteristics in landfalling winter storms observed during CALJET, *Mon. Weather Rev.*, 134, 2072–2094, doi:10.1175/MWR3166.1.
- Kirshbaum, D. J., and R. B. Smith (2009), Orographic precipitation in the tropics: Large-eddy simulations and theory, *J. Atmos. Sci.*, 66, 2559–2578, doi:10.1175/2009JAS2990.1.
- Kirshbaum, D. J., G. H. Bryan, R. Rotunno, and D. R. Durran (2007), The triggering of orographic rainbands by small-scale topography, *J. Atmos. Sci.*, 64, 1530–1549, doi:10.1175/JAS3924.1.
- Kodama, Y.-M., A. Ohta, M. Katsumata, S. Mori, S. Satoh, and H. Ueda (2005), Seasonal transitions of predominant precipitation type and lightning activity over tropical monsoon areas derived from TRMM observations, *Geophys. Res. Lett.*, 32, L14710, doi:10.1029/2005GL022986.
- Koteswaram, P., and C. A. George (1958), On the formation of monsoon depressions in the Bay of Bengal, *Indian J. Meteorol. Geophys.*, 9, 9–22.
- Krishnamurti, T. N., M. Kanamitsu, R. Godbole, C.-B. Chang, F. Carr, and J. H. Chow (1975), Study of a monsoon depression: I. Synoptic structure, *J. Meteorol. Soc. Jpn.*, 53, 227–239.
- Kummerow, C., W. Barnes, T. Kozu, J. Shiue, and J. Simpson (1998), The Tropical Rainfall Measuring Mission (TRMM) sensor package, *J. Atmos. Oceanic Technol.*, 15, 809–817, doi:10.1175/1520-0426(1998)015<0809:TTRMMT>2.0.CO;2.
- Kummerow, C., et al. (2000), The status of the Tropical Rainfall Measuring Mission (TRMM) after two years in orbit, *J. Appl. Meteorol.*, 39, 1965–1982, doi:10.1175/1520-0450(2001)040<1965:TSOTTR>2.0.CO;2.
- Lang, J. T., and A. P. Barros (2002), An investigation of the onsets of the 1999 and 2000 monsoons in central Nepal, *Mon. Weather Rev.*, 130, 1299–1316, doi:10.1175/1520-0493(2002)130<1299:AIOTOO>2.0.CO;2.
- Li, Y., and R. B. Smith (2010), The detection and significance of diurnal pressure and potential vorticity anomalies east of the Rockies, *J. Atmos. Sci.*, 67, 2734–2751, doi:10.1175/2010JAS3423.1.
- Lin, Y.-L., S. Chiao, T.-A. Wang, M. L. Kaplan, and R. P. Weglarz (2001), Some common ingredients for heavy orographic rainfall, *Weather Forecasting*, 16, 633–660, doi:10.1175/1520-0434(2001)016<0633:SCIFHO>2.0.CO;2.
- Locatelli, J. D., and P. V. Hobbs (1987), The mesoscale and microscale structure and organization of clouds and precipitation in midlatitude cyclones: Part XIII. Structure of a warm front, *J. Atmos. Sci.*, 44, 2290–2309, doi:10.1175/1520-0469(1987)044<2290:TMAMSA>2.0.CO;2.
- Mapes, B. E., T. T. Warner, and M. Xu (2003), Diurnal patterns of rainfall in northwestern South America: Part III. Diurnal gravity waves and nocturnal convection offshore, *Mon. Weather Rev.*, 131, 830–844, doi:10.1175/1520-0493(2003)131<0830:DPORIN>2.0.CO;2.
- Marengo, J. A., W. R. Soares, C. Saulo, and M. Nicolini (2004), Climatology of the low level jet east of the Andes as derived from the NCEP-NCAR reanalyses: Characteristics and temporal variability, *J. Clim.*, 17, 2261–2280, doi:10.1175/1520-0442(2004)017<2261:COTLJE>2.0.CO;2.
- Marwitz, J. D. (1983), The kinematics of orographic airflow during Sierra storms, *J. Atmos. Sci.*, 40, 1218–1227, doi:10.1175/1520-0469(1983)040<1218:TKOOAD>2.0.CO;2.
- Marwitz, J. D. (1987), Deep orographic storms over the Sierra Nevada: Part I. Thermodynamic and kinematic structure, *J. Atmos. Sci.*, 44, 159–173, doi:10.1175/1520-0469(1987)044<0159:DOSOTS>2.0.CO;2.
- Matejka, T. J., R. A. Houze Jr., and P. V. Hobbs (1980), Microphysics and dynamics of clouds associated with mesoscale rainbands in tropical cyclones, *Q. J. R. Meteorol. Soc.*, 106, 29–56, doi:10.1002/qj.49710644704.
- Medina, S. (2005), Orographic enhancement of mid-latitude cyclone precipitation, Ph. D. dissertation, Univ. of Wash., Seattle.
- Medina, S., and R. A. Houze Jr. (2003), Air motions and precipitation growth in alpine storms, *Q. J. R. Meteorol. Soc.*, 129, 345–371, doi:10.1256/qj.02.13.
- Medina, S., B. F. Smull, R. A. Houze Jr., and M. Steiner (2005), Cross-barrier flow during orographic precipitation events: Results from MAP and IMPROVE, *J. Atmos. Sci.*, 62, 3580–3598, doi:10.1175/JAS3554.1.
- Medina, S., E. Sukovich, and R. A. Houze Jr. (2007), Vertical structures of precipitation in cyclones crossing the Oregon Cascades, *Mon. Weather Rev.*, 135, 3565–3586, doi:10.1175/MWR3470.1.
- Medina, S., R. A. Houze Jr., A. Kumar, and D. Niyogi (2010), Summer monsoon convection in the Himalayan region: Terrain and land cover effects, *Q. J. R. Meteorol. Soc.*, 136, 593–616.
- Minder, J. R., D. R. Durran, G. H. Roe, and A. M. Anders (2008), The climatology of small-scale orographic precipitation over the Olympic Mountains: Patterns and processes, *Q. J. R. Meteorol. Soc.*, 134, 817–839, doi:10.1002/qj.258.
- Nagle, R. E., and S. M. Serebreny (1962), Radar precipitation echo and satellite cloud observations of a maritime cyclone, *J. Appl. Meteorol.*, 1, 279–295, doi:10.1175/1520-0450(1962)001<0279:RPEASC>2.0.CO;2.
- Negri, A. J., T. L. Bell, and L. Xu (2002), Sampling of the diurnal cycle of precipitation using TRMM, *J. Atmos. Oceanic Technol.*, 19, 1333–1344, doi:10.1175/1520-0426(2002)019<1333:SOTDCO>2.0.CO;2.
- Neiman, P. J., F. M. Ralph, A. B. White, D. E. Kingsmill, and P. O. G. Persson (2002), The statistical relationship between upslope flow and rainfall in California's coastal mountains: Observations during CALJET, *Mon. Weather Rev.*, 130, 1468–1492, doi:10.1175/1520-0493(2002)130<1468:TSRBUF>2.0.CO;2.
- Neiman, P. J., F. M. Ralph, G. A. Wick, J. D. Lundquist, and M. D. Dettinger (2008), Meteorological characteristics and overland precipitation impacts of atmospheric rivers affecting the west coast of North America based on eight years of SSM/I satellite observations, *J. Hydrometeorol.*, 9, 22–47, doi:10.1175/2007JHM855.1.

- Newell, R. E., N. E. Newell, Y. Zhu, and C. Scott (1992), Tropospheric rivers? A pilot study, *Geophys. Res. Lett.*, **19**, 2401–2404, doi:10.1029/92GL02916.
- Nogués-Paegle, J., and K. C. Mo (1997), Alternating wet and dry conditions over South America during summer, *Mon. Weather Rev.*, **125**, 279–291, doi:10.1175/1520-0493(1997)125<0279:AWADCO>2.0.CO;2.
- Nuissier, O., V. Ducrocq, D. Ricard, C. Lebeaupin, and S. Anquetin (2008), A numerical study of three catastrophic precipitating events over southern France: I. Numerical framework and synoptic ingredients, *Q. J. R. Meteorol. Soc.*, **134**, 111–130, doi:10.1002/qj.200.
- Parish, T. R. (1982), Barrier winds along the Sierra Nevada Mountains, *J. Appl. Meteorol.*, **21**, 925–930, doi:10.1175/1520-0450(1982)021<0925:BWATSN>2.0.CO;2.
- Passarelli, R. E., and H. Boehme (1983), The orographic modulation of pre-warm-front precipitation in southern New England, *Mon. Weather Rev.*, **111**, 1062–1070, doi:10.1175/1520-0493(1983)111<1062:TOMOPW>2.0.CO;2.
- Peterson, T. C., L. O. Grant, W. R. Cotton, and D. C. Rogers (1991), The effect of decoupled low-level flow on winter orographic clouds and precipitation in the Yampa River valley, *J. Appl. Meteorol.*, **30**, 368–386, doi:10.1175/1520-0450(1991)030<0368:TEODLL>2.0.CO;2.
- Ralph, F. M., P. J. Neiman, and G. A. Wick (2004), Satellite and CALJET aircraft observations of atmospheric rivers over the eastern North Pacific Ocean during the winter of 1997/98, *Mon. Weather Rev.*, **132**, 1721–1745, doi:10.1175/1520-0493(2004)132<1721:SACAOO>2.0.CO;2.
- Ralph, F. M., P. J. Neiman, and R. Rotunno (2005), Dropsonde observations in low-level jets over the northeastern Pacific Ocean from CALJET-1998 and PACJET-2001: Mean vertical-profile and atmospheric-river characteristics, *Mon. Weather Rev.*, **133**, 889–910, doi:10.1175/MWR2896.1.
- Rasmussen, K. L., and R. A. Houze Jr. (2011), Orogenic convection in subtropical South America as seen by the TRMM satellite, *Mon. Weather Rev.*, **139**(8), 2399–2420, doi:10.1175/MWR-D-10-05006.1.
- Reeves, H. D., and Y.-L. Lin (2007), The effects of a mountain on the propagation of a preexisting convective system for blocked and unblocked flow regimes, *J. Atmos. Sci.*, **64**, 2401–2421, doi:10.1175/JAS3959.1.
- Reeves, H. D., and R. Rotunno (2008), Orographic flow response to variations in upstream humidity, *J. Atmos. Sci.*, **65**, 3557–3570, doi:10.1175/2008JAS2762.1.
- Reeves, H. D., Y.-L. Lin, and R. Rotunno (2008), Dynamic forcing and mesoscale variability of heavy precipitation events over the Sierra Nevada mountains, *Mon. Weather Rev.*, **136**, 62–77, doi:10.1175/2007MWR2164.1.
- Roe, G. H. (2005), Orographic precipitation, *Annu. Rev. Earth Planet. Sci.*, **33**, 645–671, doi:10.1146/annurev.earth.33.092203.122541.
- Roe, G. H., D. R. Montgomery, and B. Hallet (2003), Orographic precipitation and the relief of mountain ranges, *J. Geophys. Res.*, **108**(B6), 2315, doi:10.1029/2001JB001521.
- Romatschke, U., and R. A. Houze Jr. (2010), Extreme summer convection in South America, *J. Clim.*, **23**, 3761–3791, doi:10.1175/2010JCLI3465.1.
- Romatschke, U., and R. A. Houze Jr. (2011a), Characteristics of precipitating convective systems in the premonsoon season of South Asia, *J. Hydrometeorol.*, **12**, 157–180, doi:10.1175/2010JHM1311.1.
- Romatschke, U., and R. A. Houze Jr. (2011b), Characteristics of precipitating convective systems in the South Asian monsoon, *J. Hydrometeorol.*, **12**, 3–26, doi:10.1175/2010JHM1289.1.
- Romatschke, U., S. Medina, and R. A. Houze Jr. (2010), Regional, seasonal, and diurnal variations of extreme convection in the South Asian region, *J. Clim.*, **23**, 419–439, doi:10.1175/2009JCLI3140.1.
- Rotunno, R., and R. Ferretti (2001), Mechanisms of intense alpine rainfall, *J. Atmos. Sci.*, **58**, 1732–1749, doi:10.1175/1520-0469(2001)058<1732:MOIAR>2.0.CO;2.
- Rotunno, R., and R. A. Houze Jr. (2007), Lessons on orographic precipitation from the Mesoscale Alpine Programme, *Q. J. R. Meteorol. Soc.*, **133**, 811–830, doi:10.1002/qj.67.
- Rotunno, R., J. B. Klemp, and M. L. Weisman (1988), A theory for strong, long-lived squall lines, *J. Atmos. Sci.*, **45**, 463–485, doi:10.1175/1520-0469(1988)045<0463:ATFSLL>2.0.CO;2.
- Saha, K., and S. Saha (1988), Thermal budget of a monsoon depression in the Bay of Bengal during FGGE-MONEX 1979, *Mon. Weather Rev.*, **116**, 242–255, doi:10.1175/1520-0493(1988)116<0242:TBOAMD>2.0.CO;2.
- Saulo, A. C., M. Nicolini, and S. C. Chou (2000), Model characterization of the South American low-level flow during the 1997–1998 spring-summer season, *Clim. Dyn.*, **16**, 867–881, doi:10.1007/s003820000085.
- Schumacher, P. N., D. J. Knight, and L. F. Bosart (1996), Frontal interaction with the Appalachian Mountains: Part I. A climatology, *Mon. Weather Rev.*, **124**, 2453–2468, doi:10.1175/1520-0493(1996)124<2453:FIWTAM>2.0.CO;2.
- Seity, Y., S. Soula, P. Tabary, and G. Scialom (2003), The convective storm system during IOP 2a of MAP: Cloud-to-ground lightning flash production in relation to dynamics and micro-physics, *Q. J. R. Meteorol. Soc.*, **129**, 523–542, doi:10.1256/qj.02.03.
- Shapiro, L. J., and H. E. Willoughby (1982), The response of balanced hurricanes to local sources of heat and momentum, *J. Atmos. Sci.*, **39**, 378–394, doi:10.1175/1520-0469(1982)039<0378:TROBHT>2.0.CO;2.
- Shukla, J. (1978), CISK-barotropic-baroclinic instability and the growth of monsoon depressions, *J. Atmos. Sci.*, **35**, 495–508, doi:10.1175/1520-0469(1978)035<0495:CBBIAT>2.0.CO;2.
- Smith, R. B. (1979), The influence of mountains on the atmosphere, *Adv. Geophys.*, **21**, 87–230, doi:10.1016/S0065-2687(08)60262-9.
- Smith, R. B. (2003), A linear upslope-time-delay model for orographic precipitation, *J. Hydrol.*, **282**, 2–9, doi:10.1016/S0022-1694(03)00248-8.
- Smith, R. B. (2006), Progress on the theory of orographic precipitation, *Spec. Pap. Geol. Soc. Am.*, **398**, 1–16, doi:10.1130/2006.2398(01).
- Smith, R. B., and I. Barstad (2004), A linear theory of orographic precipitation, *J. Atmos. Sci.*, **61**, 1377–1391, doi:10.1175/1520-0469(2004)061<1377:ALTOOP>2.0.CO;2.
- Smith, R. B., P. Schafer, D. Kirshbaum, and E. Regina (2009), Orographic enhancement of precipitation inside Hurricane Dean, *J. Hydrometeorol.*, **10**, 820–831, doi:10.1175/2008JHM1057.1.
- Smolarkiewicz, P. K., and R. Rotunno (1989), Low Froude number flow past three-dimensional obstacles: Part I. Baroclinically generated lee vortices, *J. Atmos. Sci.*, **46**, 1154–1164, doi:10.1175/1520-0469(1989)046<1154:LFNFPT>2.0.CO;2.
- Steiner, M., O. Bousquet, R. A. Houze Jr., B. F. Smull, and M. Mancini (2003), Airflow within major Alpine river valleys under heavy rainfall, *Q. J. R. Meteorol. Soc.*, **129**, 411–431, doi:10.1256/qj.02.08.
- Tang, X.-D., M.-J. Yang, and Z.-M. Tan (2011), A modeling study of orographic convection and mountain waves in the landfalling Typhoon Nari (2001), *Q. J. R. Meteorol. Soc.*, doi:10.1002/qj.933, in press.
- Tripoli, G. J., and W. R. Cotton (1989), Numerical study of an observed orogenic mesoscale convective system: Part 1. Simulated genesis and comparison with observations, *Mon. Weather Rev.*, **117**, 273–304, doi:10.1175/1520-0493(1989)117<0273:NSOAOO>2.0.CO;2.
- Vera, C., et al. (2006), The South American Low-Level Jet Experiment, *Bull. Am. Meteorol. Soc.*, **87**, 63–77, doi:10.1175/BAMS-87-1-63.

- Vivekanandan, J., D. S. Zrnic, S. M. Ellis, R. Oye, A. V. Ryzhkov, and J. Straka (1999), Cloud microphysics retrieval using S-band polarization radar measurements, *Bull. Am. Meteorol. Soc.*, 80, 381–388, doi:10.1175/1520-0477(1999)080<0381:CMRUSB>2.0.CO;2.
- Webster, P. J., et al. (2002), The JASMINE pilot study, *Bull. Am. Meteorol. Soc.*, 83, 1603–1630, doi:10.1175/BAMS-83-11-1603.
- Weston, K. J. (1972), The dry-line of northern India and its role in cumulonimbus convection, *Q. J. R. Meteorol. Soc.*, 98, 519–531, doi:10.1002/qj.49709841704.
- White, A. B., P. J. Neiman, F. M. Ralph, D. E. Kingsmill, and P. O. G. Persson (2003), Coastal orographic rainfall processes observed by radar during the California Land-Falling Jets Experiment, *J. Hydrometeorol.*, 4, 264–282, doi:10.1175/1525-7541(2003)4<264:CORPOB>2.0.CO;2.
- Willoughby, H. E. (1998), Tropical cyclone eye thermodynamics, *Mon. Weather Rev.*, 126, 3053–3067, doi:10.1175/1520-0493(1998)126<3053:TCET>2.0.CO;2.
- Witcraft, N. C., Y.-L. Lin, and Y.-H. Kuo (2005), Dynamics of orographic rain associated with the passage of a tropical cyclone over a mesoscale mountain, *Terr. Atmos. Oceanic Sci.*, 16, 1133–1161.
- Xie, S. P., H. Xu, N. H. Saji, Y. Wang, and W. T. Liu (2006), Role of narrow mountains in large-scale organization of Asian monsoon convection, *J. Clim.*, 19, 3420–3429, doi:10.1175/JCLI3777.1.
- Yu, C.-K., and L.-W. Cheng (2008), Radar observations of intense orographic precipitation associated with Typhoon Xangsane, 2000, *Mon. Weather Rev.*, 136, 497–521, doi:10.1175/2007MWR2129.1.
- Yu, C.-K., and B. F. Smull (2000), Airborne Doppler observations of a landfalling cold front upstream of steep coastal orography, *Mon. Weather Rev.*, 128, 1577–1603, doi:10.1175/1520-0493(2000)128<1577:ADOOAL>2.0.CO;2.
- Yuter, S. E., and R. A. Houze Jr. (2003), Microphysical modes of precipitation growth determined by S-band vertically pointing radar in orographic precipitation during MAP, *Q. J. R. Meteorol. Soc.*, 29, 455–476, doi:10.1256/qj.01.216.
- Zhu, Y., and R. E. Newell (1994), Atmospheric rivers and bombs, *Geophys. Res. Lett.*, 21, 1999–2002, doi:10.1029/94GL01710.
- Zhu, Y., and R. E. Newell (1998), A proposed algorithm for moisture fluxes from atmospheric rivers, *Mon. Weather Rev.*, 126, 725–735, doi:10.1175/1520-0493(1998)126<0725:APAFMF>2.0.CO;2.
- Zipser, E. J. (1977), Mesoscale and convective-scale downdrafts as distinct components of squall-line circulation, *Mon. Weather Rev.*, 105, 1568–1589, doi:10.1175/1520-0493(1977)105<1568:MACDAD>2.0.CO;2.
- Zipser, E. J., D. J. Cecil, C. Liu, S. W. Nesbitt, and D. P. Yorty (2006), Where are the most intense thunderstorms on Earth?, *Bull. Am. Meteorol. Soc.*, 87, 1057–1071, doi:10.1175/BAMS-87-8-1057.
- Zuidema, P. (2003), Convective clouds over the Bay of Bengal, *Mon. Weather Rev.*, 131, 780–798, doi:10.1175/1520-0493(2003)131<0780:CCOTBO>2.0.CO;2.

R. A. Houze Jr., Department of Atmospheric Sciences, University of Washington, Seattle, WA 98195-1640, USA. (houze@atmos.washington.edu)